Delft University of Technology
Faculty of Civil Engineering and Geosciences

Master Thesis

CIE5060

Combination parametric resonance of an oscillator that moves uniformly along a beam on a periodically inhomogeneous foundation

Graduation candidate:

Joep van Oostrum (4143787)

Graduation committee:

Dr.ir. K.N. van Dalen

Ir. A. Faragau

Dr.ir. F.P. van der Meer

Prof.dr. A.V. Metrikine

March 21, 2021

Contents

Abstract

A new form of high-speed transportation, which involves a magnetically levitated vehicle that travels through a vacuum tube, is currently under development. Those parts of the trajectory along which the tube is supported by columns—which possess both axial and bending stiffness—requires the use of a model that allows to study a form of instability that is inherent to this type of support. Specifically, the stability is studied of a point mass with a lateral and vertical degree-of-freedom that moves with constant velocity along an infinite Euler-Bernoulli beam on coupled lateral-vertical periodically inhomogeneous foundation. The beam model is able to deflect in both the lateral and vertical direction and the concentrated mass is attached to this beam by a lateral and vertical contact spring. With the help of a perturbation method it is shown that the system's vibrations can become unstable. As for the model that only exhibits degrees-of-freedom in the vertical direction, the underlying physical phenomenon is parametric resonance, which occurs because of the periodic variation of the foundation stiffnesses. For the lateral-vertical model, this form of instability is referred to as combination parametric resonance, which yields four instability domains in the velocity-mass parameter space as opposed to the one domain for the vertical-only model. The center lines of these four domains depend strongly on the period of inhomogeneity; the larger the period, the higher the velocity at which instability occurs. Vehicle-structure interaction (i.e. the maglev system) also affects the center lines considerably; including contact springs between the beam and the point mass reduces the velocity at which instability occurs. To obtain the complete instability domains and to be able to investigate the mitigating effect of foundation damping, the method from another paper is recommended to be used for follow-up research.

Chapter 1

Introduction

The backdrop of this thesis project is the *Hyperloop* transportation system; a mode of transportation that involves a magnetically levitated vehicle [4, 19], or *pod*, travelling through a sealed tube from which air is extracted. These two key characteristics remove the two constraints to which most forms of transportation are subjected: rolling resistance and air resistance. Eliminating both types of friction enables the pod to reach velocities beyond those of a high-speed train ($\sim$ 300 km/h) and even enables it to go faster than a commercial passenger aircraft ($\sim$ 900 km/h) while concurrently requiring less fuel. This competitive edge in terms of speed and energy efficiency makes the Hyperloop system a commercially viable alternative to the two aforementioned modes of transportation. However, in terms of its trajectory towards a full-scale operable means of transport, the development of the Hyperloop system is still in its infancy and requires to take on many technical challenges. One of which is to ensure that the pod's vibrations remain limited along the entire route; both underground as well as above ground. It is therefore important to determine under what conditions the vehicle becomes unstable and to establish how these conditions can be mitigated if not completely eliminated.

According to the concept design [9], the steel tube above ground is placed on support columns, which makes the Hyperloop system susceptible to a particular type of dynamic instability known as *parametric resonance*; a form of instability caused by periodic variation of one of the system's parameters. Besides setting an upper limit on the pod's cruising speed—which, once exceeded, would make the pod disperse waves in the guiding structure that leads to exponential growth of its oscillations—the lower velocity range now also becomes a concern due to this additional instability phenomenon. In fact, these two forms of instability are already well described in existing literature; combinations of vehicle mass and velocity that causes the vehicle's vibration amplitude to grow exponentially with time are designated in the velocity-mass parameter space by enclosed domains. It is mentioned that throughout this report the instability associated with the higher velocity range is referred to as *wave-induced instability* for brevity and ease of communication, even though parametric instability can also be considered as instability caused by wave formation. Because the support columns possess axial as well as bending stiffness, the foundation model in both the vertical and lateral direction exhibits the same periodic inhomogeneity; now two system parameters vary periodically instead of one, which necessitates to investigate not just parametric resonance but *combination parametric resonance* as well. Moreover, the maglev system makes the vehicle have its own degrees-of-freedom, which requires to account for vehicle-structure interaction when investigating the system's stability.

The goal of this report is to present the center lines of the instability domains associated with combination parametric resonance. In particular, Verichev & Metrikine (2003) offer the possibility to derive these lines; in this article, parametric resonance of a beam model that only exhibits vertical degrees-of-freedom is studied by means of a perturbation method. Extending the model by including a lateral foundation, which is coupled to its vertical counterpart, and following the same approach as is used by Verichev & Metrikine (2003) allows to compute combinations of vehicle mass and velocity that constitute the center lines of the instability domains. Additionally, to account for the magnetic levitation of the vehicle (the *maglev system*), the model is augmented by including contact springs between the vehicle and guiding structure, which enables to investigate the effect of vehicle-structure interaction on the instability domains' centers. Despite the notion of a coupling between the magnetic suspension along the vertical direction and the magnetic guidance along the lateral direction, this effect is not taken into account in the final model.

The model that is ultimately used to derive the center lines is built step by step. Starting off in Chapter 2 with the introduction of the concept of the *equivalent stiffness* and presenting the different types of beam motion, the third chapter is subsequently used to derive the instability domain for an oscillator that moves with constant velocity along a beam on a homogeneous base. After letting the reader get acquainted with the concept of parametric resonance by means of *Mathieu's equation* in Chapter 4, the characteristic equations that are derived in Chapter 3 are used in Chapter 5 and 6. The fifth chapter adds complexity to the model of Chapter 3 by replacing the homogeneous base by a harmonically varying foundation. In an attempt to capture the effect of the maglev system, a linear contact spring is included in the model of Chapter 6. This last model is extended in the lateral direction in Chapter 7 by adding the same periodic support along the y-axis; a coupling with its counterpart along the z-axis makes it possible to derive the center lines for combination parametric resonance. Final thoughts on the preceded material and recommendations for further research are included in Chapter 8.

Chapter 2

Wave-induced instability of a point mass moving uniformly along an axially compressed infinite Timoshenko beam on homogeneous foundation

Throughout this report the vehicle-structure model is reduced to an equivalent oscillator in order to investigate its stability. The purpose of this chapter is to let the reader become acquainted with the concept of the *equivalent stiffness*; a function that emerges when deriving the equivalent oscillator's characteristic equation and which enables plotting the instability domain. Furthermore, the four types of beam motion are described and presented graphically, which will be used for explanatory purposes in the next chapters. All this is done in the context of investigating the stability of a vehicle that moves with constant velocity along an axially compressed Timoshenko beam on visco-elastic foundation. This chapter builds on reference [22].

2.1 Equations of motion

The governing equations that describe a uniformly moving point mass along an axially compressed infinite Euler-Bernoulli beam on homogeneous visco-elastic foundation are given as [8]:

$$\begin{aligned} &\rho A\frac{\partial^2 w}{\partial t^2} + EI\frac{\partial^4 w}{\partial x^4} + N\frac{\partial^2 w}{\partial x^2} + \nu_f\frac{\partial w}{\partial t} + k_f w = -\delta\left(x - Vt\right) m\frac{d^2 w_0}{dt^2} \\ &w_0 = w|_{x=Vt} \end{aligned} \tag{2.1}$$

and the governing equations that describe a uniformly moving point mass along an axially compressed infinite Timoshenko beam on homogeneous visco-elastic foundation read [20]:

$$\begin{aligned}
&\rho A\frac{\partial^2 w}{\partial t^2} + GA\beta\left(\frac{\partial \varphi}{\partial x} - \frac{\partial^2 w}{\partial x^2}\right) + N\frac{\partial^2 w}{\partial x^2} + \nu_f\frac{\partial w}{\partial t} + k_f w = -\delta\left(x - Vt\right)m\frac{d^2 w_0}{dt^2}\\
&\rho I\frac{\partial^2 \varphi}{\partial t^2} + GA\beta\left(\varphi - \frac{\partial w}{\partial x}\right) - \left(E - \frac{N}{A}\right)I\frac{\partial^2 \varphi}{\partial x^2} = 0\\
&w_0 = w|_{x=Vt}
\end{aligned} \tag{2.2}$$

The following set of dimensionless parameters and variables is adopted:

$$\begin{aligned}
&\kappa = \frac{c^2 A}{\omega_0^2 I}, \quad \gamma = \frac{c_p^2}{c^2}, \quad T = \frac{N}{\rho A c^2}, \quad \nu = \frac{\nu_f}{\rho A \omega_0}, \quad \alpha = \frac{V}{c}, \quad M = \frac{m\omega_0}{\rho A c},\\
&\tau = \omega_0 t, \quad y = x\frac{\omega_0}{c}, \quad W_0\left(\tau\right) = w_0\left(t\right)\frac{\omega_0}{c}, \quad W\left(y,\tau\right) = w\left(x,t\right)\frac{\omega_0}{c}
\end{aligned} \tag{2.3}$$

in which $c_p = \sqrt{E/\rho}$ and $c_s = \sqrt{G/\rho}$ are the compressional respectively shear wave velocity in the beam, $c = c_s\sqrt{\beta}$ and $\omega_0 = \sqrt{k_f/(\rho A)}$ is the cut-off frequency of the beam on elastic foundation. Eq. (2.1) can then be rewritten as:

$$\begin{aligned}
&\frac{\partial^2 W}{\partial \tau^2} + \frac{\gamma}{\kappa}\frac{\partial^4 W}{\partial y^4} + T\frac{\partial^2 W}{\partial y^2} + \nu\frac{\partial W}{\partial \tau} + W = -\delta\left(y - \alpha\tau\right)M\frac{d^2 W_0}{d\tau^2}\\
&W_0 = W|_{y=\alpha\tau}
\end{aligned} \tag{2.4}$$

and Eq. (2.2) as:

$$\begin{aligned}
&\frac{\partial^2 W}{\partial \tau^2} + \frac{\partial \varphi}{\partial y} - \frac{\partial^2 W}{\partial y^2} + T\frac{\partial^2 W}{\partial y^2} + \nu\frac{\partial W}{\partial \tau} + W = -\delta\left(y - \alpha\tau\right)M\frac{d^2 W_0}{d\tau^2}\\
&\frac{\partial^2 \varphi}{\partial \tau^2} + \kappa\left(\varphi - \frac{\partial W}{\partial y}\right) - \left(\gamma - T\right)\frac{\partial^2 \varphi}{\partial y^2} = 0\\
&W_0 = W|_{y=\alpha\tau}
\end{aligned} \tag{2.5}$$

2.2 Interpretation of the equivalent beam stiffness

This section merely discusses the equivalent stiffness $\chi_{eq}\left(q\right)$; its derivation from Eq. (2.4) and Eq. (2.5) is omitted. The reader is referred to Chapter 3 for a detailed description of the derivation procedure. To be consistent with the dimensionless formulation of Eq. (2.3), a dimensionless angular frequency and wavenumber, q respectively r, are employed throughout the remainder of this chapter. Let us start the discussion by addressing the signage of the plots depicted in Fig. (2.1) and Fig. (2.2). Since the considered stiffness function is derived by reducing the beam system to an equivalent one-mass oscillator, it is only reasonable to compare it to the elementary SDoF system. Deriving the latter's characteristic equation by transforming its homogeneous equation of motion to the Laplace domain and replacing s by $i\omega_n$:

$$-\omega_n^2 m + i\omega_n c + k = 0 \tag{2.6}$$

provides insight into the three components of the equivalent stiffness. From characteristic Eq. (2.6) it can be readily observed that the negative real part is associated with inertia while the positive real part relates to the system's elasticity. The second term, related to damping, is imaginary and can be either positive or negative; implying the system to be either stable respectively unstable. The sign of $\chi_{eq}(q)$ in Fig. (2.1) and Fig. (2.2) should be likewise interpreted. See Tab. (2.1).

$\mathrm{Re}\,\chi_{\mathrm{eq}}$	$\mathrm{Im}\,\chi_{\mathrm{eq}}$	**Model**	$\mathrm{Re}\,\chi_{\mathrm{eq}}$	$\mathrm{Im}\,\chi_{\mathrm{eq}}$	**Model**	$\mathrm{Re}\,\chi_{\mathrm{eq}}$	$\mathrm{Im}\,\chi_{\mathrm{eq}}$	**Model**
> 0	> 0	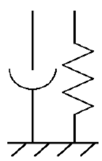	< 0	> 0	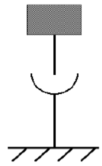	0	> 0	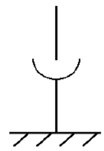
> 0	< 0	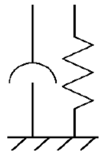	< 0	< 0	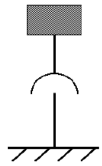	0	< 0	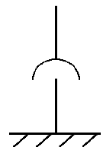

Table 2.1: Interpretation of the equivalent stiffness by means of the SDoF analogy [22].

A resemblance between the single-degree-of-freedom system's characteristic equation and that of the equivalent oscillator:

$$-Mq^2 + \chi_{eq}(q) = 0 \tag{2.7}$$

seems evident, though it needs to be noted that Eq. (2.7) is derived from inhomogeneous equations—Eq. (2.4) and Eq. (2.5)—and that the first term on the left-hand side of Eq. (2.7) originates from the inhomogeneous right-hand side of these equations of motion while the stiffness term stems completely from the EoM's left-hand side; which explains why $\chi_{eq}(q)$ expresses the equivalent oscillator's mechanical components: inertia, damping and stiffness.

Continuing the discussion on the interpretation of Fig. (2.1) and Fig. (2.2) is aided by the dispersion curves presented in Fig. (2.3) and Fig. (2.4). For the stationary situation ($\alpha = 0$) the blue curves in Fig. (2.1) and Fig. (2.2) show one respectively two abrupt changes in the gradient. According to reference [22] the corresponding frequencies are associated with horizontal tangency between the kinematic invariant[1] and the dispersion curve. This is indeed confirmed when reading the valuations of these cut-off frequencies from the vertical axis in Fig. (2.3) and Fig. (2.4); the blue curve in both the left and right panel of Fig. (2.1) shows an abrupt change of the gradient around $q_1 = 1$ while in Fig. (2.2) an additional kink can be observed around $q_2 = 35$. Staying with the stationary situation, the Euler-Bernoulli respectively Timoshenko model distinguishes three respectively six cases related to the energy content of the contact point. Whether or not energy dissipates from this point depends on the formation of propagating waves that radiate away from the contact point. In the dispersion plane this is indicated by intersections between the dispersion curve and the kinematic invariant. See Tab. (2.2). No crossing between these two lines implies that no propagating waves are generated, which means that no energy is consumed by the beam at the contact point [22]. Tangency between the two

[1]The kinematic invariant dictates that the phase of the radiated waves should mirror the phase of the excitation source at the contact point between this source and the beam. The resulting relation between the angular frequency and wavenumber is pivotal to get insight into the beam's motion.

lines indicates the accumulation of energy at the point of contact between the beam and excitation source.

	$q < q_1$	$q = q_1$	$q_1 < q < q_2$	$q = q_2$	$q > q_2$
EB	none	rigid vibrations	two waves		
Timo	none	rigid vibrations	two waves	rigid vibrations and two waves	four waves

Table 2.2: Wave formation in the beam for $\alpha = 0$. The first and second cut-off frequencies are denoted by q_1 respectively q_2.

The question now is: how do these observations from the dispersion planes translate to the blue curves in Fig. (2.1) and Fig. (2.2)? Mapping the aforementioned distinctive cases onto the blue curves in the two figures above, the cut-off frequencies bound qualitatively different wave formations [22]. See Tab. (2.2). For the Euler-Bernoulli beam, as for the Timoshenko beam, excitation below the first cut-off frequency q_1 corresponds to a visco-elastic response ($\mathrm{Re}(\chi_{eq}) > 0$ and $\mathrm{Im}(\chi_{eq}) > 0$). The imaginary part of the equivalent stiffness lies slightly above zero, indicating that energy dissipates from the contact point, even though it was concluded previously that no propagating waves are excited within this frequency range. However, unlike the dispersion relation, the equivalent stiffness is derived by including the foundation viscosity, which forms another energy sink.

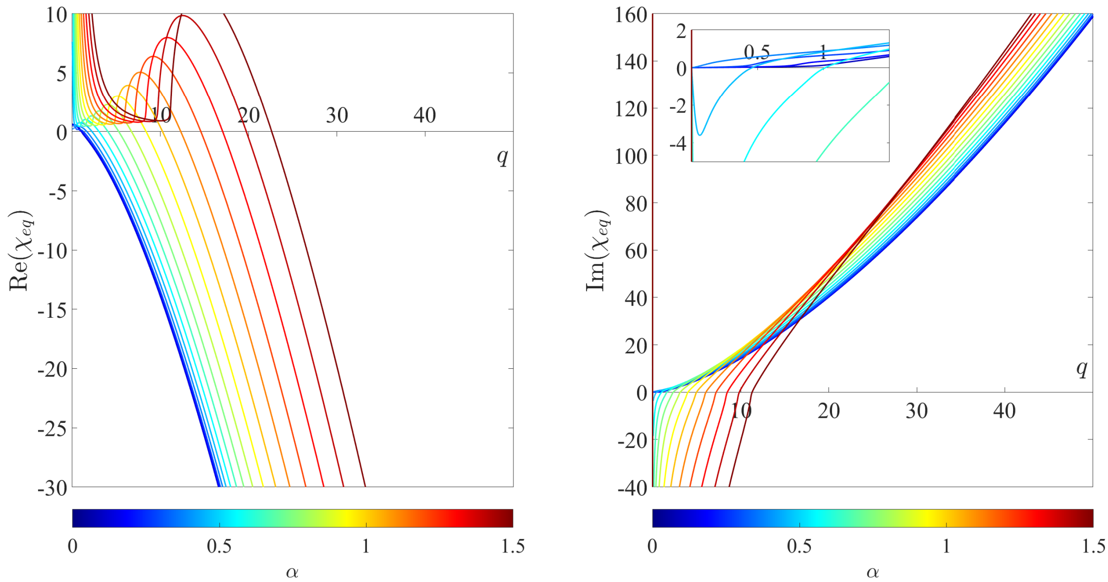

Figure 2.1: The real and imaginary part of the equivalent stiffness of the Euler-Bernoulli beam on visco-elastic foundation along which a point mass moves with constant velocity. The stiffness is a function of the point mass's vibratory frequency q and is plotted for a range of velocity values α. The used parameter values are: $N = 0$ N, $k_f = 1 \times 10^8$ N/m^2 and $\nu_f = 1 \times 10^4$ Ns/m^2.

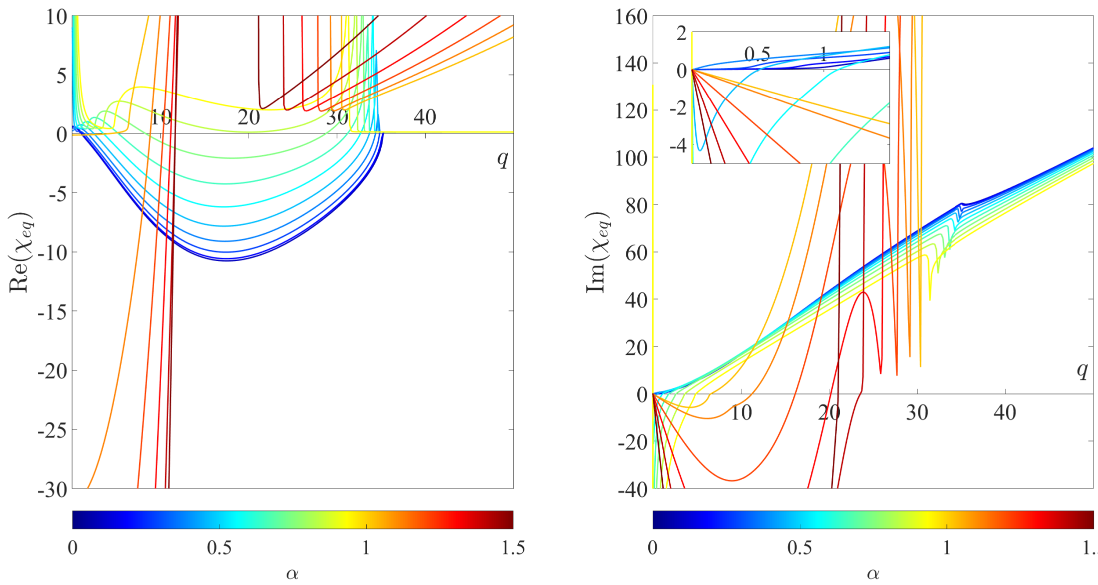

Figure 2.2: The real and imaginary part of the equivalent stiffness of the Timoshenko beam on visco-elastic foundation along which a point mass moves with constant velocity. The stiffness is a function of the point mass's vibratory frequency q and is plotted for a range of velocity values α. The used parameter values are: $N = 0$ N, $k_f = 1 \times 10^8$ N/m^2 and $\nu_f = 1 \times 10^4$ Ns/m^2.

Once the first resonance frequency q_1 is exceeded—the resonance amplitude is made finite by the presence of foundation damping which also slightly decreases the associated frequency; cf. the amplitude-frequency characteristic (also known as the *frequency-response function*) of an undamped and damped SDoF system—the equivalent oscillator behaves visco-inertial ($\mathrm{Re}(\chi_{eq}) < 0$ and $\mathrm{Im}(\chi_{eq}) > 0$); in addition to the foundation damping, two propagating waves extract energy from the oscillating point mass. This explains the increase in the imaginary part of the equivalent stiffness of both beam models. For the Euler-Bernoulli beam though, no qualitative change of motion can be observed beyond q_1. In contrast, the Timoshenko model does show a change once its second resonance frequency q_2 is reached. The fact that around this frequency the real part vanishes—which also holds for the first cut-off frequency—is no surprise; resonance causes a significant amplification of the system's response, which renders its stiffness virtually empty. After all, fundamentally, stiffness is defined as the ratio between excitation and response: $\lim_{w\to\infty} k = F/w = 0$. The real part remains zero beyond q_2 due to the fact that within this frequency band only propagating waves are excited; four in total—the horizontal kinematic invariant intersects both the first and second branch of Timoshenko's dispersion relation twice. See also the magenta colored panel in Fig. (2.6). Thus, for the frequency range $q > q_2$, the Timoshenko beam behaves purely viscous at the contact point: $\mathrm{Re}(\chi_{eq}) = 0$ and $\mathrm{Im}(\chi_{eq}) > 0$.

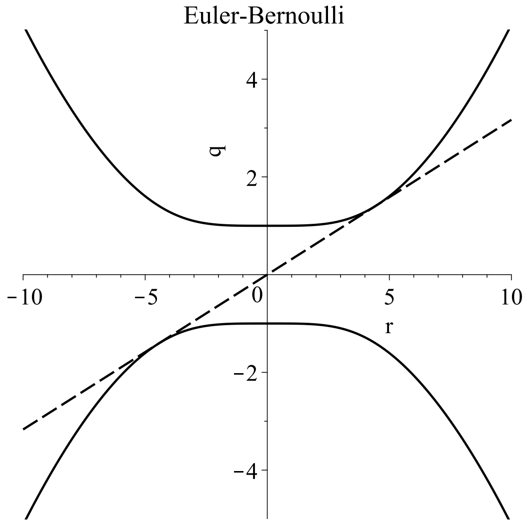

Figure 2.3: The positive and negative dispersion curves of the Euler-Bernoulli beam on elastic foundation (solid lines) and the kinematic invariant indicating the minimum phase velocity (dashed line) for $N = 0$ N and $k_f = 1 \times 10^8$ N/m^2.

Finally, the more relevant case of the moving point mass ($\alpha > 0$) is considered. Once the excitation source starts moving uniformly along the elastic guide, the kinematic invariant in the dispersion plane rotates; the slope of which indicates the vehicle's velocity. See the dashed lines in Fig. (2.3) and Fig. (2.4). The kinematic invariant is then defined as:

$$q = Q + r\alpha \tag{2.8}$$

in which q is the angular frequency of the excited wave, r is the wavenumber, α the vehicle's velocity and Q the excitation frequency. This latter quantity is indicated in the dispersion plane by the intersection between the kinematic invariant and the vertical axis. As for the stationary situation, propagating waves are generated once the invariant crosses the dispersion curve while resonance occurs in case they are tangent to one another.

Returning to Fig. (2.1) and Fig. (2.2), for both beam models, the imaginary part of the equivalent stiffness drops below zero between $0.3 < \alpha < 0.4$; see the inset plot in the figures; the velocity starts at zero and increases with steps of 0.1. This negative damping destabilizes the system and is caused by the excitation of anomalous Doppler waves, which are generated once the vehicle's velocity is greater than the minimum phase velocity [13, 22]. See the dashed lines in Fig. (2.3) and Fig. (2.4). More specifically, from reference [13] it is known that intersection between the kinematic invariant and the dispersion curve in the lower half of the dispersion plane indicates the excitation of the anomalous Doppler waves. This explains why negative damping ($\mathrm{Im}(\chi_{eq}) < 0$) occurs in the lower range of q; for an increasingly smaller α-value, Q ought to be reduced in order to let the kinematic invariant cross the lower dispersion curve. Note that along the horizontal axis of Fig. (2.1) and Fig. (2.2) the stationary case is implied: $q = Q$.

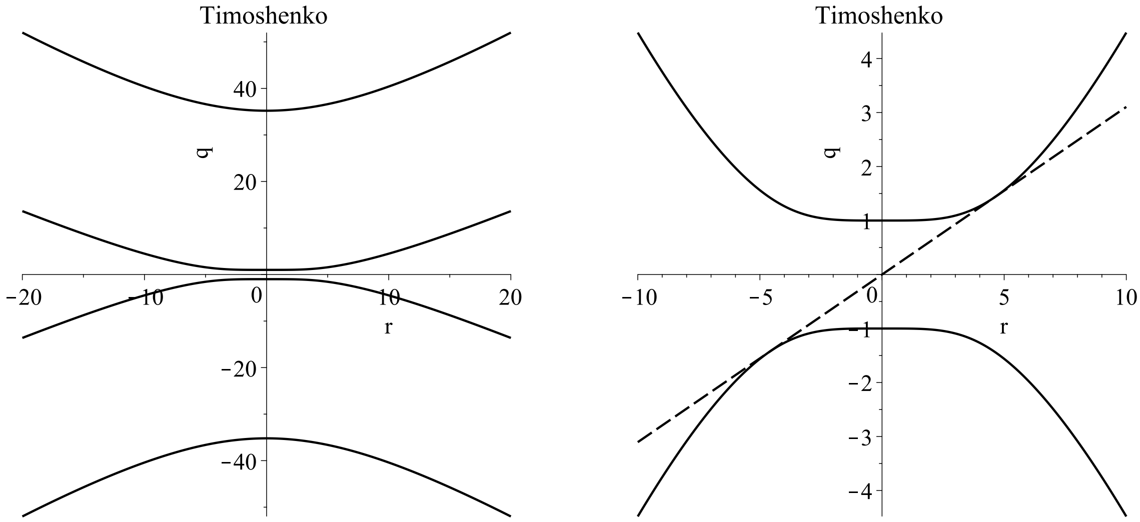

Figure 2.4: The positive and negative dispersion curves of the Timoshenko beam on elastic foundation (solid lines) and the kinematic invariant indicating the minimum phase velocity (dashed line) for $N = 0$ N and $k_f = 1 \times 10^8$ N/m^2.

2.3 Types of beam motion

Instead of solving the relation that describes the curves in Fig. (2.3) and Fig. (2.4) with respect to the angular frequency q, the dispersion relation is solved with respect to the wavenumber r, which allows to graphically present this relation in a way that provides more insight into the beam's motion. For the Euler-Bernoulli model, three cases can be distinguished, depending on the excitation frequency. See the colored panels in Fig. (2.5). The red panel indicates the situation in which the excitation frequency is below the cut-off frequency (the green panel), while the blue panel is positioned above this threshold value. Note that these panels can be interpreted as two-dimensional representations of the kinematic invariant for which the vehicle velocity is equated to zero. To gain insight into the beam's motion associated with each panel, the four types of wavenumbers are to be substituted in the following waveform:

$$W(y, \tau) = \tilde{W} e^{i(q\tau - ry)} \tag{2.9}$$

The wavenumber r can be real, imaginary, complex or zero. Substituting each case in Eq. (2.9) yields the following four types of beam motion.

$r = 0$:

$$W(\tau) = \tilde{W} e^{iq\tau} \tag{2.10}$$

This motion shows no variation with respect to the spatial coordinate y, it only dependence on the time coordinate τ; indicating rigid vibrations as those of an SDoF system.

$r = \pm r$:

$$\begin{aligned} W(y,\tau) &= \tilde{W} e^{i(q\tau - ry)} \\ W(y,\tau) &= \tilde{W} e^{i(q\tau + ry)} \end{aligned} \tag{2.11}$$

Harmonic waves with constant amplitude travel through the beam in the positive and negative y-direction.

$r = \pm ir$:

$$\begin{aligned} W(y,\tau) &= \tilde{W} e^{ry} e^{iq\tau} \\ W(y,\tau) &= \tilde{W} e^{-ry} e^{iq\tau} \end{aligned} \tag{2.12}$$

The beam exhibits vibrations that decay exponentially with increasing distance from the excitation source. The first equation expresses the vibration of the left beam domain while the second expresses the right beam domain's deflection.

$r = \pm r_{\mathrm{Re}} \pm i r_{\mathrm{Im}}$:

$$\begin{aligned} W(y,\tau) &= \tilde{W} e^{r_{\mathrm{Im}} y} e^{i(q\tau - r_{\mathrm{Re}} y)} \\ W(y,\tau) &= \tilde{W} e^{-r_{\mathrm{Im}} y} e^{i(q\tau - r_{\mathrm{Re}} y)} \\ W(y,\tau) &= \tilde{W} e^{r_{\mathrm{Im}} y} e^{i(q\tau + r_{\mathrm{Re}} y)} \\ W(y,\tau) &= \tilde{W} e^{-r_{\mathrm{Im}} y} e^{i(q\tau + r_{\mathrm{Re}} y)} \end{aligned} \tag{2.13}$$

Harmonic waves of which the amplitude decays exponentially with increasing distance from the excitation source; commonly referred to as *evanescent waves* [8]. The first and third equation apply to the left beam domain while the second and fourth apply to the right domain.

Returning to the dispersion curves presented in Fig. (2.5), we are now able to see which motions are generated in the Euler-Bernoulli beam depending on the excitation frequency. Below the cut-off frequency four propagating waves with attenuating amplitude are excited. At the level of the green panel, the stationary vehicle makes the system vibrate rigidly. This complies with the observation made in the previous section: tangency between the kinematic invariant and the dispersion curve indicates the vehicle velocity to be equal to the group velocity of the dispersed waves, which implies that energy does not propagate away from the excitation source, but instead, accumulates at the contact point, which in turn leads to resonance. The foundation damping then limits the linearly increasing amplitude. As a third possibility, excitation above the cut-off frequency yields yet another motion picture: propagating waves with constant amplitude as well as vibrations that decay exponentially with increasing distance from the excitation source.

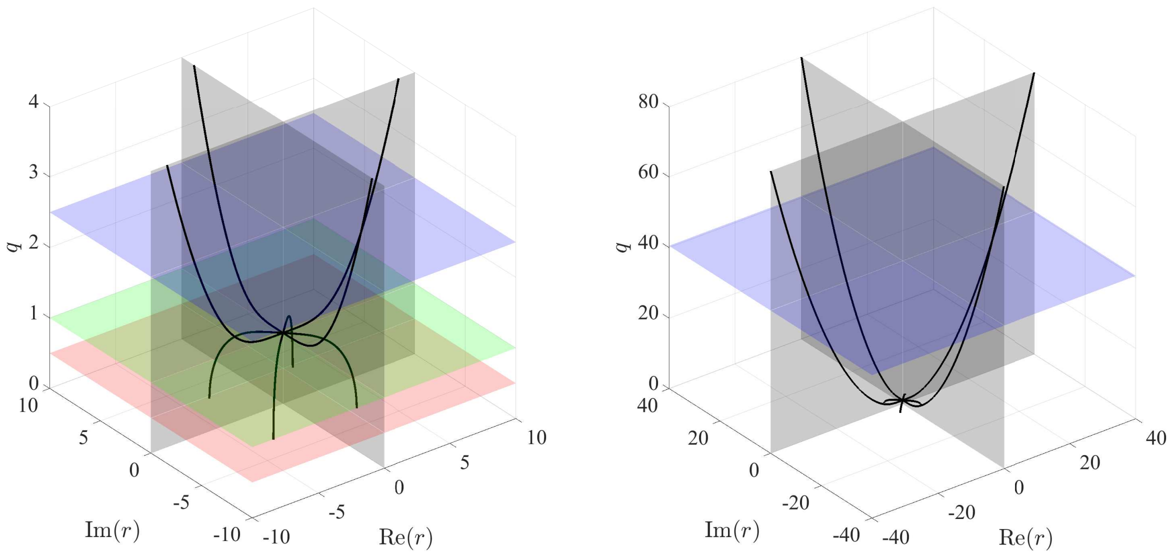

Figure 2.5: An alternative graphical depiction of the dispersion relation for the Euler-Bernoulli beam on elastic foundation for $N = 0$ N and $k_f = 1 \times 10^8$ N/m^2. The colored panels indicate qualitatively different beam motions depending on the angular frequency of the excitation source.

Further elevation of the angular frequency q presents no qualitative change of the motion of the Euler-Bernoulli beam. However, in Timoshenko's case, two other combinations of beam motions appear. At the level of the cyan colored panel at the right of Fig. (2.6), Timoshenko's beam will be subjected to rigid vibrations and simultaneously exhibit harmonic waves with constant amplitude. Increasing q again leads to the dispersion of propagating waves only; that is, harmonic waves with constant amplitude; cf. Eq. (2.11).

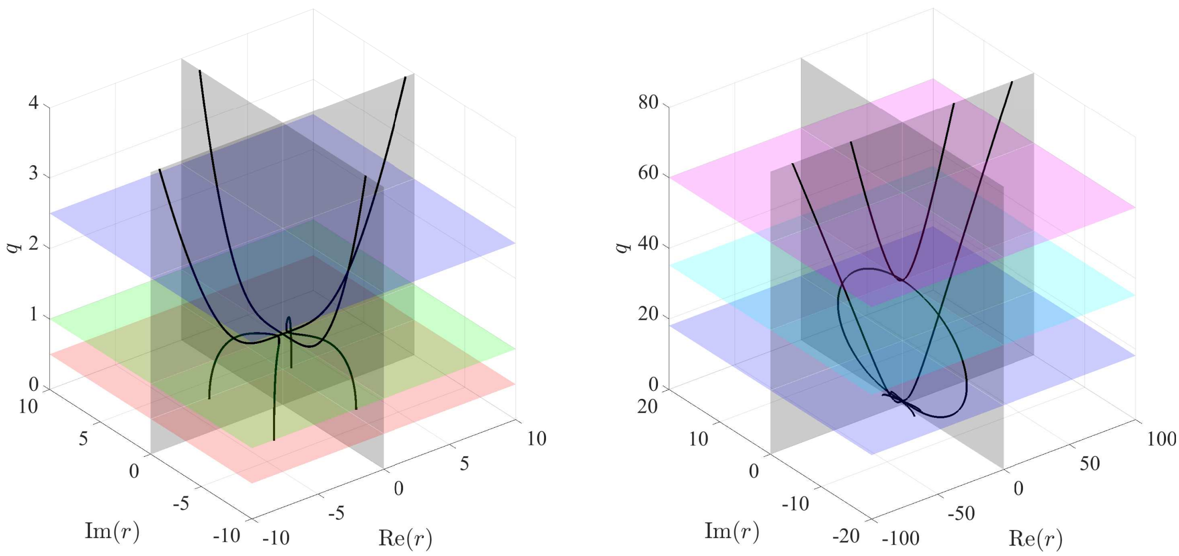

Figure 2.6: An alternative graphical depiction of the dispersion relation for the Timoshenko beam on elastic foundation for $N = 0$ N and $k_f = 1 \times 10^8$ N/m^2. The colored panels indicate qualitatively different beam motions depending on the angular frequency of the excitation source.

	$q < q_1$	$q = q_1$	$q_1 < q < q_2$	$q = q_2$	$q > q_2$
EB	$r = \pm r_{\mathrm{Re}} \pm i r_{\mathrm{Im}}$	$r = 0$	$r = \pm r,\ \pm ir$		
Timo	$r = \pm r_{\mathrm{Re}} \pm i r_{\mathrm{Im}}$	$r = 0$	$r = \pm r_{\mathrm{Re}},\ \pm i r_{\mathrm{Im}}$	$r = 0,\ \pm r$	$r = \pm r_1,\ \pm r_2$

Table 2.3: Types of beam motion dependent on the angular frequency of the excitation source q. The first and second cut-off frequencies are denoted by q_1 respectively q_2.

2.4 Parameter study of the instability domain

In this last section the instability domains of both beam models are presented. How they are derived is explained in the next chapter; the objective here is to simply point out how they are to be interpreted and to see how they are affected by changing parameters that can show significant variability in the field.

The areas enclosed at the right of the curves plotted in Fig. (2.7) to Fig. (2.9) designate combinations of mass and velocity that lead to instability, while areas at the left of the straight vertical lines express unconditional stability; no matter the magnitude of the point mass, the system's vibrations will not start growing exponentially with time. Once the minimum phase velocity is exceeded, the value of the concentrated mass must be limited in order to preserve stability; the greater the velocity, the more the mass's valuation ought to be restricted.

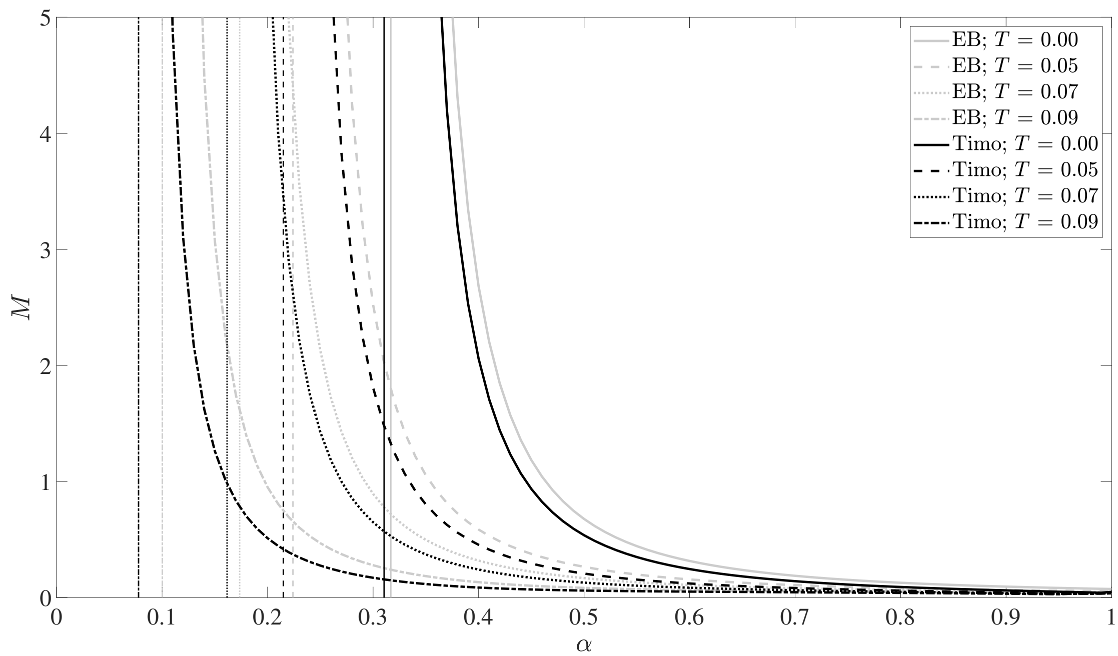

Figure 2.7: Instability domain of the Euler-Bernoulli model (grey curves) and Timoshenko model (black curves) for different axial forces and for $k_f = 1 \times 10^8\ \mathrm{N\,m^{-2}}$ and $\nu_f = 1 \times 10^4\ \mathrm{N\,s\,m^{-2}}$. The minimum phase velocities are indicated by the corresponding vertical lines.[2]

T [-]	Euler-Bernoulli	Timoshenko
0	0.317	0.310
0.05	0.224	0.215
0.07	0.174	0.162
0.09	0.100	0.078

Table 2.4: Minimum phase velocity for different axial forces.[2]

Looking at the effect of axial forcing presented in Fig. (2.7), both the Euler-Bernoulli and Timoshenko model return an instability domain that shifts leftward with increasing compression force. This implies a more critical, a more dangerous situation that is prone to instability. It also complies with physical intuition; after all, axial compression ultimately leads to buckling (static instability). As to the difference between the beam models, it appears Timoshenko retreats more rapidly towards the left with increasing T relative to Euler-Bernoulli's beam. The fact that the latter beam model presents a higher critical velocity is caused by the infinite shear stiffness it exhibits; characteristic of Timoshenko's beam is that it accounts for the deformation associated with shear forcing and therefore is by its very nature more flexible. See also Fig. (2.8).

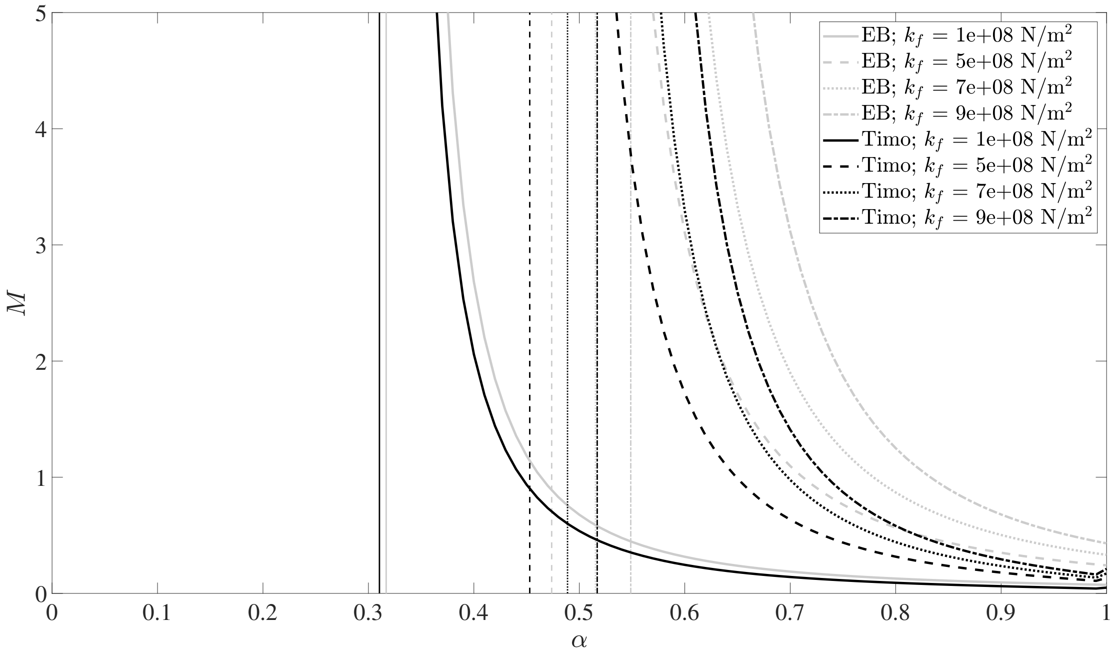

Figure 2.8: Instability domain of the Euler-Bernoulli model (grey curves) and Timoshenko model (black curves) for different foundation stiffnesses and for $T = 0$ and $\nu_f = 1 \times 10^4\ \mathrm{N\,s\,m^{-2}}$. The minimum phase velocities are indicated by the corresponding vertical lines.[2]

[2]The actual minimum phase velocities are greater, because their current valuation is based on an elastic foundation model, which excludes damping.

k_f [N m^{-2}]	Euler-Bernoulli	Timoshenko
1×10^8	0.317	0.310
5×10^8	0.474	0.453
7×10^8	0.515	0.489
9×10^8	0.549	0.517

Table 2.5: Minimum phase velocity for different stiffness values.[2]

Considering the effect of the foundation parameters, Fig. (2.8) and Fig. (2.9) reveal that both the foundation's elasticity and viscosity have an oppressive effect on the instability; increasing either or both parameters leads to a rightward shift of the instability domain. Here as well, Timoshenko's model increasingly lags behind Euler-Bernoulli due to the difference in shear stiffness. In an overall sense, it is thus fair to conclude that added stiffness and/or viscosity—whether this is incorporated in the beam or foundation—leads to a more favourable, a safer situation with a higher critical velocity that marks the onset of conditional stability.

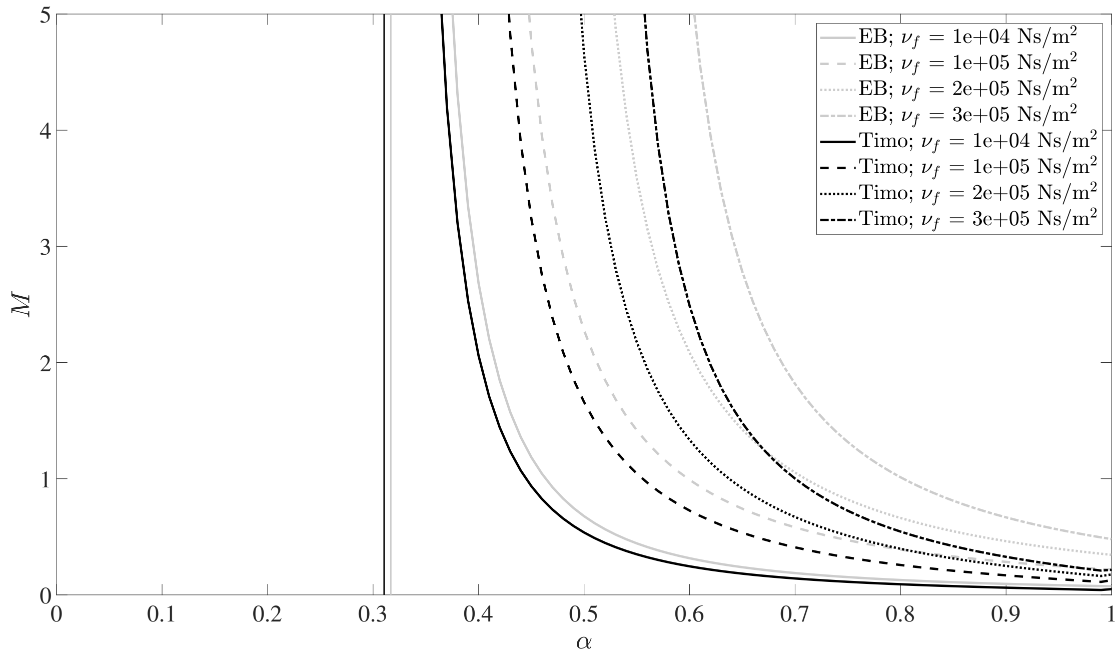

Figure 2.9: Instability domain of the Euler-Bernoulli model (grey curves) and Timoshenko model (black curves) for different foundation viscosities and for $T = 0$ and $k_f = 1 \times 10^8$ N m^{-2}.

To conclude, even though for classical railway applications the height-length ratio of the beam is sufficiently small such that the effect of shearing may be neglected, in the Hyperloop case this assumption no longer applies given the large diameter of the tube through which the pod moves. Regardless, throughout the continuation of this report the Euler-Bernoulli beam is employed to model the guiding system. This simplification is justified by the fact that this project has been research of an exploratory kind which necessitates follow-up research that should be focused on obtaining more accurate results.

Chapter 3

Wave-induced instability of an oscillator moving uniformly along an infinite Euler-Bernoulli beam on homogeneous foundation

The article of Metrikine & Dieterman [15] is revisited; the equivalent oscillator's characteristic equation is derived with more detail, but without the use of a dimensionless formulation and excluding axial forcing. Furthermore, a spring between the point mass and the beam is included, which allows to investigate the effect of vehicle-structure interaction on the instability domain's boundary; the characteristic equation is adapted accordingly, after which the D-decomposition method is used to determine this boundary.

3.1 Derivation of the characteristic equation

The model that is used to derive the characteristic equation is presented in Fig. (3.1); a point mass that moves with constant velocity along an infinite Euler-Bernoulli beam on a homogeneous visco-elastic foundation.

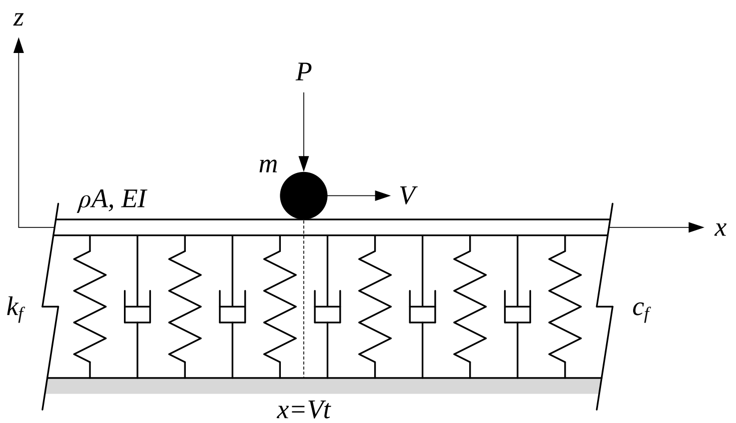

Figure 3.1: The model for investigating wave-induced instability of a point mass that moves along an elastic guide on homogeneous visco-elastic support.

The equation of motion that describes the beam's deflection is given as:

$$\begin{aligned}&\rho A\frac{\partial^2 w}{\partial t^2}(x,t)+EI\frac{\partial^4 w}{\partial x^4}(x,t)+c_f\frac{\partial w}{\partial t}(x,t)+k_f w(x,t)=\\&-\left(m\frac{d^2 w_0}{dt^2}(t)+P\right)\delta(x-Vt)\end{aligned}\tag{3.1}$$

in which $w(x,t)$ and $w_0(t)$ are the vertical deflections of the beam and mass respectively [m], ρA and EI represent the beam's distributed mass [kg m^{-1}] respectively the beam's bending stiffness [N m^2], the distributed foundation viscosity and distributed foundation stiffness are denoted by c_f [N s m^{-2}] and k_f [N m^{-2}] respectively, m is the vehicle's mass [kg], V is the vehicle's velocity [m s^{-1}], P denotes constant vertical forcing exerted on the vehicle [N] and $\delta(\ldots)$ represents Dirac's delta function [m^{-1}]. The displacement of the point mass is dictated by the continuity condition:

$$w_0(t)=w(x=Vt,t)\tag{3.2}$$

Introducing the position coordinate that follows the moving mass along the beam:

$$\xi=x-Vt\tag{3.3}$$

and replacing x by ξ in the argument of the deflection function, gives:

$$w(x,t)\Rightarrow w(\xi(x,t),t)\tag{3.4}$$

The time and space derivatives of this new deflection function are evaluated by applying the chain rule for multivariable functions [21]:

$$\frac{\partial w}{\partial t}=\frac{\partial w}{\partial \xi}\frac{\partial \xi}{\partial t}+\frac{\partial w}{\partial t}\frac{dt}{dt}=-\frac{\partial w}{\partial \xi}V+\frac{\partial w}{\partial t}\Rightarrow\frac{\partial^n w}{\partial t^n}=\left(-\frac{\partial}{\partial \xi}V+\frac{\partial}{\partial t}\right)^n w\tag{3.5}$$

$$\frac{\partial w}{\partial x}=\frac{\partial w}{\partial \xi}\frac{\partial \xi}{\partial x}=\frac{\partial w}{\partial \xi}\Rightarrow\frac{\partial^n w}{\partial x^n}=\frac{\partial^n w}{\partial \xi^n}\tag{3.6}$$

Substitution of Eq. (3.2), Eq. (3.5) and Eq. (3.6) in Eq. (3.1) gives:

$$\begin{aligned}&\rho A\left(-\frac{\partial}{\partial \xi}V+\frac{\partial}{\partial t}\right)^2 w(\xi,t)+EI\frac{\partial^4 w}{\partial \xi^4}(\xi,t)+c_f\left(-\frac{\partial}{\partial \xi}V+\frac{\partial}{\partial t}\right)w(\xi,t)+\\&k_f w(\xi,t)=-\left(m\frac{\partial^2 w}{\partial t^2}(0,t)+P\right)\delta(\xi)\end{aligned}\tag{3.7}$$

To be able to easily solve for $w(\xi,t)$, the equation of motion defined in the moving reference frame is being transformed to the Fourier-Laplace domain. The forward Fourier and Laplace transformations are defined as follows:

$$\mathcal{F}\{w(\xi,t)\}=w_k(k,t)=\int_{-\infty}^{\infty}w(\xi,t)e^{-ik\xi}d\xi\Rightarrow\mathcal{F}\left\{\frac{\partial^n w}{\partial \xi^n}(\xi,t)\right\}=(ik)^n w_k(k,t)\tag{3.8}$$

$$\mathcal{L}\{w(\xi,t)\}=w_s(\xi,s)=\int_{0}^{\infty}w(\xi,t)e^{-st}dt\Rightarrow\mathcal{L}\left\{\frac{\partial^n w}{\partial t^n}(\xi,t)\right\}=s^n w_s(\xi,s)\tag{3.9}$$

Applying Eq. (3.8) and Eq. (3.9) to Eq. (3.7) yields the following algebraic equation:[1]

$$\rho A(s-ikV)^2 w_{k,s} + EIk^4 w_{k,s} + c_f\left(s-ikV\right)w_{k,s} + k_f w_{k,s} = -\left(ms^2 \left.w_s\right|_{\xi=0} + \frac{P}{s}\right) \tag{3.10}$$

In order to find the characteristic equation, Eq. (3.10) is solved for the deflection function:

$$\begin{aligned} w_{k,s} &= -\frac{\left(ms^2 \left.w_s\right|_{\xi=0} + P/s\right)}{D\left(k,s\right)} \\ D\left(k,s\right) &= \rho A(s-ikV)^2 + EIk^4 + c_f\left(s-ikV\right) + k_f \end{aligned} \tag{3.11}$$

whereupon the obtained solution is transformed back to the Laplace domain[2] by applying the inverse Fourier transform:

$$w_s\left(\xi,s\right) = \mathcal{F}^{-1}\left\{w_{k,s}\left(k,s\right)\right\} = -\left(ms^2 \left.w_s\right|_{\xi=0} + P/s\right)\frac{1}{2\pi}\int_{-\infty}^{\infty}\frac{e^{ik\xi}}{D\left(k,s\right)}dk \tag{3.12}$$

The Laplace image of the beam's deflection at the contact point—$\mathcal{L}\left\{w\left(0,t\right)\right\} = w_s(0,s)$—must be defined in order to have a completely determined expression for the beam's deflection in the Laplace domain. In finding an expression for $w_s\left(0,s\right)$, the characteristic equation of the equivalent oscillator emerges; substitute $\xi = 0$ in Eq. (3.12) and collect for $w_s\left(0,s\right)$:

$$\begin{aligned} & w_s\left(0,s\right) = -\left(ms^2 \left.w_s\right|_{\xi=0} + P/s\right)\frac{1}{2\pi}\int_{-\infty}^{\infty}\frac{1}{D\left(k,s\right)}dk \Rightarrow \\ & \left(ms^2 + \chi_{eq}\left(s\right)\right)w_s\left(0,s\right) = -P/s \end{aligned} \tag{3.13}$$

in which:

$$\chi_{eq}\left(s\right) = \left(\frac{1}{2\pi}\int_{-\infty}^{\infty}\frac{1}{D\left(k,s\right)}dk\right)^{-1} \tag{3.14}$$

It is now evident from the SDoF analogy[2] that Eq. (3.13) governs the mass's vertical motion. And since the equivalent oscillator represents this point mass, which moves with constant velocity along the beam on visco-elastic foundation, its characteristic equation can be discerned from Eq. (3.13) once the excitation term is omitted ($P = 0$):

$$ms^2 + \chi_{eq}\left(s\right) = 0 \tag{3.15}$$

[1] The Laplace transformation is applied over time to capture the beam's transient motion, which results from the concentrated mass and the point load being applied to the beam at $t = 0$. After all, using the Fourier transform instead, would suggest that the point mass and constant forcing P have always been in contact with the beam, which is false. See the second term of equation 7 in reference [15].

[2] Compare to the SDoF system. Assuming homogeneous initial conditions, the characteristic equation of the damped SDoF system can be conveniently derived by means of the Laplace transform: $\mathcal{L}\left\{m\ddot{x}\left(t\right) + c\dot{x}\left(t\right) + kx\left(t\right) = 0\right\} \Rightarrow \left(ms^2 + cs + k\right)X\left(s\right) = 0 \Rightarrow s_{1,2} = -n \pm \sqrt{n^2 - \omega_n^2}$, in which $n = c/\left(2m\right)$ and $\omega_n = \sqrt{k/m}$. In linear models, the system's stability is not affected by the initial conditions. The expression for the vibration reads: $x\left(t\right) = \sum_{j=1}^{2} C_j e^{s_j t}$. Assuming sub-critical damping ($n < \omega_n$): $x\left(t\right) = e^{-nt}\left(A\cos\left(\omega_1 t\right) + B\sin\left(\omega_1 t\right)\right)$, in which $\omega_1 = \sqrt{\omega_n^2 - n^2}$. Note how the amplitude increases exponentially with time in case $n < 0$, or, stated differently, in case $\mathrm{Re}(s) > 0$.

in which $\chi_{eq}(s)$ expresses the equivalent stiffness of the foundation-beam system underneath the moving mass; see Chapter 2 on how to interpret this quantity.

The ultimate goal is to determine the equivalent oscillator's natural frequency and since this frequency is governed by the imaginary part of the characteristic exponent, s in characteristic Eq. (3.15) is replaced by $i\omega_n$. In addition, to be able to derive the instability boundary, the D-decomposition method [5] also requires s to be replaced by $i\omega_n$. The updated characteristic equation reads:

$$-m\omega_n^2 + \chi_{eq}(\omega_n) = 0 \tag{3.16}$$

with:

$$\begin{aligned} \chi_{eq}(\omega_n) &= \left(\frac{1}{2\pi} \int\limits_{-\infty}^{\infty} \frac{1}{D(k,\omega_n)} dk \right)^{-1} \\ D(k,\omega_n) &= -\rho A(\omega_n - kV)^2 + EIk^4 + ic_f(\omega_n - kV) + k_f \end{aligned} \tag{3.17}$$

Eq. (3.17) exhibits an improper integral that can be evaluated by means of the *contour integration method* [1]. The first step is to generalize the integrand function by replacing its real argument k by the complex argument z such that k is recovered if $z \in \mathbb{R}$. This procedure is known as *analytic continuation* and it allows to evaluate the integral along a closed contour Γ (a loop) in the complex z-plane:

$$\oint_\Gamma \frac{1}{D(z,\omega_n)} dz \tag{3.18}$$

In [15] the choice is made to close the contour in the upper half-plane, counter-clockwise. The loop integral then decomposes into:

$$\oint_\Gamma \frac{1}{D(z,\omega_n)} dz = \int\limits_{-\infty}^{\infty} \frac{1}{D(k,\omega_n)} dk + \int_{arc} \frac{1}{D(z,\omega_n)} dz \tag{3.19}$$

The left-hand side can be evaluated by making use of the *residue theory* [1]:

$$\oint_\Gamma \frac{1}{D(z,\omega_n)} dz = 2\pi i \sum_{j=1}^{2} \mathrm{Res} \left[\frac{1}{D(z,\omega_n)} \right]_{z=z_j} \tag{3.20}$$

in which the residue of the generalized integrand can be computed as [1]:

$$\mathrm{Res} \left[\frac{1}{D(z,\omega_n)} \right] = \left(\frac{\partial D}{\partial z}(z,\omega_n) \right)^{-1} \tag{3.21}$$

The argument values for which the integrand function is non-analytic (singular) are denoted by z_j and are referred to as the *poles* of the integrand. These poles are actually the roots of the polynomial $D(z,\omega_n) = 0$ in z; that is, the wavenumbers that satisfy the dispersion relation in Eq. (3.17). Note that Eq. (3.20) should exhibit a minus sign on the right-hand side in case the contour is closed clockwise instead of anticlockwise. As for the second term on the right-hand side of Eq. (3.19), the integral evaluates to zero because of the arc's radius going to infinity [1]. Consequently, the original integral can be expressed as:

$$\int_{-\infty}^{\infty} \frac{1}{D\left(k,\omega_n\right)} dk = 2\pi i \sum_{j=1}^{2} \left(\frac{\partial D}{\partial k}\left(k,\omega_n\right)\right)^{-1}_{k=k_j} \tag{3.22}$$

and the equivalent stiffness as:

$$\chi_{eq}\left(\omega_n\right) = \left(i \sum_{j=1}^{2} \left(\frac{\partial D}{\partial k}\left(k,\omega_n\right)\right)^{-1}_{k=k_j} \right)^{-1} \tag{3.23}$$

Only poles k_j that possess a positive imaginary part are of interest because of the choice to close the contour in the upper half of the complex k-plane. And since the dispersion relation $D(k,\omega_n)$ is a polynomial of the fourth order in k, two of the four wavenumber roots are mirrored in the real axis; they appear as each other's complex conjugates. Therefore the summation counter in Eq. (3.23) runs from 1 to 2.

3.2 Augmenting the characteristic equation

The model is extended by including a spring with constant stiffness k_{con} at the contact point between the moving point mass and the beam. This updated equivalent oscillator is depicted in Fig. (3.2). Note that Eq. (3.2) is now no longer valid.

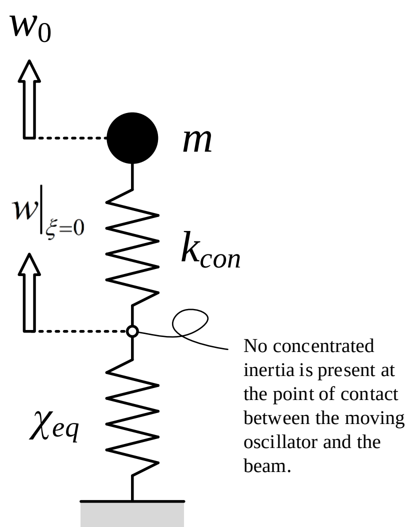

Figure 3.2: The equivalent oscillator with contact spring.

Newton's second law of motion is transformed to the Laplace domain so as to be able to find the characteristic equation associated with the new oscillator:

$$\mathcal{L}\left\{F_{net} = m\ddot{w}_0\left(t\right)\right\} \Rightarrow F_{net} = ms^2 w_0\left(s\right) \tag{3.24}$$

The displacement method is applied in the Laplace domain to find the net force acting at each degree-of-freedom:

$$\begin{aligned} -k_{con}w_0\left(s\right) + k_{con}w\left(0,s\right) &= ms^2 w_0\left(s\right) \\ k_{con}w_0\left(s\right) - k_{con}w\left(0,s\right) - \chi_{eq}\left(s\right)w\left(0,s\right) &= 0 \end{aligned} \tag{3.25}$$

Note that no concentrated inertia is present at the contact point. Putting Eq. (3.25) in vector-matrix format:

$$\begin{bmatrix} ms^2 + k_{con} & -k_{con} \\ -k_{con} & k_{con} + \chi_{eq}(s) \end{bmatrix} \begin{bmatrix} w_0(s) \\ w(0,s) \end{bmatrix} = \begin{bmatrix} 0 \\ 0 \end{bmatrix} \tag{3.26}$$

and letting the determinant of the coefficient matrix vanish while replacing the Laplace parameter s by $i\omega_n$ yields the augmented characteristic equation:

$$-m\omega_n^2 + \frac{k_{con}\chi_{eq}(\omega_n)}{k_{con} + \chi_{eq}(\omega_n)} = 0 \tag{3.27}$$

in which the equivalent spring stiffness $\chi_{eq}(\omega_n)$ is defined by Eq. (3.23). Note that the second term on the left-hand side of Eq. (3.27) is in fact the expression for the equivalent stiffness of two springs connected in series:

$$k_{eq} = \left(\frac{1}{k_1} + \frac{1}{k_2}\right)^{-1} = \left(\frac{k_1 + k_2}{k_1 k_2}\right)^{-1} = \frac{k_1 k_2}{k_1 + k_2} \tag{3.28}$$

as expected when looking at Fig. (3.2).

3.3 The instability domain

The D-decomposition method [5] is employed to determine the instability domain and investigate how its boundary is affected by the interaction between the vehicle and the beam. To this end, the mapping rule with respect to the point mass is defined; solving Eq. (3.27) for m gives:

$$\begin{aligned} m &= \frac{\chi'(\omega_n)}{\omega_n^2} \\ \chi'(\omega_n) &= \frac{k_{con}\chi_{eq}(\omega_n)}{k_{con} + \chi_{eq}(\omega_n)} \end{aligned} \tag{3.29}$$

Note how $\chi_{eq}(\omega_n)$ is recovered from $\chi'(\omega_n)$ for $k_{con} \to \infty$. The adopted parameter values are listed in Tab. (3.1), which are copied from reference [23] for comparison purposes. Note that these parameters have a classical railway application and do not represent the Hyperloop system.

$\rho = 7849\ \mathrm{kg\,m^{-3}}$	$A = 7.687 \times 10^{-3}\ \mathrm{m^2}$	$I = 3.055 \times 10^{-5}\ \mathrm{m^4}$
$E = 2 \times 10^{11}\ \mathrm{N\,m^{-2}}$	$k_f = 1 \times 10^{8}\ \mathrm{N\,m^{-2}}$	$c_f = 10\ \mathrm{N\,s\,m^{-2}}$

Table 3.1: Parameter set for computing the instability domain's boundary and calculating the minimum phase velocity.

Because the instability domain for (combination) parametric resonance is computed for $c_f = 0\ \mathrm{N\,s\,m^{-2}}$ in Chapter 5 to 7, one might wonder why in this chapter, for the case of wave-induced instability, $c_f > 0\ \mathrm{N\,s\,m^{-2}}$ is considered. The reason is that one of the two poles k_j in Eq. (3.23) becomes real when $V > V_{ph}^{min}$, see Fig. (5.2); the adopted contour does not account for this and Eq. (3.23) would return an incorrect valuation of the equivalent stiffness. Adding a small amount of damping resolves this issue, since the real root then becomes complex again with a small imaginary part; making the evaluated integral, from a numerical point of view, an approximation of the actual integral that needs to be calculated. Another explanation is that the absence of damping would render the D-decomposition useless; the root s of the equivalent oscillator's characteristic Eq. (3.15) would no longer possess a real part,[2] which is a problem when trying to determine the critical mass by means of the D-decomposition method [15].

The instability domain is presented in Fig. (3.3). It is clearly shown that the critical mass—beyond which the motion is unstable—decreases with increasing velocity. The physical explanation for this is that instability can only occur if anomalous Doppler waves are radiated by the moving mass. As the moving mass on the beam has its natural frequency, the real part of the latter should be small enough in order to excite the anomalous waves; otherwise, the kinematic invariant line will not cross the negative-frequency branch of the dispersion curve [13]. See Fig. (3.4). And the smaller the velocity, the smaller should be this frequency. That is why one needs larger mass at smaller velocities and smaller mass at larger velocities. It also explains why the critical mass decreases with decreasing spring stiffness k_{con}.

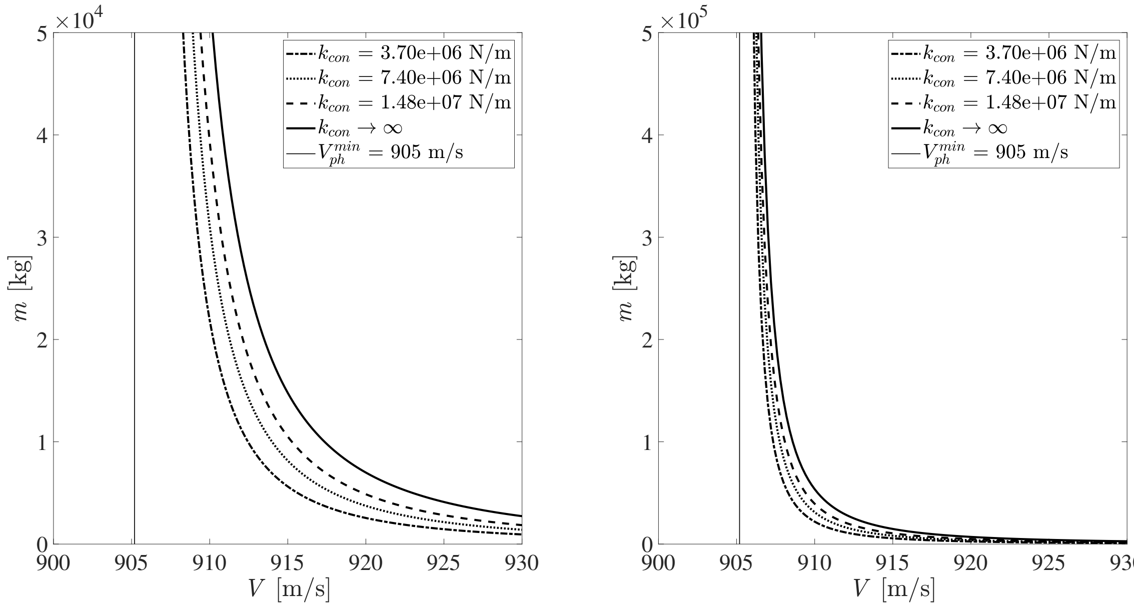

Figure 3.3: The effect of vehicle-structure interaction on the boundary of the instability domain.

For $c_f \to 0$, the curves in Fig. (3.3) converge towards the vertical line, which indicates the minimum phase velocity [15]. See Fig. (3.4). In reference [15] as well as Chapter 2 it is shown that the instability boundary shifts to lower velocity-mass values when the foundation stiffness and foundation damping are decreased. A similar effect now seems to be observed in Fig. (3.3) when the stiffness of the contact spring is reduced. However, this is not the case. In fact, the vertical asymptot towards which the curve converges for $m \to \infty$ does not shift to the left with decreasing k_{con}; only the critical mass decreases.

Note that the aforementioned asymptot does not refer to the vertical line in Fig. (3.3): $V_{asymp} > V_{ph}^{min}$ if $c_f > 0$.

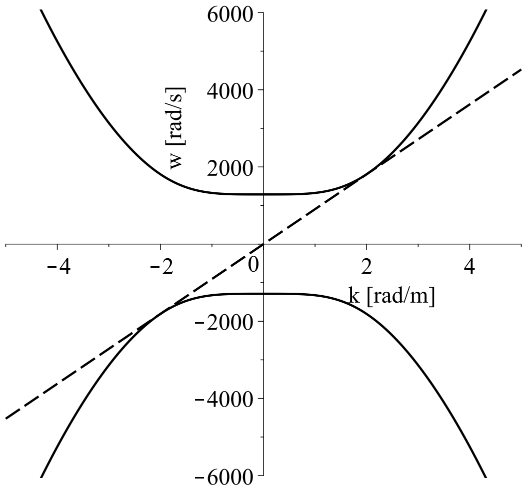

Figure 3.4: Dispersion curves for flexural waves in the Euler-Bernoulli beam on homogeneous elastic foundation. The dashed line represents the kinematic invariant and its slope designates the minimum phase velocity ($V_{ph}^{min} = 905$ m/s). See section 5.2.

Characteristic Eq. (3.16) and Eq. (3.27) are employed in Chapter 5 respectively Chapter 6 to investigate parametric instability of the moving point mass respectively the moving oscillator. For this form of instability as well, the oscillator model allows to study the effect of vehicle-structure interaction on the instability domain.

Chapter 4

Mathieu's equation and parametric resonance

Before we build on the models from Chapter 3 to investigate the instability phenomenon known as *parametric resonance*, this intermediate chapter offers an introduction to this form of instability by means of two elementary SDoF models. Parametric resonance is a form of instability that occurs in dynamic systems exhibiting time- and/or space-dependent parameters. The two models considered below are an oscillator of which the spring stiffness varies harmonically with time and a pendulum of which the distance between the fulcrum and concentrated mass is subjected to periodic shortening and lengthening.

4.1 The first instability domain

The two considered parametric SDoF systems are depicted in Fig. (4.1).

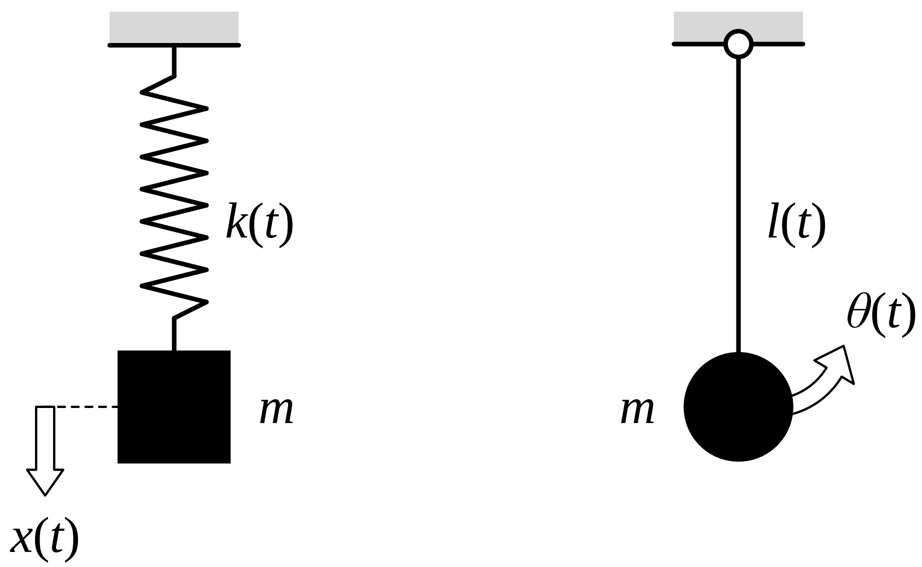

Figure 4.1: An oscillator with a time-dependent spring stiffness (l) and a pendulum with a varying suspension length (r).

The motion of an SDoF system with a time-varying parameter that does not exhibit damping and is without any source of external excitation can be described by a homogeneous ODE with a time-dependent coefficient. For the oscillator, this differential equation reads:

$$m\ddot{x} + k\left(t\right)x = 0 \tag{4.1}$$

The choice is made to let the spring stiffness vary harmonically with time, with small amplitude μk_0 around a non-zero equilibrium value k_0 and with frequency ω_p:

$$k\left(t\right) = k_0\left(1 + \mu\cos\left(\omega_p t\right)\right) \tag{4.2}$$

Dividing Eq. (4.1) by the mass m makes the system's natural or eigenfrequency follow the same time signature as the spring stiffness. The resulting equation is referred to as *Mathieu's equation*:

$$\ddot{x} + \omega_0^2\left(1 + \mu\cos\left(\omega_p t\right)\right)x = 0 \tag{4.3}$$

with $\omega_0 = \sqrt{k_0/m}$ being the natural frequency of the non-parametric system; that is, the oscillator whose spring stiffness does not dependent on time. Mathieu's equation can also be derived for the pendulum. Starting from the equation that governs its motion ($\theta \ll 1$):

$$l\left(t\right)\ddot{\theta} + g\theta = 0 \tag{4.4}$$

and assigning the same time function to the changing length:

$$l\left(t\right) = l_0\left(1 + \mu\cos\left(\omega_p t\right)\right) \tag{4.5}$$

gives:

$$\ddot{\theta} + \omega_0^2\left(1 + \mu\cos\left(\omega_p t\right)\right)^{-1}\theta = 0 \tag{4.6}$$

with $\omega_0 = \sqrt{g/l_0}$. Since the amplitude of the varying length is small ($\mu \ll 1$), the time-dependent coefficient in front of the second term on the left-hand side of Eq. (4.6) can be approximated by a first order Taylor polynomial with respect to $\mu\cos(\omega_p t)$; yielding Mathieu's equation once more:

$$\ddot{\theta} + \omega_0^2\left(1 - \mu\cos\left(\omega_p t\right)\right)\theta = 0 \tag{4.7}$$

Eq. (4.3) and Eq. (4.7) can be solved numerically, but it is also possible to propose an analytical solution that approximates the frequency interval that is associated with unstable motion of the system; a type of instability that is able to occur in systems that exhibit time- and/or space-dependent parameters and is referred to as parametric resonance. The condition for parametric resonance according to references [11, 18] is:

$$\omega_p = 2\omega_0/n\ , \quad n \in \mathbb{N}_1 \tag{4.8}$$

As for classical resonance, the excitation frequency needs to coincide with the system's natural frequency by a certain ratio in order for the system's oscillations to grow indefinitely. This becomes clear when Eq. (4.3) is rewritten as: $\ddot{x} + \omega_0^2 x = -\omega_0^2\mu\cos\left(\omega_p t\right)x$; note that the forcing term on the right-hand side is proportional to the system's degree-of-freedom. Also note that for classical resonance the ratio ω_p/ω_0 ought to be 1 while for parametric resonance it is $2/n$.

Aiming to find the first instability domain, $n = 1$, the natural frequency in Eq. (4.8) is perturbed by a small amount $\mu\delta$, after which the updated expression for the frequency of inhomogeneity ω_p is substituted in Mathieu's equation for the oscillator:

$$\ddot{x} + \omega_0^2\left(1 + \mu\cos\left(2\left(\omega_0 + \mu\delta\right)t\right)\right)x = 0 \tag{4.9}$$

Assuming the motion of the parametric oscillator is periodic, the following solution is proposed as a first order approximation:

$$x(t) = a(\mu t)\cos((\omega_0 + \mu\delta)t) + b(\mu t)\sin((\omega_0 + \mu\delta)t) \tag{4.10}$$

in which the coefficients $a(\mu t)$ and $b(\mu t)$ are slowly varying time functions compared to the trigonometric operators. Combining Eq. (4.9) and Eq. (4.10), assuming the functions $a(\mu t)$ and $b(\mu t)$ are described by exponentials—making $d^n a/dt^n$ proportional to $\mu^n a$ and $d^n b/dt^n$ to $\mu^n b$—and collecting terms proportional to μ^1, yields:

$$\begin{aligned}
&-2\dot{a}\omega_0 \sin((\omega_0 + \mu\delta)t) - 2a\omega_0\mu\delta\cos((\omega_0 + \mu\delta)t) + \\
&2\dot{b}\omega_0\cos((\omega_0 + \mu\delta)t) - 2b\omega_0\mu\delta\sin((\omega_0 + \mu\delta)t) + \\
&a\omega_0^2\mu\cos(2(\omega_0 + \mu\delta)t)\cos((\omega_0 + \mu\delta)t) + \\
&b\omega_0^2\mu\cos(2(\omega_0 + \mu\delta)t)\sin((\omega_0 + \mu\delta)t) = 0
\end{aligned} \tag{4.11}$$

Using the following trigonometric identities:

$$\cos\theta\cos\varphi = \frac{\cos(\theta - \varphi) + \cos(\theta + \varphi)}{2} \tag{4.12}$$

$$\cos\theta\sin\varphi = \frac{\sin(\theta + \varphi) - \sin(\theta - \varphi)}{2} \tag{4.13}$$

and omitting terms that exhibit the frequency '$3(\omega_0 + \mu\delta)$', reduces Eq. (4.11) to:

$$\begin{aligned}
&-2\left(\ \dot{a} + b\mu\delta + b\omega_0\mu/4\ \right)\omega_0\sin((\omega_0 + \mu\delta)t) + \\
&\ 2\left(\ \dot{b} - a\mu\delta + a\omega_0\mu/4\ \right)\omega_0\cos((\omega_0 + \mu\delta)t) = 0
\end{aligned} \tag{4.14}$$

In order to satisfy Eq. (4.14), expressions for the slowly varying functions $a(\mu t)$ and $b(\mu t)$ that fulfill the following coupled ODEs need to be derived:

$$\begin{aligned}
&\dot{a} + b(\delta + \omega_0/4\ )\mu = 0 \\
&\dot{b} - a(\delta - \omega_0/4\ )\mu = 0
\end{aligned} \tag{4.15}$$

Combining both gives:

$$\ddot{a} + a(\delta - \omega_0/4\ )(\delta + \omega_0/4\ )\mu^2 = 0 \tag{4.16}$$

which can be solved for a by searching for it in the following form:

$$a(t) = \sum_{n=1}^{2} C_n e^{s_n t} \tag{4.17}$$

Substitution in Eq. (4.16) and requiring the solution to be non-trivial ($C_n \neq 0$) gives the following characteristic equation:

$$s_n^2 + \left(\delta^2 - \omega_0^2/16\ \right)\mu^2 = 0 \tag{4.18}$$

Whatever the type of instability, the mathematical criterion for instability to occur—including parametric resonance—is that one of the characteristic exponents s_n must possess a positive real part; making the amplitude of the oscillations grow exponentially with time; cf. Eq. (4.10) and Eq. (4.17). However, since the second order polynomial of Eq. (4.18) does not include a first order term with respect to s_n—after all, the system is without viscous damping—the criterion simplifies to:[1]

$$s_n^2 > 0 \tag{4.19}$$

or, as follows from Eq. (4.18):

$$\omega_0^2/16 \; - \delta^2 > 0 \tag{4.20}$$

The frequency interval that renders the parametric oscillator unstable can now be derived by solving Eq. (4.20) for δ:

$$-\omega_0/4 \; < \delta < \omega_0/4 \tag{4.21}$$

and substituting this result into the first order perturbation of the first condition for parametric resonance:

$$\omega_p = 2\left(\omega_0 + \mu\delta\right) \tag{4.22}$$

The instability domain can then be presented as:

$$2\omega_0\left(1 - \mu/4\;\right) < \omega_p < 2\omega_0\left(1 + \mu/4\;\right) \tag{4.23}$$

To obtain a more accurate approximation of this interval, the proposed solution ought to include terms with frequencies that differ from $\omega_0 + \mu^q\delta$ by integer multiples of $2(\omega_0 + \mu^q\delta)$ [11]:

$$x\left(t\right) = \sum_{p=1}^{q} a_p\left(\mu^q t\right)\cos\left(\left(2p-1\right)\left(\omega_0 + \mu^q\delta\right)t\right) + b_p\left(\mu^q t\right)\sin\left(\left(2p-1\right)\left(\omega_0 + \mu^q\delta\right)t\right) \tag{4.24}$$

See Appendix A for the second order calculation.

4.2 Energy analysis

Before attempting to determine the coefficient functions $a(\mu t)$ and $b(\mu t)$, a qualitative energy analysis of the pendulum is described. The total mechanical energy of the system consists of a kinetic and potential contribution:

$$\mathcal{E} = \mathcal{K} + \mathcal{P} = \frac{1}{2}ml^2\dot{\theta}^2 + mgl\left(1 - \cos\theta\right) \tag{4.25}$$

Idealized by considering there to be no non-conservative forces at work—friction at the fulcrum is neglected—the total mechanical energy is time-invariant in the non-parametric case[2]; the system's energy content is constant and completely provided by the initial conditions. However, the amount of energy can grow over time by periodically shortening and extending the pendulum's arm by an amount Δl. According to reference [7], the pendulum can be rendered unstable by shortening the arm when the mass is at its lowest point ($\mathcal{K} = \mathcal{K}_{max}, \mathcal{P} = 0$) and extending the arm by the same amount once the mass reaches its highest point ($\mathcal{K} = 0, \mathcal{P} = \mathcal{P}_{max}$); with every cycle more energy is added at $\theta = 0$ than is subtracted at $\theta = \theta_{max}$. After all, at $\theta = \theta_{max}$ the maximum potential

[1] $as^2 + bs + c = 0 \to s_{1,2} = \left(-b \pm \sqrt{b^2 - 4ac}\right)/\left(2a\right) \to$ for $a = 1$ and $b = 0$: $s_{1,2} = \pm\sqrt{-4c}/2 \to c < 0$ for $s_{1,2}$ to be real. To express this condition in terms of the roots, s_n is squared: $s_n^2 = -c \to s_n^2 > 0$.

[2] Refers to the pendulum with constant arm.

energy reduces because of a decrease of the vertical distance between the mass and the horizontal reference line while the kinetic energy remains zero at that instant. And while the kinetic energy reduces at $\theta = 0$ because of a decreasing moment of inertia—$m(l–\Delta l)^2$—the potential energy increases.

In order to obtain fully determined expressions for the slowly varying functions $a(\mu t)$ and $b(\mu t)$, we need to return to Eq. (4.18) and solve it with respect to s_n:

$$s_{1,2} = \pm\mu\sqrt{\omega_0^2/16 \ - \delta^2} \tag{4.26}$$

Substitution in Eq. (4.17) gives:

$$a\left(\mu t\right) = C_1 e^{\mu t\sqrt{\omega_0^2/16\ - \delta^2}} + C_2 e^{-\mu t\sqrt{\omega_0^2/16\ - \delta^2}} \tag{4.27}$$

and by Eq. (4.15), $b(\mu t)$ reads:

$$b\left(\mu t\right) = C_3 e^{\mu t\sqrt{\omega_0^2/16\ - \delta^2}} + C_4 e^{-\mu t\sqrt{\omega_0^2/16\ - \delta^2}} \tag{4.28}$$

with:

$$C_3 = -C_1 \frac{\sqrt{\omega_0^2/16\ - \delta^2}}{\delta + \omega_0/4}, \quad C_4 = C_2 \frac{\sqrt{\omega_0^2/16\ - \delta^2}}{\delta + \omega_0/4} \tag{4.29}$$

The coefficients C_1 and C_2 are determined by the initial conditions $x(t = 0)$ and $dx/dt(t = 0)$. Looking at the format of Eq. (4.27) and Eq. (4.28), it was correct to assume in the derivation of the frequency interval of Eq. (4.23) that the functions $a(\mu t)$ and $b(\mu t)$ are described by exponentials. Interesting to note is that constant coefficients $a(\mu t) = A$ and $b(\mu t) = B$ in Eq. (4.10) are associated with the boundaries of the instability domain; substituting either the lower or upper boundary of δ from Eq. (4.21) in Eq. (4.27) and Eq. (4.28), one can observe these coefficient functions transforming into constant coefficients; making $s_{1,2} = 0$.[3] This notion allows to derive the frequency interval more rapidly; substitution of $a = A$ and $b = B$ in Eq. (4.15) yields the boundaries from Eq. (4.21):

$$\delta = \pm\omega_0/4 \tag{4.30}$$

To demonstrate the effect of the time-varying spring stiffness on the oscillator's motion, the constants C_1 and C_2 are solved for by substituting Eq. (4.27) and Eq. (4.28) in Eq. (4.10) and making use of the following initial conditions:

$$x\left(t = 0\right) = x_0, \quad \dot{x}\left(t = 0\right) = v_0 \tag{4.31}$$

C_1 and C_2 are then found to be defined as:

$$C_1 = \frac{1}{2}x_0 + \frac{8\left(\omega_0/4\ + \delta\right)}{\omega_0\left(\mu - 4\right)\sqrt{\omega_0^2 - 16\delta^2}}v_0 \tag{4.32}$$

$$C_2 = \frac{1}{2}x_0 - \frac{8\left(\omega_0/4\ + \delta\right)}{\omega_0\left(\mu - 4\right)\sqrt{\omega_0^2 - 16\delta^2}}v_0 \tag{4.33}$$

Adopting the parameter set of Tab. (4.1)

[3] $b(\mu t) = B = 0$

$m = 100$ kg	$k_0 = 10\ \mathrm{N\,m^{-1}}$	$\mu = 0.3$	$x_0 = 1$ m	$v_0 = 1\ \mathrm{m\,s^{-1}}$

Table 4.1: Parameter set for plotting the oscillator's displacement and energy content as functions of time.

the expression for the oscillator's displacement from Eq. (4.10) is plotted in Fig. (4.2) for two different δ's; one that lies outside the interval of Eq. (4.21) and one that is at the center of the instability domain.

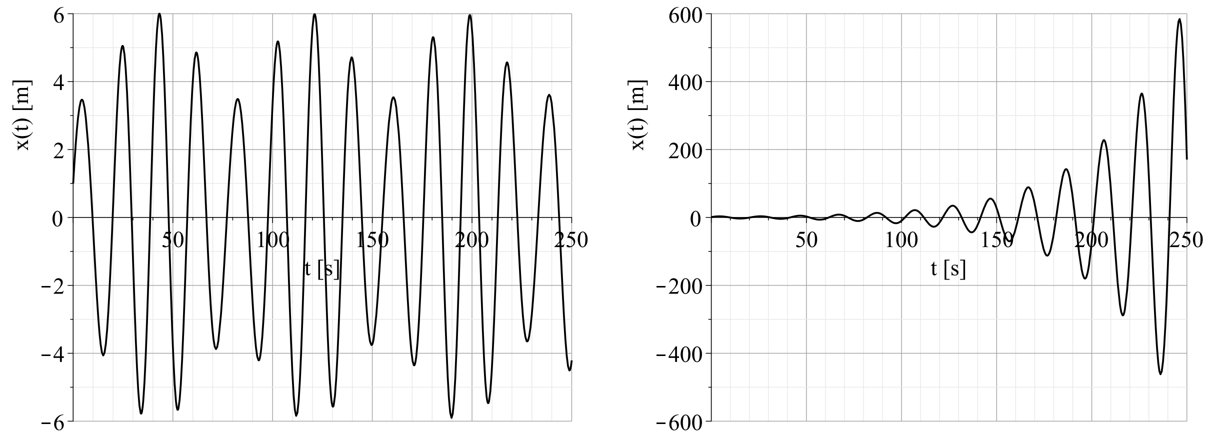

Figure 4.2: Motion of the parametric oscillator for $\delta = \omega_0/2$ (l) and $\delta = 0$ (r).

Another way to demonstrate that the intervals of Eq. (4.21) and Eq. (4.23) are associated with instability is by considering the time dependency of the total mechanical energy of the parametric oscillator. Again, the energy content is composed of a kinetic and potential part:

$$\mathcal{E} = \mathcal{K} + \mathcal{P} = \frac{1}{2}m\dot{x}^2 + \frac{1}{2}k\left(t\right)x^2 \tag{4.34}$$

Substituting Eq. (4.2) and Eq. (4.10) in Eq. (4.34) and using the parameter set of Tab. (4.1), the sum of the kinetic and potential energy can be plotted as is done in Fig. (4.3) and Fig. (4.4) as functions of time for two different δ-values.

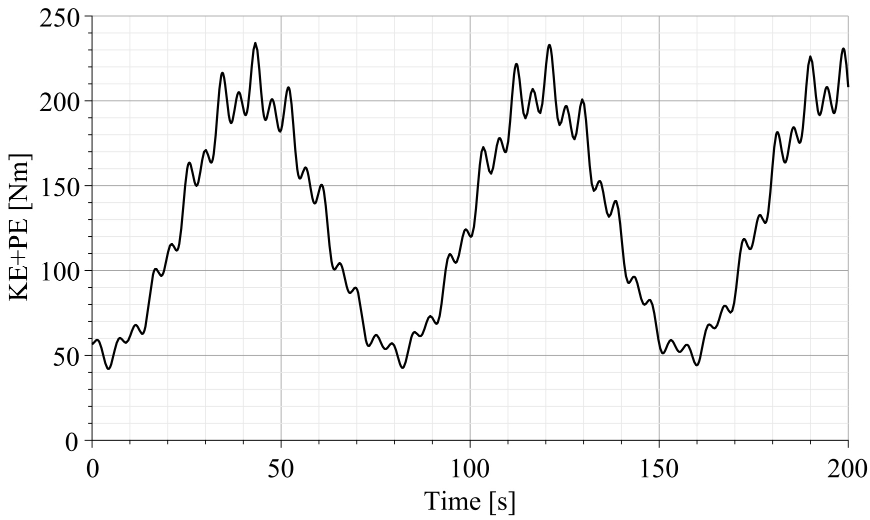

Figure 4.3: Variation of the oscillator's mechanical energy for $\delta = \omega_0/2$ ($\omega_p/\omega_0 = 2.3$).

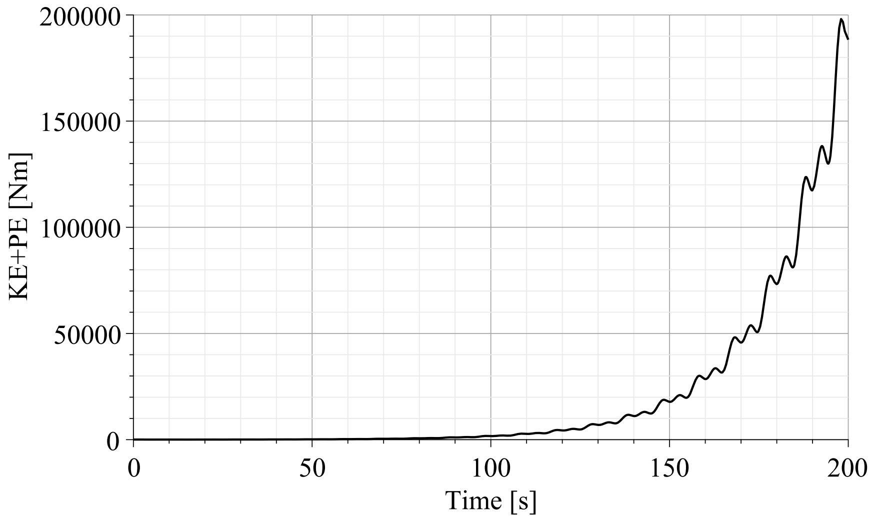

Figure 4.4: Variation of the oscillator's mechanical energy for $\delta = 0$ ($\omega_p/\omega_0 = 2$).

In accordance with Eq. (4.23), the system's oscillations and energy content grow exponentially with time in case $1.85 < \omega_p/\omega_0 < 2.15$; outside this interval the energy fluctuates around 140 N m and is bounded between 40 N m and 240 N m. This energy analysis clearly demonstrates that the parametric oscillator is a non-conservative system. After all, its non-parametric equivalent does not exhibit a time dependency. See Fig. (4.5).

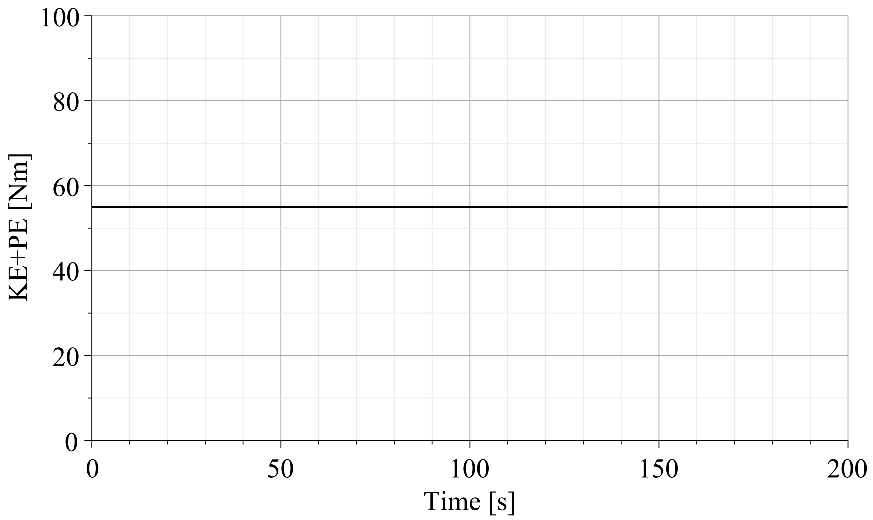

Figure 4.5: The mechanical energy of the non-parametric oscillator is time-invariant.

By setting μ equal to 0, the perturbation of the mean spring stiffness is removed and the expression for the motion $x(t)$ of the conservative mass-spring system is recovered from Eq. (4.10):

$$x\,(t) = x_0 \cos\left(\omega_0 t\right) + \frac{v_0}{\omega_0} \sin\left(\omega_0 t\right) \tag{4.35}$$

Inserting $k(t) = k_0$ and Eq. (4.35) in Eq. (4.34) yields the conservative system's energy content:

$$\mathcal{E} = \mathcal{K} + \mathcal{P} = \frac{1}{2} m v_0^2 + \frac{1}{2} k_0 x_0^2 = \frac{1}{2} \times 100 \times 1^2 + \frac{1}{2} \times 10 \times 1^2 = 55\ \mathrm{N\,m} \tag{4.36}$$

See Fig. (4.5). Comparing Eq. (4.10) to Eq. (4.35) suggests that Landau & Lifshitz [11] took inspiration from the solution for the non-parametric system to propose an expression for the motion of the parametric system; letting the coefficients slowly vary with time while adding a minor perturbation to the frequency in the argument of the trigonometric operators, makes it possible to capture the effect of the harmonically time-varying natural frequency in Mathieu's equation.[4]

4.3 The second instability domain

Eq. (4.8) already alluded to multiple frequency intervals. In fact, according to Eq. (4.8) there are as many instability domains as there are positive integer numbers; that is, an infinite amount. The second frequency interval, which precedes the first interval from Eq. (4.23) reads:

$$\omega_0 \left(1 - 5\mu^2/24\,\right) < \omega_p < \omega_0 \left(1 + \mu^2/24\,\right) \tag{4.37}$$

The derivation of this second instability domain is presented in Appendix B. Note how the width of the second frequency interval is of a second order of smallness with respect to the perturbation parameter $\mathcal{O}(\mu^2)$ while the range of the first instability domain is of a first order of smallness $\mathcal{O}(\mu^1)$; suggesting proportionality to μ^n, with n from Eq. (4.8)

[4]Eq. (4.24) suggests that Landau & Lifshitz used some form of the Fourier series to solve Mathieu's equation. This seems reasonable, since it is likely that the motion of the parametric SDoF system is periodic.

[2]. The effect of this increasing order on the instability domain is visualized in Fig. (4.6) for $\mu = 0.3$.

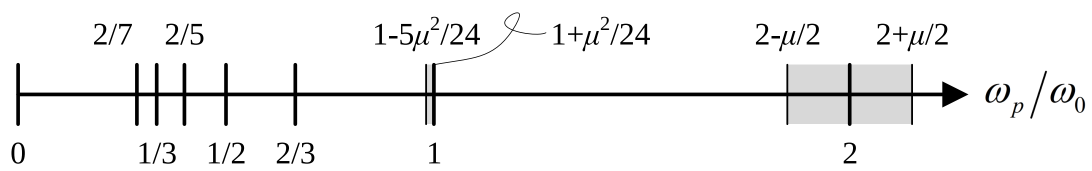

Figure 4.6: The first seven frequency intervals associated with parametric resonance.

Note the rapid decrease of the interval width; the second interval already exhibits boundaries that almost completely coincide with the center. Also note how the interval centers lie increasingly closer to one another with increasing interval order; the distance between the sixth and seventh instability domain is smaller than the distance between the first and second interval.

4.4 The effect of damping

One may wonder what happens to the instability domain in case damping is included in the system. See Fig. (4.7). To find out, the damped Mathieu equation is solved in exactly the same manner as is done in the previous sections.

$$\ddot{x} + 2\mu n\dot{x} + \omega_0^2 \left(1 + \mu \cos\left(\omega_p t\right)\right) x = 0 \tag{4.38}$$

The damping factor n $(= c/(2m))$ is made proportional to the amplitude coefficient μ [10]. Restricting the analysis to a first order approximation of the first frequency interval, Eq. (4.10) is substituted in Eq. (4.38) while ω_p is replaced by $2(\omega_0 + \mu\delta)$; assuming the functions $a(\mu t)$ and $b(\mu t)$ are described by exponentials and collecting terms proportional to μ^1 yields:

$$\begin{aligned}
&-2\dot{a}\omega_0 \sin\left(\left(\omega_0 + \mu\delta\right) t\right) - 2a\omega_0\mu\delta \cos\left(\left(\omega_0 + \mu\delta\right) t\right) + \\
&\quad 2\dot{b}\omega_0 \cos\left(\left(\omega_0 + \mu\delta\right) t\right) - 2b\omega_0\mu\delta \sin\left(\left(\omega_0 + \mu\delta\right) t\right) - \\
&\quad 2a\mu n\omega_0 \sin\left(\left(\omega_0 + \mu\delta\right) t\right) + 2b\mu n\omega_0 \cos\left(\left(\omega_0 + \mu\delta\right) t\right) + \\
&\quad a\omega_0^2\mu \cos\left(2\left(\omega_0 + \mu\delta\right) t\right) \cos\left(\left(\omega_0 + \mu\delta\right) t\right) + \\
&\quad b\omega_0^2\mu \cos\left(2\left(\omega_0 + \mu\delta\right) t\right) \sin\left(\left(\omega_0 + \mu\delta\right) t\right) = 0
\end{aligned} \tag{4.39}$$

Using Eq. (4.12) and Eq. (4.13) and omitting terms that exhibit the frequency '$3(\omega_0+\mu\delta)$', reduces Eq. (4.39) to:

$$\begin{aligned}
&-2\left(\ \dot{a} + b\mu\delta + a\mu n + b\omega_0\mu/4\ \right)\omega_0 \sin\left(\left(\omega_0 + \mu\delta\right) t\right) + \\
&\quad 2\left(\ \dot{b} - a\mu\delta + b\mu n + a\omega_0\mu/4\ \right)\omega_0 \cos\left(\left(\omega_0 + \mu\delta\right) t\right) = 0
\end{aligned} \tag{4.40}$$

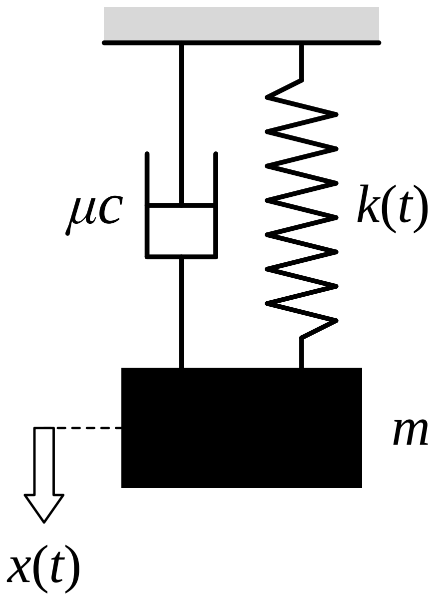

Figure 4.7: A visco-elastic oscillator with time-dependent spring stiffness.

The following system of two coupled homogeneous ODEs with constant coefficients needs to be solved in order to fulfill Eq. (4.40):

$$\begin{aligned} \dot{a} + a\mu n + b\,(\,\delta + \omega_0/4\,)\,\mu &= 0 \\ \dot{b} + b\mu n - a\,(\,\delta - \omega_0/4\,)\,\mu &= 0 \end{aligned} \tag{4.41}$$

To solve Eq. (4.41) with respect to a and b, the following solutions are proposed:

$$a\,(t) = C_a e^{st}, \quad b\,(t) = C_b e^{st} \tag{4.42}$$

Combining Eq. (4.41) and Eq. (4.42) yields a system of two algebraic equations:

$$\begin{bmatrix} s + \mu n & (\delta + \omega_0/4\,)\,\mu \\ -\,(\delta - \omega_0/4\,)\,\mu & s + \mu n \end{bmatrix} \begin{bmatrix} C_a \\ C_b \end{bmatrix} = \begin{bmatrix} 0 \\ 0 \end{bmatrix} \tag{4.43}$$

Requiring the solution to be non-trivial—$C_a \neq 0$ and $C_b \neq 0$—the determinant of the coefficient matrix of Eq. (4.43) needs to vanish, or, stated differently, the following characteristic equation needs to be satisfied:

$$s^2 + 2\mu n s + \mu^2 \left(n^2 + (\delta + \omega_0/4\,)\,(\delta - \omega_0/4\,)\right) = 0 \tag{4.44}$$

Solve for the characteristic exponent:

$$s_{1,2} = -\mu n \pm \frac{\mu}{4}\sqrt{\omega_0^2 - 16\delta^2} \tag{4.45}$$

As mentioned above, $s_{1,2}$ ought to possess a positive real part for instability to occur, and since all parameters—with the exception of δ—are positive (and real), the first term of Eq. (4.45) is real and negative while the second term is real for $|\delta| < \omega_0/4$. So in order to derive a range for δ that is associated with parametric resonance, one of the two roots of Eq. (4.44) needs to be positive with $|\delta| < \omega_0/4$. Meeting this condition results in the following interval for δ:

$$-\frac{1}{4}\sqrt{\omega_0^2 - 16n^2} < \delta < \frac{1}{4}\sqrt{\omega_0^2 - 16n^2} \tag{4.46}$$

and in terms of ω_p:

$$2\omega_0 - \frac{\mu}{2}\sqrt{\omega_0^2 - 16n^2} < \omega_p < 2\omega_0 + \frac{\mu}{2}\sqrt{\omega_0^2 - 16n^2} \tag{4.47}$$

Both Eq. (4.46) and Eq. (4.47) show that the damping factor n needs to remain below the threshold value of $\omega_0/4$ in order for the width of the instability domain to be greater than zero. To see what happens in case the boundaries are zero or even complex, Eq. (4.10) needs to be fully determined. Substituting Eq. (4.45) in Eq. (4.42) and defining the initial conditions as x_0 and v_0, allows to derive the expressions for C_a and C_b:

$$C_a = x_0 \tag{4.48}$$

$$C_b = \frac{\left(n - \sqrt{\omega_0^2/16 \; - \delta^2}\right)\mu x_0 + v_0}{\mu\delta + \omega_0} \tag{4.49}$$

The parameter set of Tab. (4.1) is used to plot Eq. (4.10) for three different damping factors. See Fig. (4.8) to Fig. (4.10).

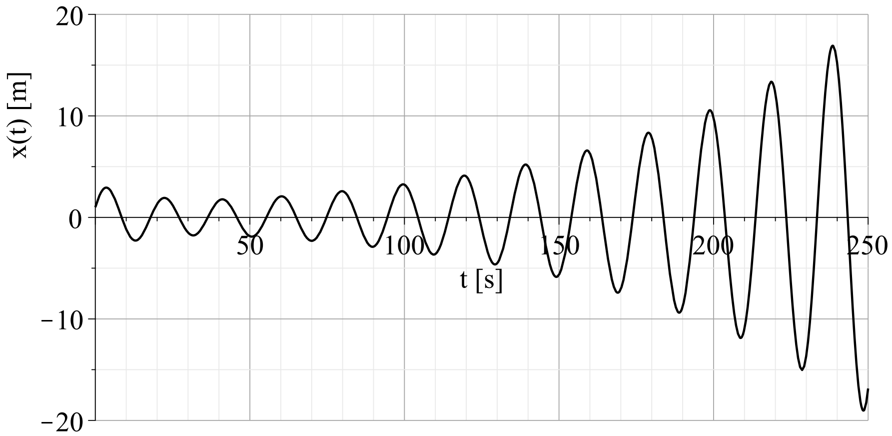

Figure 4.8: Motion of the damped parametric oscillator for $\delta = 0$ and $n = \omega_0/8$.

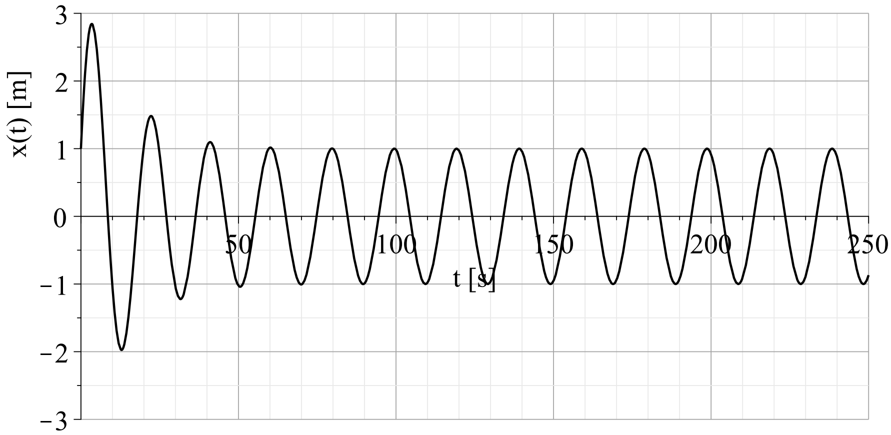

Figure 4.9: Motion of the damped parametric oscillator for $\delta = 0$ and $n = \omega_0/4$.

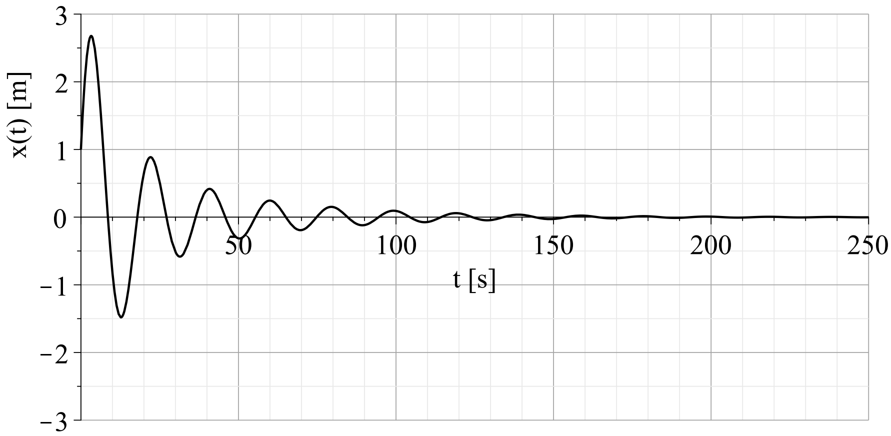

Figure 4.10: Motion of the damped parametric oscillator for $\delta = 0$ and $n = \omega_0/2$.

At the center of the instability zone ($\delta = 0$) the oscillations grow exponentially with time in case the zone has a non-zero width; that is, if $n < \omega_0/4$; making one of the characteristic exponents positive. See Fig. (4.8). For $n = \omega_0/4$ one root of the characteristic equation vanishes, leaving the other to be negative. As a result, the oscillations ultimately reach a steady-state in which the effect of the harmonic component associated with the negative root has completely subsided; cf. Fig. (4.9). The third and final scenario is presented by Fig. (4.10) in which $n > \omega_0/4$ renders both roots negative; negating the effect of both harmonic components as time progresses. It can thus be concluded that the inclusion of (linear viscous) damping in a parametric system prevents this system from becoming unstable as long as $n \geq \omega_0/4$.

As an alternative to the solution procedure adopted above, one can also make use of the *perturbation method* as described in references [10, 18]. It is this method that will be employed to solve the problems of the next three chapters.

Chapter 5

Parametric resonance of a point mass moving uniformly along an infinite Euler-Bernoulli beam on harmonically inhomogeneous foundation

Building on the gained knowledge from the previous two chapters, we are now able to study the phenomenon of parametric resonance in the beam model. This is done by revisiting the article of Verichev & Metrikine [23]; intuitive reasoning is replaced by more explicit explanations and certain concepts are clarified more elaborately. Furthermore, the reader is provided with an outline of how the plotted data is computed.

5.1 Model and governing equations

The considered model is presented in Fig. (5.1); a point mass that moves with constant velocity along an infinite Euler-Bernoulli beam on a harmonically inhomogeneous visco-elastic foundation.

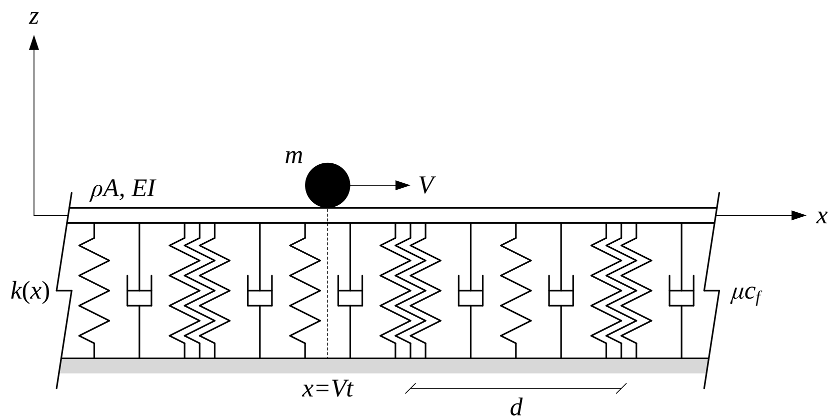

Figure 5.1: The model for investigating vertical parametric resonance of a point mass that moves along an elastic guide on harmonically inhomogeneous visco-elastic support.

The equation of motion, which governs the beam's (small) vertical vibrations, reads—as follows from dynamic equilibrium of vertical forces acting on an infinitesimal beam segment:

$$\rho A \frac{\partial^2 w}{\partial t^2} + EI \frac{\partial^4 w}{\partial x^4} + \mu c_f \frac{\partial w}{\partial t} + k\left(x\right) w = 0 \tag{5.1}$$

with:

$$k\left(x\right) = k_f\left(1 + \mu \cos\left(\chi x\right)\right), \quad \chi = 2\pi/d \tag{5.2}$$

The interface conditions ensure continuity of the beam's displacement, rotation and curvature at the point of contact between the point mass and the beam:

$$\left[w\right]_{x=Vt} = \left[\frac{\partial w}{\partial x}\right]_{x=Vt} = \left[\frac{\partial^2 w}{\partial x^2}\right]_{x=Vt} = 0 \tag{5.3}$$

The square brackets indicate the difference between the bracketed quantity at the right and left of the contact point; e.g., $\lim_{\xi \to 0} \left(w\left(x = Vt + \xi, t\right) - w\left(x = Vt - \xi, t\right)\right) = \left[w\right]_{x=Vt}$. Continuity of the beam's shear force distribution is interrupted by the presence of the point mass:

$$EI \left[\frac{\partial^3 w}{\partial x^3}\right]_{x=Vt} = -m \frac{d^2 w_0}{dt^2} - mg \tag{5.4}$$

How Eq. (5.4) is derived, is presented in Appendix C. Note that the self-weight of the point mass is not able to make the system unstable; it does not depend on any of the system's degrees-of-freedom.[1] Because of this, the second term on the right-hand side of Eq. (5.4) is omitted henceforth. Finally, the point mass and the beam are in continuous contact with one another:

$$w\left(x = Vt, t\right) = w_0\left(t\right) \tag{5.5}$$

Compare the above formulation with the description of the model from Chapter 3; instead of using the Dirac delta function to describe the interface between the left and right beam domain, interface conditions are used to describe the model of Fig. (5.1). This is done because the delta function does not lend itself for the perturbation method as is used in reference [23]. In addition to the parameters and variables introduced in Chapter 3, the following additional quantity symbols are employed:

- μ = amplitude coefficient [-]
- k_f = mean foundation stiffness [N/m^2]
- χ = wavenumber of inhomogeneity [rad/m]
- d = period of inhomogeneity [m]
- g = gravitational acceleration [m/s^2]

[1] In general, for instability to occur in a dynamic system, it ought to include an external source that continuously provides the system with energy—allowing its oscillations to grow unlimited with time. Modelling such a system and writing up its governing equations, one can see excitation terms appearing that exhibit proportionality to the system's own degrees-of-freedom; cf. the first term on the right-hand side of Eq. (5.4).

Because the variation of the foundation stiffness is small compared to its mean value ($\mu \ll 1$), a perturbation method [17, 18] is used to solve Eq. (5.1) with respect to the beam's deflection $w(x,t)$; it is assumed that the solution to the homogeneous system $w^{(0)}(x,t)$ is not affected considerably by the inclusion of a small harmonic inhomogeneity. The solution is searched for in the following form—of the first order with respect to the perturbation parameter μ:

$$w\left(x,t\right) = w^{(0)}\left(x,t\right) + \mu w^{(1)}\left(x,t\right) \tag{5.6}$$

$$w_0\left(t\right) = w_0^{(0)}\left(t\right) + \mu w_0^{(1)}\left(t\right) \tag{5.7}$$

with $\mu w^{(1)} \ll w^{(0)}$ and $\mu w_0^{(1)} \ll w_0^{(0)}$. Substituting Eq. (5.6) and Eq. (5.7) in the governing equations and collecting terms proportional to μ^0 yields the set of governing equations for the unperturbed problem:

$$\begin{aligned}
&\rho A \frac{\partial^2 w^{(0)}}{\partial t^2} + EI \frac{\partial^4 w^{(0)}}{\partial x^4} + k_f w^{(0)} = 0 \\
&\left[w^{(0)}\right]_{x=Vt} = \left[\frac{\partial w^{(0)}}{\partial x}\right]_{x=Vt} = \left[\frac{\partial^2 w^{(0)}}{\partial x^2}\right]_{x=Vt} = 0 \\
&EI\left[\frac{\partial^3 w^{(0)}}{\partial x^3}\right]_{x=Vt} = -m\frac{d^2 w_0^{(0)}}{dt^2} \\
&w^{(0)}\Big|_{x=Vt} = w_0^{(0)}
\end{aligned} \tag{5.8}$$

Collecting terms proportional to μ^1 yields the set of governing equations for the (first order) perturbed problem:

$$\begin{aligned}
&\rho A \frac{\partial^2 w^{(1)}}{\partial t^2} + EI \frac{\partial^4 w^{(1)}}{\partial x^4} + k_f w^{(1)} = -c_f \frac{\partial w^{(0)}}{\partial t} - k_f w^{(0)} \cos\left(\chi x\right) \\
&\left[w^{(1)}\right]_{x=Vt} = \left[\frac{\partial w^{(1)}}{\partial x}\right]_{x=Vt} = \left[\frac{\partial^2 w^{(1)}}{\partial x^2}\right]_{x=Vt} = 0 \\
&EI\left[\frac{\partial^3 w^{(1)}}{\partial x^3}\right]_{x=Vt} = -m\frac{d^2 w_0^{(1)}}{dt^2} \\
&w^{(1)}\Big|_{x=Vt} = w_0^{(1)}
\end{aligned} \tag{5.9}$$

The equations of motion of (5.8) and (5.9) are solved consecutively; once the solution to the unperturbed problem $w^{(0)}$ is derived from (5.8), it is substituted at the right-hand side of the equation of motion of (5.9) where it, combined with the harmonic variation of the foundation stiffness and the uniformly distributed foundation damping, composes the forcing term.

5.2 Solution to the unperturbed problem

This problem is partly studied in Chapter 3; no expression for the beam's vertical deflection was derived, only the characteristic equation of the equivalent oscillator—that is, the single-degree-of-freedom system that allows to analyze the moving concentrated mass as such. Exploiting this analogy further, the general solution to the problem of the freely vibrating oscillator reads:

$$w_0^{(0)}\left(t\right) = W_A e^{i\omega_n t} + W_B e^{-i\omega_n t} \tag{5.10}$$

which indeed is the adopted expression for the mass's vertical displacement. Note that the coefficients W_A and W_B are determined by the mass's initial conditions. As for the elementary SDoF system, the natural frequency ω_n is inferred from the characteristic equation; for the equivalent oscillator, this equation reads as:

$$-m\omega_n^2 + \left(i \sum_{j=1}^{2} \left(\frac{\partial D}{\partial k}\left(k, \omega_n\right) \right)^{-1}_{k=k_j} \right)^{-1} = 0 \tag{5.11}$$

with:

$$D\left(k, \omega_n\right) = -\rho A (\omega_n - kV)^2 + EIk^4 + ic_f\left(\omega_n - kV\right) + k_f \tag{5.12}$$

The poles k_j in Eq. (5.11) are obtained by equating the dispersion relation of Eq. (5.12) to zero and solving it for k. Of the four ensuing roots, only those two that possess a positive imaginary part are of interest; recall, the contour is closed in the upper half of the complex k-plane; see Chapter 3. Eq. (5.11) is subsequently solved for ω_n by means of a numerical approach; letting ω_n run along a range of real positive values, starting at zero, while observing which two consecutive values make the left-hand side of Eq. (5.11) switch sign, the natural frequency is then found by linear interpolating between these two values. Performing this procedure for multiple valuations of the mass and its velocity, the dependency of ω_n on these two parameters can be presented graphically. See Fig. (5.2).

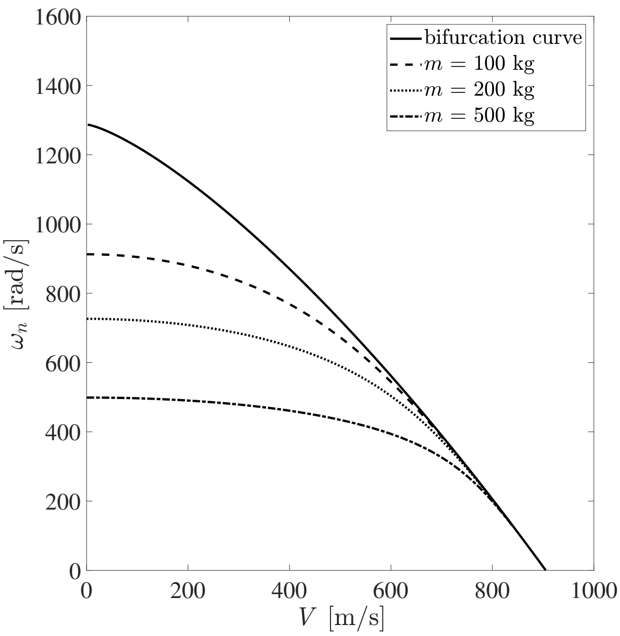

Figure 5.2: The equivalent oscillator's natural frequency ω_n as a function of the point mass m and the mass's velocity V.

The solid curve separates three regimes, each in which the vehicle disperses a different kind of wave into the beam. Dependent on the combination of its velocity and vibratory frequency—below, on or above the curve—the vehicle either generates evanescent waves, rigid vibrations or harmonic waves respectively; cf. Chapter 2. The associated motion of the vehicle is referred to as sub-critical, critical respectively super-critical.

$\rho = 7849\ \mathrm{kg\,m^{-3}}$	$A = 7.687 \times 10^{-3}\ \mathrm{m^2}$	$I = 3.055 \times 10^{-5}\ \mathrm{m^4}$
$E = 2 \times 10^{11}\ \mathrm{N\,m^{-2}}$	$k_f = 1 \times 10^{8}\ \mathrm{N\,m^{-2}}$	$c_f = 0\ \mathrm{N\,s\,m^{-2}}$

Table 5.1: Parameter set for plotting the curves of Fig. (5.2) and Fig. (6.2).

How the bifurcation curve in Fig. (5.2) is constructed, is illustrated in Fig. (5.3); effectively by tracing the tangency between the kinematic invariant and the dispersion curve for wavenumbers between k_0 and k_1. For a non-vibrating excitation source ($\Omega_1 = 0$ rad/s) that moves with constant velocity, the minimum phase velocity with which waves are dispersed in the beam is obtained by equating the group velocity to the phase velocity and solving this with respect to the wavenumber; back-substitution of the real positive wavenumber in either one of the velocity definitions returns the minimum phase velocity V_1. In case the excitation source does vibrate ($0 < \Omega \leq \omega_0$), the aforementioned equation needs to include one extra term: $V_{gr} = V_{ph} - \Omega/k$.

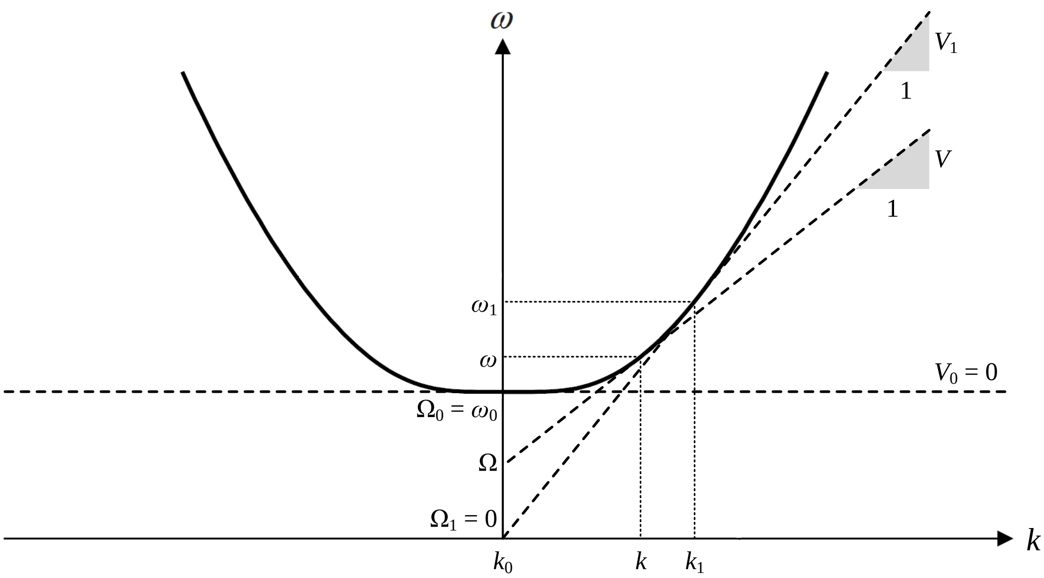

Figure 5.3: Deriving the bifurcation curve.

The dispersion relation [8, 16] for bending waves in the Euler-Bernoulli beam on uniformly distributed elastic foundation is derived by substituting an assumed waveform:

$$w(x,t) = We^{i(\omega t - kx)} \tag{5.13}$$

in the equation of motion for this beam model:

$$\rho A \frac{\partial^2 w}{\partial t^2} + EI \frac{\partial^4 w}{\partial x^4} + k_f w = 0 \tag{5.14}$$

The non-trivial solution ($W \neq 0$) then reads:

$$-\omega^2 \rho A + k^4 EI + k_f = 0 \tag{5.15}$$

which constitutes the dispersion relation. Solving this relation with respect to the wave-frequency ω provides us with two roots; the positive one describes the dispersion curve in Fig. (5.3):

$$\omega = \sqrt{\frac{EI}{\rho A} k^4 + \omega_0^2}, \quad \omega_0 = \sqrt{\frac{k_f}{\rho A}} = 1287 \text{ rad/s} \tag{5.16}$$

In order to determine the angular frequency ω and wavenumber k with which waves—as described by Eq. (5.13)—are dispersed in the beam due to a general excitation source:

$$F(t) = F_0 e^{i\Omega t} \tag{5.17}$$

that moves with constant velocity V along the guide, the following relationship is inferred [13]:

$$\omega - kV = \Omega \Rightarrow \omega = \Omega + kV \tag{5.18}$$

This relationship states that the phase of the induced wave '$\omega t - kx$' mirrors the phase of the oscillating force 'Ωt' at $x = Vt$ and is referred to as the *kinematic invariant* [6]. A graphical representation of Eq. (5.18) is provided by the dashed lines in Fig. (5.3); intersection with the dispersion curve indicates the excitation of propagating waves of which the frequencies and wavenumbers are designated by the coordinates of the intersection points. However, in Fig. (5.3) the dashed lines do not cross the dispersion curve, but are tangent to this curve; the horizontal kinematic invariant indicates a stationary excitation source that vibrates at the *cut-off frequency* ω_0 [16], while the tilted kinematic invariant crossing the axes' origin implies a non-vibrating excitation source that moves with minimum phase velocity along the guide. The phase and group velocity of waves that propagate through the beam, being defined respectively as:

$$V_{ph} = \frac{\omega}{k} = \sqrt{\frac{EI}{\rho A} k^2 + \left(\frac{\omega_0}{k}\right)^2} \tag{5.19}$$

$$V_{gr} = \frac{d\omega}{dk} = \frac{2EIk^3}{\sqrt{\rho A \left(EIk^4 + k_f\right)}} \tag{5.20}$$

allow for the derivation of the minimum phase velocity; equating the right-hand sides of Eq. (5.19) and Eq. (5.20) and solving for the wavenumber, provides four roots, one of which is real and positive, i.e. $k_1 = \sqrt[4]{k_f/EI}$. Back-substitution of this wavenumber in either Eq. (5.19) or Eq. (5.20) yields the expression for the minimum phase velocity:

$$V_1 = V_{ph}^{min} = \sqrt[4]{\frac{4EI\omega_0^2}{\rho A}} = 905 \text{ m/s} \tag{5.21}$$

Note how the velocity-frequency pairs $(V_0, \Omega_0) = (0, 1287)$ and $(V_1, \Omega_1) = (905, 0)$ denote the two outer points of the bifurcation curve in Fig. (5.2). In order to find an expression for the points in between, the same procedure is repeated; except now, the definition of the phase velocity needs to be extended by an extra term:

$$V_{ph} - \frac{\Omega}{k} \tag{5.22}$$

Equating this to the definition of the group velocity and solving it with respect to the wavenumber k returns eight roots, two of which are real and positive but only one goes from k_1 to k_0 when the forcing frequency Ω elevates from zero to the cut-off frequency ω_0; cf. Fig. (5.3). This wavenumber is defined as:

$$k(\Omega) = \left(\frac{\rho A \Omega^2 + 2k_f - \sqrt{\rho A \Omega^2 \left(\rho A \Omega^2 + 8k_f\right)}}{2EI} \right)^{1/4} \tag{5.23}$$

Note how $k(\Omega = 0) = k_1$ and $k(\Omega = \omega_0) = k_0 = 0$. Substituting Eq. (5.23) back in either Eq. (5.20) or Eq. (5.22) yields the expression for the critical velocity:

$$V = V_{cr}(\Omega) = \left(\frac{8EI\left(\rho A \Omega^2 + 2k_f - \sqrt{\rho A \Omega^2 \left(\rho A \Omega^2 + 8k_f\right)}\right)^3}{\rho^2 A^2 \left(\rho A \Omega^2 + 4k_f - \sqrt{\rho A \Omega^2 \left(\rho A \Omega^2 + 8k_f\right)}\right)^2} \right)^{1/4} \tag{5.24}$$

which describes the bifurcation curve in Fig. (5.2).

Returning to the problem of the moving mass, it needs to be noted that 'free' vibrations are investigated; no external forcing with an inherent frequency is exerted on the beam. Thus, for this problem, the natural frequency of the equivalent oscillator ω_n is in fact the excitation frequency Ω. Consequently, the bifurcation curve may be compared to the dashed curves in Fig. (5.2). As is shown in reference [13], once the kinematic invariant crosses the dispersion curve, anomalous Doppler waves are dispersed in the beam, which render the system unstable. Also, tangency between the invariant and the curve implies that the excitation source moves with a velocity equal to the waves' group velocity; the associated energy does not propagate away from the source, but accumulates at the loading point, which leads to resonance. Neither wave-induced instability nor classical resonance is the aim of this research and so, as to be able to investigate under what conditions instability arises as a result of periodically varying foundation stiffness, it is required to let the kinematic invariant remain below the dispersion curve. Given Tab. (5.1), Fig. (5.2) shows that this requirement is met for three different mass valuations. In fact, as long as $m \geq 0$, the natural frequency function is bounded by the bifurcation curve.

The only remaining task to solve the unperturbed problem completely, is to come up with an expression for the beam's deflection. Given the general complex waveform of Eq. (5.13), the expression for the vertical displacement of the mass by Eq. (5.10) and adopting a local coordinate system that follows this moving mass ($\xi = x - Vt$) the following solution is proposed:[2]

$$w^{(0)}(x,t) = \begin{cases} W_{A1} e^{i\left(\Omega t - k_1^A \xi\right)} + W_{A2} e^{i\left(\Omega t - k_2^A \xi\right)} + \\ W_{B1} e^{-i\left(\Omega t + k_1^B \xi\right)} + W_{B2} e^{-i\left(\Omega t + k_2^B \xi\right)}, \quad \xi \geq 0 \\ \\ W_{A3} e^{i\left(\Omega t - k_3^A \xi\right)} + W_{A4} e^{i\left(\Omega t - k_4^A \xi\right)} + \\ W_{B3} e^{-i\left(\Omega t + k_3^B \xi\right)} + W_{B4} e^{-i\left(\Omega t + k_4^B \xi\right)}, \quad \xi \leq 0 \end{cases} \tag{5.25}$$

The wavenumbers $k_{1,2,3,4}^{A,B}$ are derived from Eq. (5.15) combined with Eq. (5.18). Note the resemblance to dispersion Eq. (5.12); the same waveform of Eq. (5.13) is assumed, except the phase exhibits different signage: $\omega t + kx$ instead of $\omega t - kx$. Because we are

[2] A more rigorous derivation of the beam's deflection field is presented in reference [15].

solely interested in the mass's sub-critical behaviour, accordingly, the kinematic invariant ought to remain below the dispersion curve, which makes these wavenumbers complex: $\mathrm{Im}\left(k_{1,2}^{A,B}\right) < 0$ and $\mathrm{Im}\left(k_{3,4}^{A,B}\right) > 0$. See Eq. (2.13) and Fig. (2.5). The W-coefficients are determined by the interface and continuity conditions of Eq. (5.8) [13]. See Appendix D.

5.3 Analysis of the perturbed problem

In this section, the system of Eq. (5.9) is analyzed in order to determine under which conditions parametric resonance occurs. Substituting Eq. (5.25) in the perturbed equation of motion while setting $c_f = 0$—according to Chapter 4, the first criterion for parametric resonance is not affected by the exclusion of damping—and employing the following identity from Euler's formula:

$$\cos(\chi x) = \frac{e^{i\chi x} + e^{-i\chi x}}{2} \tag{5.26}$$

the right-hand side of the perturbed equation of motion can then be written out as:

$$\rho A \frac{\partial^2 w^{(1)}}{\partial t^2} + EI \frac{\partial^4 w^{(1)}}{\partial x^4} + k_f w^{(1)} =$$
$$-\frac{k_f}{2} \begin{cases} W_{A1} e^{i\left(k_1^A V + \Omega\right)t} e^{i\left(\chi - k_1^A\right)x} + W_{A2} e^{i\left(k_2^A V + \Omega\right)t} e^{i\left(\chi - k_2^A\right)x} + \\ W_{A1} e^{i\left(k_1^A V + \Omega\right)t} e^{-i\left(\chi + k_1^A\right)x} + W_{A2} e^{i\left(k_2^A V + \Omega\right)t} e^{-i\left(\chi + k_2^A\right)x} + \\ W_{B1} e^{i\left(k_1^B V - \Omega\right)t} e^{i\left(\chi - k_1^B\right)x} + W_{B2} e^{i\left(k_2^B V - \Omega\right)t} e^{i\left(\chi - k_2^B\right)x} + \\ W_{B1} e^{i\left(k_1^B V - \Omega\right)t} e^{-i\left(\chi + k_1^B\right)x} + W_{B2} e^{i\left(k_2^B V - \Omega\right)t} e^{-i\left(\chi + k_2^B\right)x}, & x \geq Vt \\ \\ W_{A3} e^{i\left(k_3^A V + \Omega\right)t} e^{i\left(\chi - k_3^A\right)x} + W_{A4} e^{i\left(k_4^A V + \Omega\right)t} e^{i\left(\chi - k_4^A\right)x} + \\ W_{A3} e^{i\left(k_3^A V + \Omega\right)t} e^{-i\left(\chi + k_3^A\right)x} + W_{A4} e^{i\left(k_4^A V + \Omega\right)t} e^{-i\left(\chi + k_4^A\right)x} + \\ W_{B3} e^{i\left(k_3^B V - \Omega\right)t} e^{i\left(\chi - k_3^B\right)x} + W_{B4} e^{i\left(k_4^B V - \Omega\right)t} e^{i\left(\chi - k_4^B\right)x} + \\ W_{B3} e^{i\left(k_3^B V - \Omega\right)t} e^{-i\left(\chi + k_3^B\right)x} + W_{B4} e^{i\left(k_4^B V - \Omega\right)t} e^{-i\left(\chi + k_4^B\right)x}, & x \leq Vt \end{cases} \tag{5.27}$$

Adopting the solution procedure for ordinary inhomogeneous differential equations, the total solution is composed of two parts; the homogeneous solution—in the context of classical mechanics, this solution usually represents the free motion of the system—and the particular solution, which signifies the forced motion:

$$w^{(1)} = w_h^{(1)} + w_p^{(1)} \tag{5.28}$$

As for an inhomogeneous ordinary differential equation, the particular solution of partial differential Eq. (5.27) is found by means of the so-called *Method of Undetermined Coefficients*—this method can be employed whenever the right-hand side terms belong to a limited group of functions; them being: polynomials, exponentials and trigonometric functions [3]. The forced solution reads:

$$
w_p^{(1)}(x,t) = \begin{cases} C_{11}e^{i\left(k_1^A V+\Omega\right)t}e^{i\left(\chi-k_1^A\right)x} + C_{12}e^{i\left(k_2^A V+\Omega\right)t}e^{i\left(\chi-k_2^A\right)x} + \\ C_{21}e^{i\left(k_1^A V+\Omega\right)t}e^{-i\left(\chi+k_1^A\right)x} + C_{22}e^{i\left(k_2^A V+\Omega\right)t}e^{-i\left(\chi+k_2^A\right)x} + \\ C_{31}e^{i\left(k_1^B V-\Omega\right)t}e^{i\left(\chi-k_1^B\right)x} + C_{32}e^{i\left(k_2^B V-\Omega\right)t}e^{i\left(\chi-k_2^B\right)x} + \\ C_{41}e^{i\left(k_1^B V-\Omega\right)t}e^{-i\left(\chi+k_1^B\right)x} + C_{42}e^{i\left(k_2^B V-\Omega\right)t}e^{-i\left(\chi+k_2^B\right)x}, \quad x \geq Vt \\ \\ C_{13}e^{i\left(k_3^A V+\Omega\right)t}e^{i\left(\chi-k_3^A\right)x} + C_{14}e^{i\left(k_4^A V+\Omega\right)t}e^{i\left(\chi-k_4^A\right)x} + \\ C_{23}e^{i\left(k_3^A V+\Omega\right)t}e^{-i\left(\chi+k_3^A\right)x} + C_{24}e^{i\left(k_4^A V+\Omega\right)t}e^{-i\left(\chi+k_4^A\right)x} + \\ C_{33}e^{i\left(k_3^B V-\Omega\right)t}e^{i\left(\chi-k_3^B\right)x} + C_{34}e^{i\left(k_4^B V-\Omega\right)t}e^{i\left(\chi-k_4^B\right)x} + \\ C_{43}e^{i\left(k_3^B V-\Omega\right)t}e^{-i\left(\chi+k_3^B\right)x} + C_{44}e^{i\left(k_4^B V-\Omega\right)t}e^{-i\left(\chi+k_4^B\right)x}, \quad x \leq Vt \end{cases} \tag{5.29}
$$

The C-coefficients are determined by substituting Eq. (5.29) in Eq. (5.27) for $w^{(1)}$ and solving for the unknown coefficient per time-space signature. See Appendix D. Now that $w_p^{(1)}$ is completely determined, the free deflection field $w_h^{(1)}$ remains to be defined. To this end, the corresponding set of governing equations needs to be formulated; inserting Eq. (5.28) in Eq. (5.27)—taking into account that Eq. (5.29) forms the solution to Eq. (5.27)—as well as in the interface and continuity conditions of Eq. (5.9), the following system is obtained:

$$
\begin{aligned}
&\rho A \frac{\partial^2 w_h^{(1)}}{\partial t^2} + EI \frac{\partial^4 w_h^{(1)}}{\partial x^4} + k_f w_h^{(1)} = 0 \\
&\left[w_h^{(1)} \right]_{x=Vt} = D_{01}e^{it(V\chi+\Omega)} + D_{02}e^{-it(V\chi-\Omega)} + D_{03}e^{it(V\chi-\Omega)} + D_{04}e^{-it(V\chi+\Omega)} \\
&\left[\frac{\partial w_h^{(1)}}{\partial x} \right]_{x=Vt} = D_{11}e^{it(V\chi+\Omega)} + D_{12}e^{-it(V\chi-\Omega)} + D_{13}e^{it(V\chi-\Omega)} + D_{14}e^{-it(V\chi+\Omega)} \\
&\left[\frac{\partial^2 w_h^{(1)}}{\partial x^2} \right]_{x=Vt} = D_{21}e^{it(V\chi+\Omega)} + D_{22}e^{-it(V\chi-\Omega)} + D_{23}e^{it(V\chi-\Omega)} + D_{24}e^{-it(V\chi+\Omega)} \\
&\left[\frac{\partial^3 w_h^{(1)}}{\partial x^3} \right]_{x=Vt} = -\frac{m}{EI}\frac{d^2 w_0^{(1)}}{dt^2} + D_{31}e^{it(V\chi+\Omega)} + D_{32}e^{-it(V\chi-\Omega)} + \\
&\qquad\qquad D_{33}e^{it(V\chi-\Omega)} + D_{34}e^{-it(V\chi+\Omega)} \\
&\left. w_h^{(1)} \right|_{x=Vt} = w_0^{(1)} + D_{41}e^{it(V\chi+\Omega)} + D_{42}e^{-it(V\chi-\Omega)} + D_{43}e^{it(V\chi-\Omega)} + D_{44}e^{-it(V\chi+\Omega)}
\end{aligned} \tag{5.30}
$$

The definitions of the D-coefficients are listed in Appendix D. At this point we are not interested in a fully determined expression for the beam's deflection; this would require to solve Eq. (5.30) with respect to $w_h^{(1)}$. Fortunately, as such, the system of Eq. (5.30) does already provide sufficient insight into the effect of the foundation's harmonic inhomogeneity. This effect, which is expressed by the particular solution, presents itself at the right-hand side of the interface conditions. In particular, the four additional terms that appear on the right-hand side of the balance of vertical forces; each varying with a different time signature. Classical resonance, as is well known, occurs once the excitation frequency coincides with one of the system's natural frequencies. Following the same reasoning here—given the frequencies of the four aforementioned forcing terms—there is only one excitation frequency that allows for the derivation of a condition for parametric resonance once it is equated to the natural frequency of the unperturbed system ($\omega_n = \Omega$):

$$V\chi - \Omega = \Omega \Rightarrow V\chi = 2\Omega \tag{5.31}$$

After all, the EoM denoted in Eq. (5.30) describes the motion of the unperturbed system; cf. Eq. (5.8). The other three time signatures are not able to balance with the natural frequency, because the mass's velocity V, the wavenumber of inhomogeneity χ and the excitation frequency Ω are all greater than zero. Note the resemblance of Eq. (5.31) to the first condition for parametric resonance in systems described by Mathieu's equation: $\omega_p = 2\omega_0$. See Chapter 4.

5.4 The instability domain

Eq. (5.31) defines the instability domain's center (Chapter 4), which is a curve in the velocity-mass parameter space. See Fig. (5.4). Based on the data of Fig. (5.2), this curve is plotted by checking numerically for each mass value which combination of velocity and natural frequency Eq. (5.31) balances. Doing this for three different valuations of χ, one can observe that an increase in the period of inhomogeneity leads to an elevation of the critical mass; the velocity at which parametric instability occurs increases.

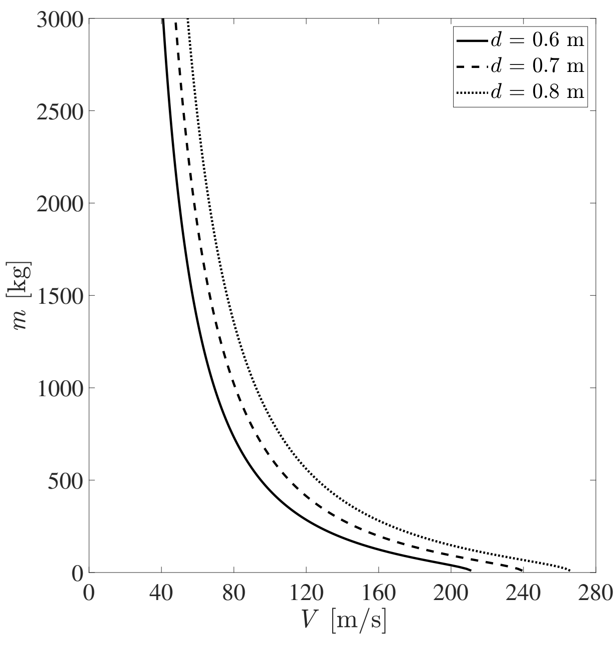

Figure 5.4: Center line of the first instability domain for three different periods of inhomogeneity.

Though a resemblance may be noted between the curves of Fig. (5.4) and those that represent the boundary of the wave-induced instability domain—see Chapter 2 and 3—it is underlined that the area at the right of the curves in Fig. (5.4) does not indicate combinations of V and m that lead to instability. In fact, the area that encloses unstable V-m

coordinates is very limited compared to the area that corresponds to wave-induced instability. Repeating the procedure outlined in [23], the domain's boundary associated with parametric instability is plotted in Fig. (5.5) for three different periods of inhomogeneity; an increase in d leads to a widening of the instability region.

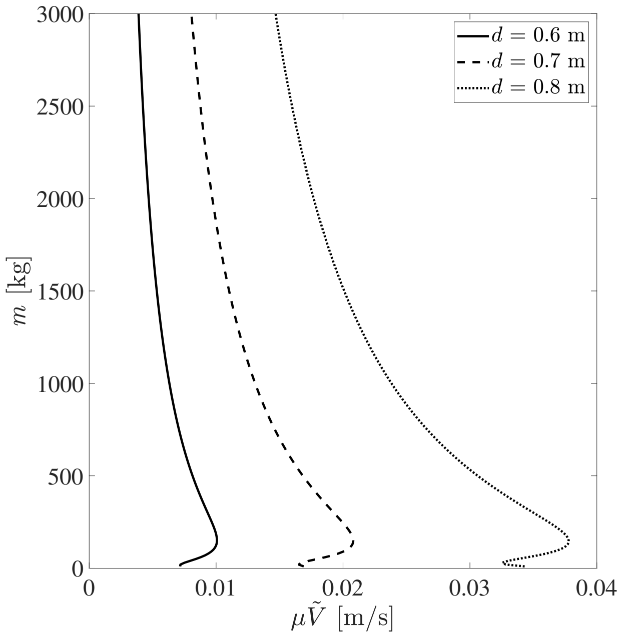

Figure 5.5: Deviation line of the first instability domain for three different periods of inhomogeneity.

The fact that the parametric instability domain—which is centered around the curve of Fig. (5.4) and bounded at the left and right by the curve of Fig. (5.5)—is a very narrow strip, is a result of the model's weak inhomogeneity ($\mu \ll 1$).

To conclude, it is checked if there is a special relationship between parametric resonance and the radiation of anomalous Doppler waves. That is, if combinations of V and m that lie inside the instability domain associated with parametric resonance give rise to the dispersion of anomalous Doppler waves exclusively outside the instability domain associated with wave-induced instability; cf. Fig. (3.3), Fig. (5.4) and Fig. (5.5). To this end, we return to the system of Eq. (5.30) and employ the four time signatures one by one as excitation frequency Ω in the dispersion relation that is formed by combining Eq. (5.15) and Eq. (5.18). Solving this relation with respect to the wavenumber k provides insight into the type of wave that is radiated; normal Doppler or anomalous Doppler. According to reference [13], wavenumbers that lie in the third quadrant of the dispersion plane are anomalous Doppler. Doing this for a combination of V and m that lies on one of the center lines of Fig. (5.4) shows that anomalous Doppler waves are indeed dispersed in the beam under the condition for parametric resonance. See Fig. (5.6). However, this also turns out to be true for a combination outside the instability domain—see Fig. (5.7)—which suggests that there is no special relation. An energy analysis should be conducted to see what is going on in more detail.

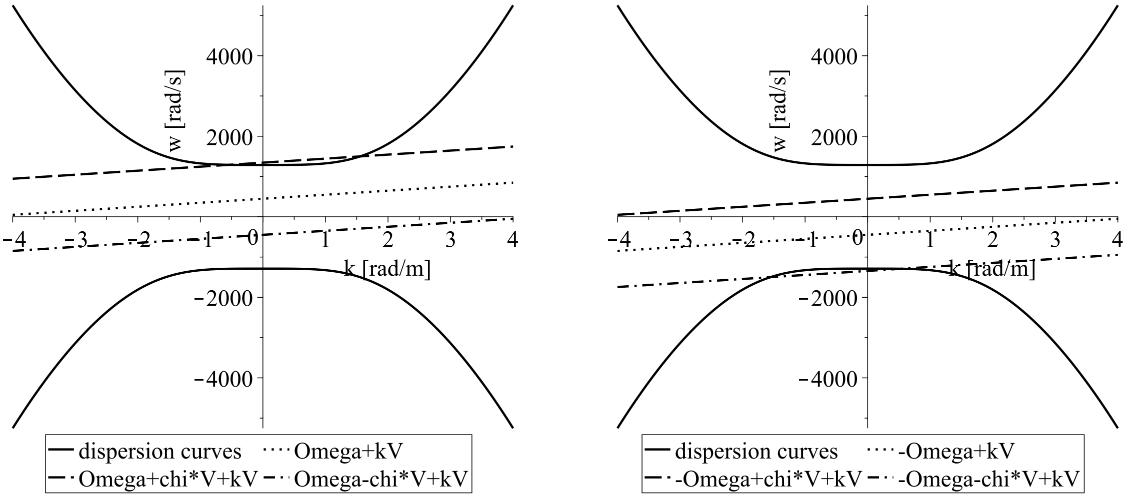

Figure 5.6: Higher-order kinematic invariants inside the domain of parametric resonance.

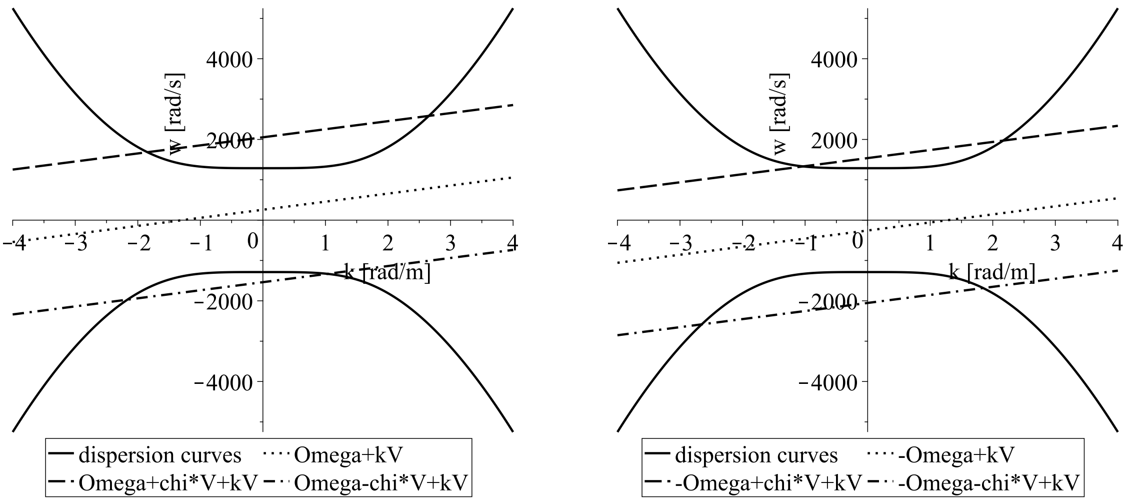

Figure 5.7: Higher-order kinematic invariants outside the domain of parametric resonance and outside the domain of wave-induced instability.

Chapter 6

Parametric resonance of an oscillator moving uniformly along an infinite Euler-Bernoulli beam on harmonically inhomogeneous foundation

The effect of vehicle-structure interaction on the instability domain's center line is investigated. To this end, the method presented in reference [23] is used again, except now, the governing equations account for the contact spring. Will it affect the critical mass in a similar manner as is observed in the case of wave-induced instability? See Chapter 3.

6.1 Model and governing equations

The model is presented in Fig. (6.1); a one-mass oscillator that moves with constant velocity along an infinite Euler-Bernoulli beam on a harmonically inhomogeneous visco-elastic foundation.

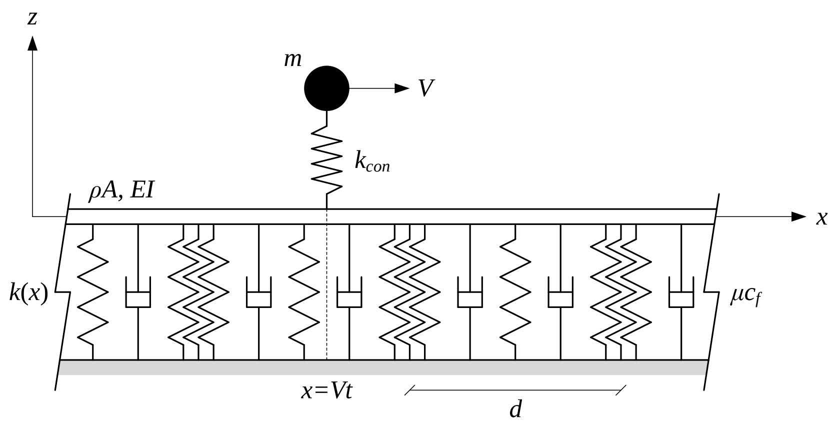

Figure 6.1: The model for investigating vertical parametric resonance of a one-mass oscillator that moves along an elastic guide on harmonically inhomogeneous visco-elastic support.

Of the governing equations, only the balance of vertical forces at the interface and the continuity condition change due to the inclusion of the contact spring:

$$EI\left[\frac{\partial^3 w}{\partial x^3}\right]_{x=Vt} = F_s, \quad m\frac{d^2 w_0}{dt^2} = -F_s - mg \tag{6.1}$$

$$F_s = k_{con}\left(w_0 - w|_{x=Vt}\right) \tag{6.2}$$

The derivations of Eq. (6.1) and Eq. (6.2) are provided in Appendix E. Henceforth, the dead weight mg is neglected. Following the exact same steps as in Chapter 5, the perturbation method yields the following unperturbed system of equations:

$$\begin{aligned}
&\rho A\frac{\partial^2 w^{(0)}}{\partial t^2} + EI\frac{\partial^4 w^{(0)}}{\partial x^4} + k_f w^{(0)} = 0\\
&\left[w^{(0)}\right]_{x=Vt} = \left[\frac{\partial w^{(0)}}{\partial x}\right]_{x=Vt} = \left[\frac{\partial^2 w^{(0)}}{\partial x^2}\right]_{x=Vt} = 0\\
&F_s^{(0)} = EI\left[\frac{\partial^3 w^{(0)}}{\partial x^3}\right]_{x=Vt}, \quad F_s^{(0)} = -m\frac{d^2 w_0^{(0)}}{dt^2}\\
&F_s^{(0)} = k_{con}\left(w_0^{(0)} - w^{(0)}\big|_{x=Vt}\right)
\end{aligned} \tag{6.3}$$

and returns the following perturbed system:

$$\begin{aligned}
&\rho A\frac{\partial^2 w^{(1)}}{\partial t^2} + EI\frac{\partial^4 w^{(1)}}{\partial x^4} + k_f w^{(1)} = -c_f\frac{\partial w^{(0)}}{\partial t} - k_f w^{(0)}\cos\left(\chi x\right)\\
&\left[w^{(1)}\right]_{x=Vt} = \left[\frac{\partial w^{(1)}}{\partial x}\right]_{x=Vt} = \left[\frac{\partial^2 w^{(1)}}{\partial x^2}\right]_{x=Vt} = 0\\
&F_s^{(1)} = EI\left[\frac{\partial^3 w^{(1)}}{\partial x^3}\right]_{x=Vt}, \quad F_s^{(1)} = -m\frac{d^2 w_0^{(1)}}{dt^2}\\
&F_s^{(1)} = k_{con}\left(w_0^{(1)} - w^{(1)}\big|_{x=Vt}\right)
\end{aligned} \tag{6.4}$$

6.2 Solution to the unperturbed problem

Including the contact spring in the model does not lead to a change of Eq. (5.10) and Eq. (5.25). After all, the only change made to the equivalent oscillator is the insertion of a spring with constant stiffness between the equivalent spring and the point mass; cf. Chapter 3. This new spring system in series does require however to edit the equivalent oscillator's characteristic equation accordingly; as derived in Chapter 3, the augmented equation reads:

$$-m\omega_n^2 + \chi'\left(\omega_n\right) = 0 \tag{6.5}$$

with:

$$\begin{aligned}
&\chi'\left(\omega_n\right) = \frac{k_{con}\chi_{eq}\left(\omega_n\right)}{k_{con} + \chi_{eq}\left(\omega_n\right)}\\
&\chi_{eq}\left(\omega_n\right) = \left(i\sum_{j=1}^{2}\left(\frac{\partial D}{\partial k}\left(k,\omega_n\right)\right)^{-1}_{k=k_j}\right)^{-1}\\
&D\left(k,\omega_n\right) = -\rho A(\omega_n - kV)^2 + EIk^4 + ic_f\left(\omega_n - kV\right) + k_f
\end{aligned} \tag{6.6}$$

The dependency of the oscillator's natural frequency ω_n on the valuation of the point mass m and the mass's constant velocity V is shown in Fig. (6.2).

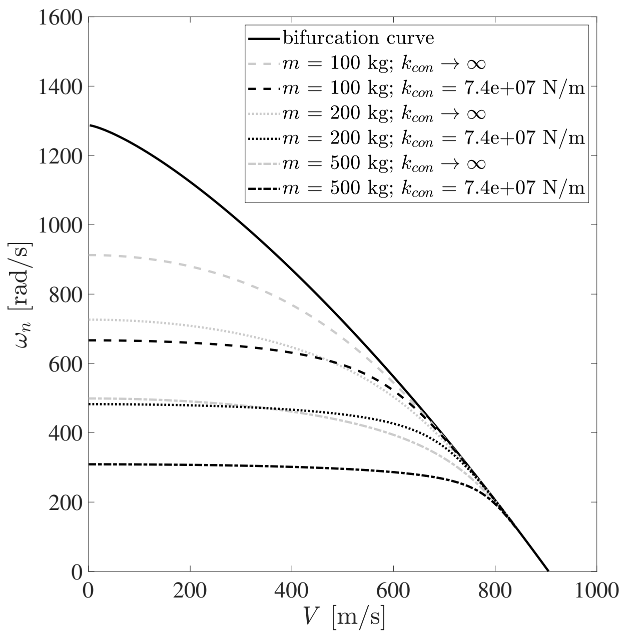

Figure 6.2: The augmented equivalent oscillator's natural frequency ω_n as a function of the point mass m and the mass's velocity V. The parameter set from Tab. (5.1) is used to plot these curves.

As it turns out, including the contact spring with finite stiffness demotes the natural frequency for every mass valuation and for every velocity; compare the dashed grey curves to their black counterparts. This change can be explained qualitatively by making a comparison to the analytical expression for the natural frequency of the elementary SDoF system: $\omega_n = \sqrt{k/m}$; decreasing the spring stiffness, which appears in the numerator of the radicand, again, reduces the natural frequency. In turn, decreasing the mass also results in an elevation of the natural frequency.

Before addressing the perturbed problem, it is pointed out that the W-coefficients in the expression for the vertical deflection field of the unperturbed beam are now defined by a different set of conditions. The four conditions that were used in the case without the contact spring read:

$$\begin{aligned} & w^{(0)\,+}\big|_{x=Vt} = w_0^{(0)}, \quad w^{(0)\,-}\big|_{x=Vt} = w_0^{(0)}, \\ & \left.\frac{\partial w^{(0)\,+}}{\partial x}\right|_{x=Vt} = \left.\frac{\partial w^{(0)\,-}}{\partial x}\right|_{x=Vt}, \\ & \left.\frac{\partial^2 w^{(0)\,+}}{\partial x^2}\right|_{x=Vt} = \left.\frac{\partial^2 w^{(0)\,-}}{\partial x^2}\right|_{x=Vt} \end{aligned} \tag{6.7}$$

in which:

$$w^{(0)\,+} = W_{A1}e^{i\left(\Omega t - k_1^A \xi\right)} + W_{A2}e^{i\left(\Omega t - k_2^A \xi\right)} + W_{B1}e^{-i\left(\Omega t + k_1^B \xi\right)} + W_{B2}e^{-i\left(\Omega t + k_2^B \xi\right)} \tag{6.8}$$

$$w^{(0)\,-} = W_{A3}e^{i\left(\Omega t - k_3^A \xi\right)} + W_{A4}e^{i\left(\Omega t - k_4^A \xi\right)} + W_{B3}e^{-i\left(\Omega t + k_3^B \xi\right)} + W_{B4}e^{-i\left(\Omega t + k_4^B \xi\right)} \tag{6.9}$$

Including the contact spring requires an additional term at the right-hand side of the first two conditions of Eq. (6.7). From Eq. (6.3), combining the second equation of the pair that constitutes the balance of forces with the continuity condition yields the following four conditions:

$$\begin{aligned} & w^{(0)\,+}\big|_{x=Vt} = w_0^{(0)} + \frac{m}{k_{con}}\frac{d^2 w_0^{(0)}}{dt^2}, \quad w^{(0)\,-}\big|_{x=Vt} = w_0^{(0)} + \frac{m}{k_{con}}\frac{d^2 w_0^{(0)}}{dt^2}, \\ & \left.\frac{\partial w^{(0)\,+}}{\partial x}\right|_{x=Vt} = \left.\frac{\partial w^{(0)\,-}}{\partial x}\right|_{x=Vt}, \quad \left.\frac{\partial^2 w^{(0)\,+}}{\partial x^2}\right|_{x=Vt} = \left.\frac{\partial^2 w^{(0)\,-}}{\partial x^2}\right|_{x=Vt} \end{aligned} \tag{6.10}$$

The mass's acceleration gives the beam an extra pull or push in the contact point via the spring. Note that $w_0^{(0)} \geq w^{(0)\,\pm}\big|_{x=Vt}$, otherwise the girder and concentrated mass would pass each other, which is not possible. Substitution of Eq. (6.8) and Eq. (6.9) in Eq. (6.10) yields for each time signature n $(= A, B)$ the following set of algebraic equations:

$$\begin{aligned} & W_{n1} + W_{n2} = W_n \left(1 - m\Omega^2/k_{con}\right) \\ & W_{n3} + W_{n4} = W_n \left(1 - m\Omega^2/k_{con}\right) \\ & k_1^n W_{n1} + k_2^n W_{n2} = k_3^n W_{n3} + k_4^n W_{n4} \\ & (k_1^n)^2 W_{n1} + (k_2^n)^2 W_{n2} = (k_3^n)^2 W_{n3} + (k_4^n)^2 W_{n4} \end{aligned} \tag{6.11}$$

The solution to the system of Eq. (6.11) reads:

$$\begin{aligned} W_{n1} &= -W_n \frac{(k_2^n - k_3^n)(k_2^n - k_4^n)}{(k_1^n + k_2^n - k_3^n - k_4^n)(k_1^n - k_2^n)} \left(1 - \frac{m\Omega^2}{k_{con}}\right) \\ W_{n2} &= +W_n \frac{(k_1^n - k_3^n)(k_1^n - k_4^n)}{(k_1^n + k_2^n - k_3^n - k_4^n)(k_1^n - k_2^n)} \left(1 - \frac{m\Omega^2}{k_{con}}\right) \\ W_{n3} &= +W_n \frac{(k_1^n - k_4^n)(k_2^n - k_4^n)}{(k_1^n + k_2^n - k_3^n - k_4^n)(k_3^n - k_4^n)} \left(1 - \frac{m\Omega^2}{k_{con}}\right) \\ W_{n4} &= -W_n \frac{(k_1^n - k_3^n)(k_2^n - k_3^n)}{(k_1^n + k_2^n - k_3^n - k_4^n)(k_3^n - k_4^n)} \left(1 - \frac{m\Omega^2}{k_{con}}\right) \end{aligned} \tag{6.12}$$

Note that the inclusion of the contact spring makes the W-coefficients a function of the excitation frequency Ω. The W-coefficients from Appendix D are retrieved for $k_{con} \to \infty$.

6.3 Analysis of the perturbed problem

The condition for parametric resonance ($V\chi = 2\Omega$) does not change, because the balance of forces at the interface exhibits the same forcing terms with the same time signatures as for the case without the contact spring (cf. Eq. (5.30)):

$$F_s^{(1)} = EI\left[\frac{\partial^3 w_h^{(1)}}{\partial x^3}\right]_{x=Vt} - EI\begin{pmatrix} D_{31}e^{it(V\chi+\Omega)} + D_{32}e^{-it(V\chi-\Omega)} + \\ D_{33}e^{it(V\chi-\Omega)} + D_{34}e^{-it(V\chi+\Omega)} \end{pmatrix} \tag{6.13}$$

$$F_s^{(1)} = -m\frac{d^2 w_0^{(1)}}{dt^2} \tag{6.14}$$

$$F_s^{(1)} = k_{con}\left(w_0^{(1)} - w_h^{(1)}\Big|_{x=Vt}\right) + k_{con}\begin{pmatrix} D_{41}e^{it(V\chi+\Omega)} + D_{42}e^{-it(V\chi-\Omega)} + \\ D_{43}e^{it(V\chi-\Omega)} + D_{44}e^{-it(V\chi+\Omega)} \end{pmatrix} \tag{6.15}$$

The C- and D-coefficients are defined in Appendix D.

6.4 The instability domain's center line

According to Fig. (6.3), the contact spring reduces the critical mass; the velocity at which parametric instability occurs decreases. In Chapter 3 a similar effect is observed for wave-induced instability; introducing a spring between the mass and beam lowers the instability domain's boundary. Unfortunately, at the moment of writing this, I am not able to provide a physical explanation for this effect in the case of parametric instability.

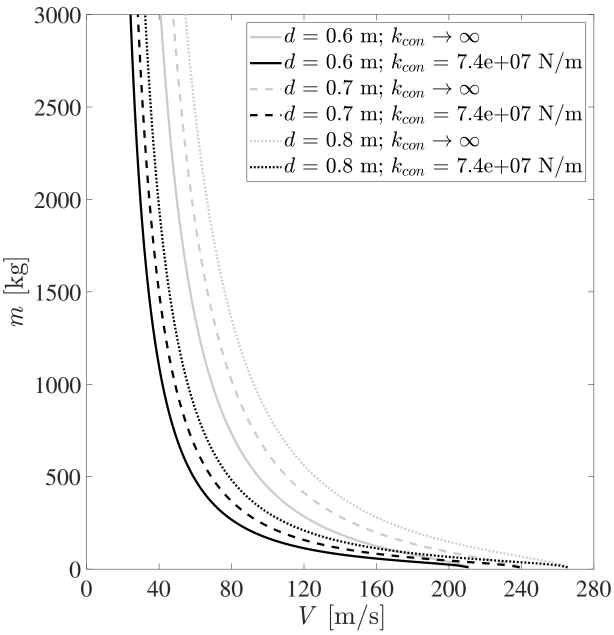

Figure 6.3: The effect of vehicle-structure interaction on the center line.

Chapter 7

Combination parametric resonance of a uniformly moving point mass connected by springs to an infinite Euler-Bernoulli beam on coupled lateral-vertical harmonically inhomogeneous foundation

Thus far, only the stability of the mass's vertical oscillations has been investigated; both wave-induced instability as well as parametric resonance were examined. But what about the lateral oscillations and the interaction with its vertical counterpart? How does an additional degree-of-freedom affect the instability zone for parametric resonance in the velocity-mass parameter space and under what conditions is this combination resonance possible? These questions are answered in this chapter by extending the method that is presented in reference [23].

7.1 Model and governing equations

The model includes a concentrated mass that moves uniformly along an infinite Euler-Bernoulli beam and is connected to this beam by a lateral and vertical contact spring. The beam itself is in both directions supported by the same harmonically inhomogeneous visco-elastic foundation in which only the elastic component varies harmonically along the x-coordinate; the damping is uniformly distributed. A stiffness coupling is created in the foundation: a displacement in one direction leads to a distributed forcing in the other direction. The second moment of area around the y- and z-axis is the same: $I_{yy} = I_{zz} = I$. See Fig. (7.1).

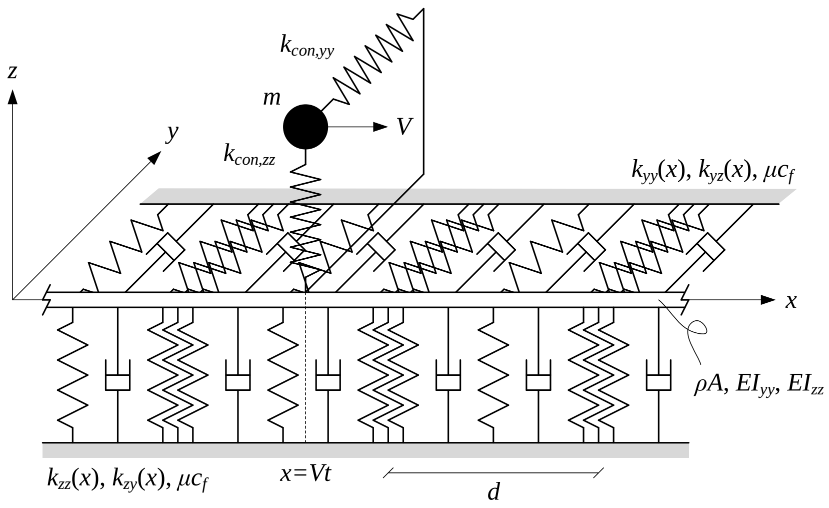

Figure 7.1: The model for investigating combination parametric resonance of a two-degrees-of-freedom one-mass oscillator that moves along an elastic guide on coupled lateral-vertical harmonically inhomogeneous visco-elastic support.

The equations that govern this model read as follows.

- The equations of motion (EoMs):

$$\rho A \frac{\partial^2 v}{\partial t^2} + EI \frac{\partial^4 v}{\partial x^4} + \mu c_f \frac{\partial v}{\partial t} + k_{yy}(x)\, v + k_{yz}(x)\, w = 0 \tag{7.1}$$

$$\rho A \frac{\partial^2 w}{\partial t^2} + EI \frac{\partial^4 w}{\partial x^4} + \mu c_f \frac{\partial w}{\partial t} + k_{zz}(x)\, w + k_{zy}(x)\, v = 0 \tag{7.2}$$

in which:

$$k_{yy}(x) = k_{f,y}\left(1 + \mu \cos(\chi x)\right) \tag{7.3}$$

$$k_{zz}(x) = k_{f,z}\left(1 + \mu \cos(\chi x)\right) \tag{7.4}$$

$$k_{yz}(x) = k_{zy}(x) = k_{f,c}\left(1 + \mu \cos(\chi x)\right) \tag{7.5}$$

- The interface conditions (ICs):

$$[v]_{x=Vt} = \left[\frac{\partial v}{\partial x}\right]_{x=Vt} = \left[\frac{\partial^2 v}{\partial x^2}\right]_{x=Vt} = 0 \tag{7.6}$$

$$[w]_{x=Vt} = \left[\frac{\partial w}{\partial x}\right]_{x=Vt} = \left[\frac{\partial^2 w}{\partial x^2}\right]_{x=Vt} = 0 \tag{7.7}$$

- The relations that constitute the balance of forces at the interface (BoFs):

$$F_{s,y} = EI \left[\frac{\partial^3 v}{\partial x^3}\right]_{x=Vt}, \quad F_{s,y} = -m \frac{d^2 v_0}{dt^2} \tag{7.8}$$

$$F_{s,z} = EI \left[\frac{\partial^3 w}{\partial x^3}\right]_{x=Vt}, \quad F_{s,z} = -m \frac{d^2 w_0}{dt^2} - mg \tag{7.9}$$

- And the spring forces/continuity conditions (CCs)[1]:

$$F_{s,y} = k_{con,yy} \left(v_0 - v|_{x=Vt} \right) \tag{7.10}$$

$$F_{s,z} = k_{con,zz} \left(w_0 - w|_{x=Vt} \right) \tag{7.11}$$

Note that $v_0 - v|_{x=Vt}$ in Eq. (7.10) is associated with the lateral contact spring being positioned along the negative y-axis—after all, a displacement of the point mass in the positive lateral direction leads to a tensile force in the lateral contact spring while positive lateral beam deflection causes the spring to compress. The reason the spring is placed along the positive y-axis in Fig. (7.1) is to maintain the figure's clarity. As to the stiffness coupling in the foundation, this is expressed by the last term on the left-hand side of Eq. (7.1) and Eq. (7.2) and model the asymmetric nature of the guide's support structure.

To come up with a solution for this system of equations and be able to investigate its stability, the same procedure as used in reference [23] is employed.

$$v = v^{(0)} + \mu v^{(1)}, \quad v_0 = v_0^{(0)} + \mu v_0^{(1)} \tag{7.12}$$

$$w = w^{(0)} + \mu w^{(1)}, \quad w_0 = w_0^{(0)} + \mu w_0^{(1)} \tag{7.13}$$

Substitution of Eq. (7.12) and Eq. (7.13) in Eq. (7.1) to Eq. (7.11) while omitting the mass's dead weight mg and collecting terms proportional to μ^0, yields the equations that describe the unperturbed system:

$$\rho A \frac{\partial^2 v^{(0)}}{\partial t^2} + EI \frac{\partial^4 v^{(0)}}{\partial x^4} + k_{f,y} v^{(0)} + k_{f,c} w^{(0)} = 0 \tag{7.14}$$

$$\rho A \frac{\partial^2 w^{(0)}}{\partial t^2} + EI \frac{\partial^4 w^{(0)}}{\partial x^4} + k_{f,z} w^{(0)} + k_{f,c} v^{(0)} = 0 \tag{7.15}$$

$$\left[v^{(0)} \right]_{x=Vt} = \left[\frac{\partial v^{(0)}}{\partial x} \right]_{x=Vt} = \left[\frac{\partial^2 v^{(0)}}{\partial x^2} \right]_{x=Vt} = 0 \tag{7.16}$$

$$\left[w^{(0)} \right]_{x=Vt} = \left[\frac{\partial w^{(0)}}{\partial x} \right]_{x=Vt} = \left[\frac{\partial^2 w^{(0)}}{\partial x^2} \right]_{x=Vt} = 0 \tag{7.17}$$

$$F_{s,y}^{(0)} = EI \left[\frac{\partial^3 v^{(0)}}{\partial x^3} \right]_{x=Vt}, \quad F_{s,y}^{(0)} = -m \frac{d^2 v_0^{(0)}}{dt^2} \tag{7.18}$$

$$F_{s,z}^{(0)} = EI \left[\frac{\partial^3 w^{(0)}}{\partial x^3} \right]_{x=Vt}, \quad F_{s,z}^{(0)} = -m \frac{d^2 w_0^{(0)}}{dt^2} \tag{7.19}$$

$$F_{s,y}^{(0)} = k_{con,yy} \left(v_0^{(0)} - v^{(0)}\big|_{x=Vt} \right) \tag{7.20}$$

$$F_{s,z}^{(0)} = k_{con,zz} \left(w_0^{(0)} - w^{(0)}\big|_{x=Vt} \right) \tag{7.21}$$

The equations that govern the perturbed system are obtained by collecting terms propor-

[1]The motivation for why these two labels are interchangeable is provided in Appendix E.

tional to μ^1:

$$\begin{aligned}\rho A\frac{\partial^2 v^{(1)}}{\partial t^2} + EI\frac{\partial^4 v^{(1)}}{\partial x^4} + k_{f,y}v^{(1)} + k_{f,c}w^{(1)} = \\ - c_f\frac{\partial v^{(0)}}{\partial t} - k_{f,y}v^{(0)}\cos(\chi x) - k_{f,c}w^{(0)}\cos(\chi x)\end{aligned} \tag{7.22}$$

$$\begin{aligned}\rho A\frac{\partial^2 w^{(1)}}{\partial t^2} + EI\frac{\partial^4 w^{(1)}}{\partial x^4} + k_{f,z}w^{(1)} + k_{f,c}v^{(1)} = \\ - c_f\frac{\partial w^{(0)}}{\partial t} - k_{f,z}w^{(0)}\cos(\chi x) - k_{f,c}v^{(0)}\cos(\chi x)\end{aligned} \tag{7.23}$$

$$\left[v^{(1)}\right]_{x=Vt} = \left[\frac{\partial v^{(1)}}{\partial x}\right]_{x=Vt} = \left[\frac{\partial^2 v^{(1)}}{\partial x^2}\right]_{x=Vt} = 0 \tag{7.24}$$

$$\left[w^{(1)}\right]_{x=Vt} = \left[\frac{\partial w^{(1)}}{\partial x}\right]_{x=Vt} = \left[\frac{\partial^2 w^{(1)}}{\partial x^2}\right]_{x=Vt} = 0 \tag{7.25}$$

$$F_{s,y}^{(1)} = EI\left[\frac{\partial^3 v^{(1)}}{\partial x^3}\right]_{x=Vt}, \quad F_{s,y}^{(1)} = -m\frac{d^2 v_0^{(1)}}{dt^2} \tag{7.26}$$

$$F_{s,z}^{(1)} = EI\left[\frac{\partial^3 w^{(1)}}{\partial x^3}\right]_{x=Vt}, \quad F_{s,z}^{(1)} = -m\frac{d^2 w_0^{(1)}}{dt^2} \tag{7.27}$$

$$F_{s,y}^{(1)} = k_{con,yy}\left(v_0^{(1)} - v^{(1)}\big|_{x=Vt}\right) \tag{7.28}$$

$$F_{s,z}^{(1)} = k_{con,zz}\left(w_0^{(1)} - w^{(1)}\big|_{x=Vt}\right) \tag{7.29}$$

7.2 Solution to the unperturbed problem

This section is subdivided into four subsections. The first sets out how the 2DoF equivalent system's stiffnesses and characteristic equation are derived by applying the method of Chapter 3 (reference [15]) to the coupled PDEs of Eq. (7.14) and Eq. (7.15). To account for the effect of the contact springs, the second subsection explains how these springs are incorporated in the definitions of the equivalent stiffnesses. The third subsection presents the equivalent system's natural frequencies as functions of the point mass and the velocity with which this mass moves. Finally, based on the equivalent system, solutions are proposed for the vibrations of the point mass and the deflection fields of the beam.

7.2.1 Derivation of the characteristic equation

The equations of motion:

$$\rho A\frac{\partial^2 v^{(0)}}{\partial t^2} + EI\frac{\partial^4 v^{(0)}}{\partial x^4} + k_{f,y}v^{(0)} + k_{f,c}w^{(0)} = -\left(m\frac{d^2 v_0^{(0)}}{dt^2} + P_y\right)\delta(x - Vt) \tag{7.30}$$

$$\rho A\frac{\partial^2 w^{(0)}}{\partial t^2} + EI\frac{\partial^4 w^{(0)}}{\partial x^4} + k_{f,z}w^{(0)} + k_{f,c}v^{(0)} = -\left(m\frac{d^2 w_0^{(0)}}{dt^2} + P_z\right)\delta(x - Vt) \tag{7.31}$$

and continuity conditions:

$$v^{(0)}\big|_{x=Vt} = v_0^{(0)} \tag{7.32}$$

$$w^{(0)}\big|_{x=Vt} = w_0^{(0)} \tag{7.33}$$

Expressing the EoMs in the moving reference frame while using Eq. (7.32) and Eq. (7.33):

$$\begin{aligned}\rho A\left(-\frac{\partial}{\partial\xi}V+\frac{\partial}{\partial t}\right)^2 v^{(0)} + EI\frac{\partial^4 v^{(0)}}{\partial\xi^4} + \\ k_{f,y}v^{(0)} + k_{f,c}w^{(0)} = -\left(m\frac{\partial^2 v^{(0)}}{\partial t^2} + P_y\right)\delta\left(\xi\right)\end{aligned} \tag{7.34}$$

$$\begin{aligned}\rho A\left(-\frac{\partial}{\partial\xi}V+\frac{\partial}{\partial t}\right)^2 w^{(0)} + EI\frac{\partial^4 w^{(0)}}{\partial\xi^4} + \\ k_{f,z}w^{(0)} + k_{f,c}v^{(0)} = -\left(m\frac{\partial^2 w^{(0)}}{\partial t^2} + P_z\right)\delta\left(\xi\right)\end{aligned} \tag{7.35}$$

and subsequently transforming them to the Fourier-Laplace domain:

$$\rho A(s-ikV)^2 v_{k,s}^{(0)} + EIk^4 v_{k,s}^{(0)} + k_{f,y}v_{k,s}^{(0)} + k_{f,c}w_{k,s}^{(0)} = -\left(ms^2\, v_s^{(0)}\big|_{\xi=0} + \frac{P_y}{s}\right) \tag{7.36}$$

$$\rho A(s-ikV)^2 w_{k,s}^{(0)} + EIk^4 w_{k,s}^{(0)} + k_{f,z}w_{k,s}^{(0)} + k_{f,c}v_{k,s}^{(0)} = -\left(ms^2\, w_s^{(0)}\big|_{\xi=0} + \frac{P_z}{s}\right) \tag{7.37}$$

Combining Eq. (7.36) and Eq. (7.37) in vector-matrix format:

$$\begin{bmatrix} D_y\left(k,s\right) & k_{f,c} \\ k_{f,c} & D_z\left(k,s\right)\end{bmatrix}\begin{bmatrix} v_{k,s}^{(0)} \\ w_{k,s}^{(0)}\end{bmatrix} = -\begin{bmatrix} ms^2\, v_s^{(0)}\Big|_{\xi=0} + P_y/s \\ ms^2\, w_s^{(0)}\Big|_{\xi=0} + P_z/s\end{bmatrix} \tag{7.38}$$

with:

$$D_y\left(k,s\right) = \rho A(s-ikV)^2 + EIk^4 + k_{f,y} \tag{7.39}$$

$$D_z\left(k,s\right) = \rho A(s-ikV)^2 + EIk^4 + k_{f,z} \tag{7.40}$$

The lateral and vertical displacement field of the unperturbed beam model in the Fourier-Laplace domain are respectively defined as:

$$v_{k,s}^{(0)} = \frac{-D_z}{D_yD_z - k_{f,c}^2}\left(ms^2\, v_s^{(0)}\big|_{\xi=0} + \frac{P_y}{s}\right) + \frac{k_{f,c}}{D_yD_z - k_{f,c}^2}\left(ms^2\, w_s^{(0)}\big|_{\xi=0} + \frac{P_z}{s}\right) \tag{7.41}$$

$$w_{k,s}^{(0)} = \frac{k_{f,c}}{D_yD_z - k_{f,c}^2}\left(ms^2\, v_s^{(0)}\big|_{\xi=0} + \frac{P_y}{s}\right) + \frac{-D_y}{D_yD_z - k_{f,c}^2}\left(ms^2\, w_s^{(0)}\big|_{\xi=0} + \frac{P_z}{s}\right) \tag{7.42}$$

Back-transformation to the Laplace domain:

$$\begin{aligned} v_s^{(0)}(\xi,s) = \mathcal{F}^{-1}\left\{v_{k,s}^{(0)}(k,s)\right\} = -\left(ms^2 v_s^{(0)}\big|_{\xi=0} + \frac{P_y}{s}\right)\frac{1}{2\pi}\int\limits_{-\infty}^{\infty}\frac{D_z e^{ik\xi}}{D_y D_z - k_{f,c}^2}dk \\ + \left(ms^2 w_s^{(0)}\big|_{\xi=0} + \frac{P_z}{s}\right)\frac{k_{f,c}}{2\pi}\int\limits_{-\infty}^{\infty}\frac{e^{ik\xi}}{D_y D_z - k_{f,c}^2}dk \end{aligned} \tag{7.43}$$

$$\begin{aligned} w_s^{(0)}(\xi,s) = \mathcal{F}^{-1}\left\{w_{k,s}^{(0)}(k,s)\right\} = \left(ms^2 v_s^{(0)}\big|_{\xi=0} + \frac{P_y}{s}\right)\frac{k_{f,c}}{2\pi}\int\limits_{-\infty}^{\infty}\frac{e^{ik\xi}}{D_y D_z - k_{f,c}^2}dk \\ - \left(ms^2 w_s^{(0)}\big|_{\xi=0} + \frac{P_z}{s}\right)\frac{1}{2\pi}\int\limits_{-\infty}^{\infty}\frac{D_y e^{ik\xi}}{D_y D_z - k_{f,c}^2}dk \end{aligned} \tag{7.44}$$

and setting $\xi = 0$ yields:

$$\begin{aligned} v_s^{(0)}(0,s) = -\left(ms^2 v_s^{(0)}\big|_{\xi=0} + \frac{P_y}{s}\right)\frac{1}{2\pi}\int\limits_{-\infty}^{\infty}\frac{D_z}{D_y D_z - k_{f,c}^2}dk \\ + \left(ms^2 w_s^{(0)}\big|_{\xi=0} + \frac{P_z}{s}\right)\frac{k_{f,c}}{2\pi}\int\limits_{-\infty}^{\infty}\frac{1}{D_y D_z - k_{f,c}^2}dk \end{aligned} \tag{7.45}$$

$$\begin{aligned} w_s^{(0)}(0,s) = \left(ms^2 v_s^{(0)}\big|_{\xi=0} + \frac{P_y}{s}\right)\frac{k_{f,c}}{2\pi}\int\limits_{-\infty}^{\infty}\frac{1}{D_y D_z - k_{f,c}^2}dk \\ - \left(ms^2 w_s^{(0)}\big|_{\xi=0} + \frac{P_z}{s}\right)\frac{1}{2\pi}\int\limits_{-\infty}^{\infty}\frac{D_y}{D_y D_z - k_{f,c}^2}dk \end{aligned} \tag{7.46}$$

Combining Eq. (7.45) and Eq. (7.46) in vector-matrix format:

$$\begin{bmatrix} 1+\psi_1 ms^2 & -k_{f,c}\psi_2 ms^2 \\ -k_{f,c}\psi_2 ms^2 & 1+\psi_3 ms^2 \end{bmatrix}\begin{bmatrix} v_s^{(0)} \\ w_s^{(0)} \end{bmatrix}_{\xi=0} = \frac{P_y}{s}\begin{bmatrix} -\psi_1 \\ k_{f,c}\psi_2 \end{bmatrix} + \frac{P_z}{s}\begin{bmatrix} k_{f,c}\psi_2 \\ -\psi_3 \end{bmatrix} \tag{7.47}$$

with:

$$\begin{aligned} \psi_1(s) = \frac{1}{2\pi}\int\limits_{-\infty}^{\infty}\frac{D_z}{D_y D_z - k_{f,c}^2}dk = \\ i\sum_{m=1}^{M}\mathrm{Res}\left[\frac{D_z}{D_y D_z - k_{f,c}^2}\right]_{k=k_m} + \frac{i}{2}\sum_{n=1}^{N}\mathrm{Res}\left[\frac{D_z}{D_y D_z - k_{f,c}^2}\right]_{k=k_n} \end{aligned} \tag{7.48}$$

$$\begin{aligned} \psi_2(s) = \frac{1}{2\pi}\int\limits_{-\infty}^{\infty}\frac{1}{D_y D_z - k_{f,c}^2}dk = \\ i\sum_{m=1}^{M}\mathrm{Res}\left[\frac{1}{D_y D_z - k_{f,c}^2}\right]_{k=k_m} + \frac{i}{2}\sum_{n=1}^{N}\mathrm{Res}\left[\frac{1}{D_y D_z - k_{f,c}^2}\right]_{k=k_n} \end{aligned} \tag{7.49}$$

$$\begin{aligned}
&\psi_3(s) = \frac{1}{2\pi}\int_{-\infty}^{\infty} \frac{D_y}{D_y D_z - k_{f,c}^2} dk = \\
&i\sum_{m=1}^{M} \mathrm{Res}\left[\frac{D_y}{D_y D_z - k_{f,c}^2}\right]_{k=k_m} + \frac{i}{2}\sum_{n=1}^{N} \mathrm{Res}\left[\frac{D_y}{D_y D_z - k_{f,c}^2}\right]_{k=k_n}
\end{aligned} \tag{7.50}$$

k_m are the complex poles of the integrand functions that possess a positive imaginary part and k_n are the integrands' real poles; that is, the roots of:

$$D_y(k,s)\, D_z(k,s) - k_{f,c}^2 = 0 \tag{7.51}$$

Considering the homogeneous equivalent of Eq. (7.47)—$P_y = P_z = 0$—the following system of algebraic equations emerges:

$$\left(\mathbf{I} + \boldsymbol{\chi}_{eq}^{-1}\mathbf{M}s^2\right)\mathbf{v}_s^{(0)}\Big|_{\xi=0} = \mathbf{0} \Rightarrow \left(\mathbf{M}s^2 + \boldsymbol{\chi}_{eq}\right)\mathbf{v}_s^{(0)}\Big|_{\xi=0} = \mathbf{0} \tag{7.52}$$

in which:

$$\begin{aligned}
&\mathbf{I} = \begin{bmatrix} 1 & 0 \\ 0 & 1 \end{bmatrix}, \quad \boldsymbol{\chi}_{eq}^{-1} = \begin{bmatrix} \psi_1 & -k_{f,c}\psi_2 \\ -k_{f,c}\psi_2 & \psi_3 \end{bmatrix}, \quad \mathbf{M} = \begin{bmatrix} m & 0 \\ 0 & m \end{bmatrix}, \\
&\mathbf{v}_s^{(0)} = \begin{bmatrix} v_s^{(0)} \\ w_s^{(0)} \end{bmatrix}, \quad \mathbf{0} = \begin{bmatrix} 0 \\ 0 \end{bmatrix}
\end{aligned} \tag{7.53}$$

The equivalent stiffness matrix reads as:

$$\boldsymbol{\chi}_{eq} = \begin{bmatrix} \chi_{yy} & \chi_{yz} \\ \chi_{zy} & \chi_{zz} \end{bmatrix} \tag{7.54}$$

with:

$$\chi_{yy}(s) = \frac{\psi_3}{\psi_1\psi_3 - k_{f,c}^2\psi_2^2} \tag{7.55}$$

$$\chi_{zz}(s) = \frac{\psi_1}{\psi_1\psi_3 - k_{f,c}^2\psi_2^2} \tag{7.56}$$

$$\chi_{yz}(s) = \chi_{zy}(s) = \frac{k_{f,c}\psi_2}{\psi_1\psi_3 - k_{f,c}^2\psi_2^2} \tag{7.57}$$

Eq. (7.52) has a non-trivial solution if the determinant of its coefficient matrix vanishes; the ensuing characteristic equation ultimately reads:

$$s^4 + s^2\left(\frac{\chi_{yy}}{m} + \frac{\chi_{zz}}{m}\right) + \frac{\chi_{yy}\chi_{zz}}{m^2} - \frac{\chi_{yz}\chi_{zy}}{m^2} = 0 \tag{7.58}$$

Reducing the Laplace parameter s to $i\omega_n$ yields:

$$\omega_n^4 - \omega_n^2\left(\omega_{yy}^2 + \omega_{zz}^2\right) + \omega_{yy}^2\omega_{zz}^2 - \omega_{yz}^4 = 0 \tag{7.59}$$

in which the partial frequencies are defined as:

$$\omega_{yy}^2(\omega_n) = \frac{\chi_{yy}(\omega_n)}{m}, \quad \omega_{zz}^2(\omega_n) = \frac{\chi_{zz}(\omega_n)}{m}, \quad \omega_{yz}^2(\omega_n) = \frac{\sqrt{\chi_{yz}(\omega_n)\chi_{zy}(\omega_n)}}{m} \tag{7.60}$$

Equating $k_{f,c}$ in Eq. (7.55) and Eq. (7.56) to zero returns the equivalent stiffness definition from Chapter 3:

$$\chi_{yy}(s) = \frac{1}{\psi_1} = \left(\frac{1}{2\pi}\int_{-\infty}^{\infty}\frac{1}{D_y(k,s)}dk\right)^{-1} \tag{7.61}$$

$$\chi_{zz}(s) = \frac{1}{\psi_3} = \left(\frac{1}{2\pi}\int_{-\infty}^{\infty}\frac{1}{D_z(k,s)}dk\right)^{-1} \tag{7.62}$$

$$\chi_{yz}(s) = \chi_{zy}(s) = 0 \tag{7.63}$$

Compare Eq. (7.61) and Eq. (7.62) to Eq. (3.14) with $c_f = 0$. After all, removing the coupling results in a beam model that is along the x-axis in both the lateral y- and vertical z-direction identical to the model from Chapter 3.

7.2.2 Augmenting the characteristic equation

Now that the equivalent stiffnesses are defined, the contact springs are taken into account by attaching them in series to the equivalent lateral and vertical spring; the augmented equivalent stiffnesses are designated by a double prime: $\chi''_{yy}, \chi''_{zz}, \chi''_{yz}$ and χ''_{zy}. To define these new equivalent stiffnesses, the displacement method is applied in the Laplace domain. After all, Eq. (7.55) to Eq. (7.57) are already defined in the Laplace domain. The following system is searched for:

$$\mathbf{F}_s^{(0)} = \boldsymbol{\chi}''\mathbf{v}_0^{(0)} \tag{7.64}$$

in which:

$$\mathbf{F}_s^{(0)} = \begin{bmatrix} F_{s,y}^{(0)} \\ F_{s,z}^{(0)} \end{bmatrix}, \quad \boldsymbol{\chi}'' = \begin{bmatrix} \chi''_{yy} & \chi''_{yz} \\ \chi''_{zy} & \chi''_{zz} \end{bmatrix}, \quad \mathbf{v}_0^{(0)} = \begin{bmatrix} v_0^{(0)} \\ w_0^{(0)} \end{bmatrix} \tag{7.65}$$

The superscript '(0)' indicates that the unperturbed problem is addressed while the subscript '0' relates to the degrees-of-freedom of the point mass; the subscript 's' indicates to the spring force in the equivalent system. Making use of the spring model depicted in Fig. (7.2)—representing the vertical part of the equivalent system—the series configuration requires the spring forces to be equal to one another; this follows from vertical force equilibrium.

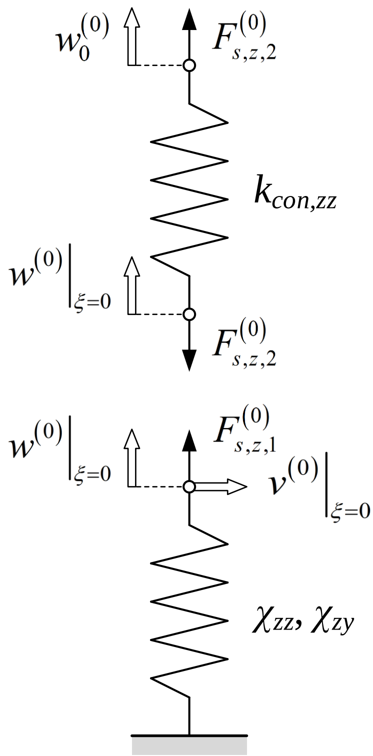

Figure 7.2: The spring model by means of which an expression for the vertical spring force $F_{s,z}$ is derived.

The spring forces read:

$$F_{s,z,1}^{(0)} = \chi_{zz}\, w^{(0)}\big|_{\xi=0} + \chi_{zy}\, v^{(0)}\big|_{\xi=0} \tag{7.66}$$

$$F_{s,z,2}^{(0)} = k_{con,zz}\left(w_0^{(0)} - w^{(0)}\big|_{\xi=0}\right) \tag{7.67}$$

An expression for the vertical beam deflection at the contact point is derived by equating these forces:

$$w^{(0)}\big|_{\xi=0} = \frac{k_{con,zz}}{k_{con,zz} + \chi_{zz}} w_0^{(0)} - \frac{\chi_{zy}}{k_{con,zz} + \chi_{zz}} v^{(0)}\big|_{\xi=0} \tag{7.68}$$

Back-substitution in Eq. (7.67) yields:

$$F_{s,z}^{(0)} = F_{s,z,1}^{(0)} = F_{s,z,2}^{(0)} = \frac{k_{con,zz}\chi_{zz}}{k_{con,zz} + \chi_{zz}} w_0^{(0)} + \frac{k_{con,zz}\chi_{zy}}{k_{con,zz} + \chi_{zz}} v^{(0)}\big|_{\xi=0} \tag{7.69}$$

The same procedure yields a similar expression for the lateral spring force:

$$F_{s,y}^{(0)} = \frac{k_{con,yy}\chi_{yy}}{k_{con,yy} + \chi_{yy}} v_0^{(0)} + \frac{k_{con,yy}\chi_{yz}}{k_{con,yy} + \chi_{yy}} w^{(0)}\big|_{\xi=0} \tag{7.70}$$

To attain the format of Eq. (7.64), the second term at the right-hand side of Eq. (7.69) and Eq. (7.70) needs to be expressed in terms of the mass's displacement instead of the beam deflection at the contact point. To this end, the continuity conditions of Eq. (7.20) and Eq. (7.21) are used:

$$F_{s,y}^{(0)} = k_{con,yy}\left(v_0^{(0)} - v^{(0)}\big|_{\xi=0}\right) \Rightarrow v^{(0)}\big|_{\xi=0} = v_0^{(0)} - F_{s,y}^{(0)}/k_{con,yy} \tag{7.71}$$

$$F_{s,z}^{(0)} = k_{con,zz}\left(w_0^{(0)} - w^{(0)}\big|_{\xi=0}\right) \Rightarrow w^{(0)}\big|_{\xi=0} = w_0^{(0)} - F_{s,z}^{(0)}/k_{con,zz} \tag{7.72}$$

Substitution in Eq. (7.69) and Eq. (7.70) gives:

$$F_{s,y}^{(0)} + \frac{k_{con,yy}\chi_{yz}}{k_{con,zz}\left(k_{con,yy}+\chi_{yy}\right)}F_{s,z}^{(0)} = \frac{k_{con,yy}\chi_{yy}}{k_{con,yy}+\chi_{yy}}v_0^{(0)} + \frac{k_{con,yy}\chi_{yz}}{k_{con,yy}+\chi_{yy}}w_0^{(0)} \tag{7.73}$$

$$F_{s,z}^{(0)} + \frac{k_{con,zz}\chi_{zy}}{k_{con,yy}\left(k_{con,zz}+\chi_{zz}\right)}F_{s,y}^{(0)} = \frac{k_{con,zz}\chi_{zz}}{k_{con,zz}+\chi_{zz}}w_0^{(0)} + \frac{k_{con,zz}\chi_{zy}}{k_{con,zz}+\chi_{zz}}v_0^{(0)} \tag{7.74}$$

In vector-matrix format:

$$\begin{bmatrix} 1 & \chi'_{yz}/k_{con,zz} \\ \chi'_{zy}/k_{con,yy} & 1 \end{bmatrix}\begin{bmatrix} F_{s,y}^{(0)} \\ F_{s,z}^{(0)} \end{bmatrix} = \begin{bmatrix} \chi'_{yy} & \chi'_{yz} \\ \chi'_{zy} & \chi'_{zz} \end{bmatrix}\begin{bmatrix} v_0^{(0)} \\ w_0^{(0)} \end{bmatrix} \tag{7.75}$$

with:

$$\begin{aligned} \chi'_{yy} &= \frac{k_{con,yy}\chi_{yy}}{k_{con,yy}+\chi_{yy}}, \quad \chi'_{yz} = \frac{k_{con,yy}\chi_{yz}}{k_{con,yy}+\chi_{yy}}, \\ \chi'_{zy} &= \frac{k_{con,zz}\chi_{zy}}{k_{con,zz}+\chi_{zz}}, \quad \chi'_{zz} = \frac{k_{con,zz}\chi_{zz}}{k_{con,zz}+\chi_{zz}} \end{aligned} \tag{7.76}$$

Looking at Eq. (7.64), the stiffness matrix's entries can now readily be inferred from Eq. (7.75); the effective stiffnesses are defined as:

$$\chi''_{yy} = \frac{k_{con,yy}k_{con,zz}\chi'_{yy} - k_{con,yy}\chi'_{yz}\chi'_{zy}}{k_{con,yy}k_{con,zz} - \chi'_{yz}\chi'_{zy}} \tag{7.77}$$

$$\chi''_{zz} = \frac{k_{con,yy}k_{con,zz}\chi'_{zz} - k_{con,zz}\chi'_{yz}\chi'_{zy}}{k_{con,yy}k_{con,zz} - \chi'_{yz}\chi'_{zy}} \tag{7.78}$$

$$\chi''_{yz} = \frac{k_{con,yy}k_{con,zz}\chi'_{yz} - k_{con,yy}\chi'_{yz}\chi'_{zz}}{k_{con,yy}k_{con,zz} - \chi'_{yz}\chi'_{zy}} \tag{7.79}$$

$$\chi''_{zy} = \frac{k_{con,yy}k_{con,zz}\chi'_{zy} - k_{con,zz}\chi'_{yy}\chi'_{zy}}{k_{con,yy}k_{con,zz} - \chi'_{yz}\chi'_{zy}} \tag{7.80}$$

Note how the original equivalent stiffnesses—Eq. (7.55) to Eq. (7.57)—are retrieved when the stiffnesses of the contact springs go to infinity:

$$k_{con,yy} \to \infty,\ k_{con,zz} \to \infty \Rightarrow \chi''_{yy} = \chi_{yy},\ \chi''_{zz} = \chi_{zz},\ \chi''_{yz} = \chi_{yz},\ \chi''_{zy} = \chi_{zy} \tag{7.81}$$

The augmented characteristic equation is now defined by Eq. (7.59) with the partial frequencies from Eq. (7.60) exhibiting the effective stiffnesses defined by Eq. (7.77) to Eq. (7.80).

7.2.3 The natural frequencies

Using the following parameter set:

$\rho = 7849\ \mathrm{kg\,m^{-3}}$	$A = 7.687 \times 10^{-3}\ \mathrm{m^2}$	$I = 3.055 \times 10^{-5}\ \mathrm{m^4}$
$E = 2 \times 10^{11}\ \mathrm{N\,m^{-2}}$	$k_{f,z} = 1 \times 10^{8}\ \mathrm{N\,m^{-2}}$	$k_{f,y} = 1.2 \times k_{f,z}$
$k_{f,c} = 0.5 \times k_{f,z}$	$k_{con,yy} = 7.4 \times 10^{7}\ \mathrm{N\,m^{-1}}$	$k_{con,zz} = 7.4 \times 10^{7}\ \mathrm{N\,m^{-1}}$

Table 7.1: Parameter set for computing the natural frequencies and center lines.

characteristic Eq. (7.59) is solved numerically as outlined in Chapter 5. The result is presented in Fig. (7.3).

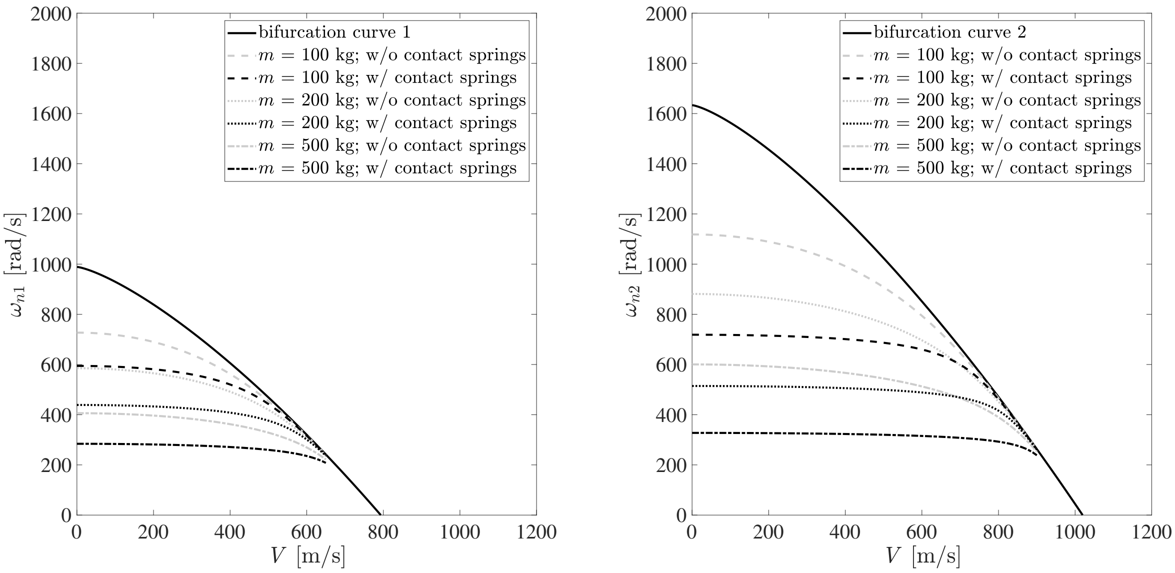

Figure 7.3: The first and second natural frequency of the equivalent 2DoF system as functions of the point mass m and the mass's velocity V.

To be able to trace the bifurcation curves, the beam's dispersion relation needs to be derived first. This relation dictates with which angular frequency and wavenumber waves are dispersed in the beam. Substituting the following assumed waveforms:

$$v^{(0)}(x,t) = Ve^{i(\omega t - kx)}, \quad w^{(0)}(x,t) = We^{i(\omega t - kx)} \tag{7.82}$$

in Eq. (7.14) and Eq. (7.15) and requiring the determinant of the ensuing coefficient matrix to vanish yields the following dispersion relation:

$$\left(-\omega^2 \rho A + k^4 EI + k_{f,y}\right)\left(-\omega^2 \rho A + k^4 EI + k_{f,z}\right) - k_{f,c}^2 = 0 \tag{7.83}$$

Solving Eq. (7.83) for the angular frequency, the dispersion curves are then described by:

$$\omega_1 = \pm\sqrt{k^4 \frac{EI}{\rho A} + \omega_{0-}^2}, \quad \omega_2 = \pm\sqrt{k^4 \frac{EI}{\rho A} + \omega_{0+}^2} \tag{7.84}$$

in which the cut-off frequencies are defined as:

$$\omega_{0\pm}^2 = \frac{k_{f,y} + k_{f,z} \pm \sqrt{4k_{f,c}^2 + \left(k_{f,y} - k_{f,z}\right)^2}}{2\rho A} \tag{7.85}$$

Eq. (7.84) is plotted in Fig. (7.4). Note how the dispersion curves converge to each other for large wavenumbers k. That is because the bending ($\propto k^4$) dominates at high k and the influence of the foundation ($\propto k^0$) is negligible. As the bending stiffness EI is the same in both the lateral and vertical direction, the dispersion curves overlap at high k; cf. Eq. (7.84).

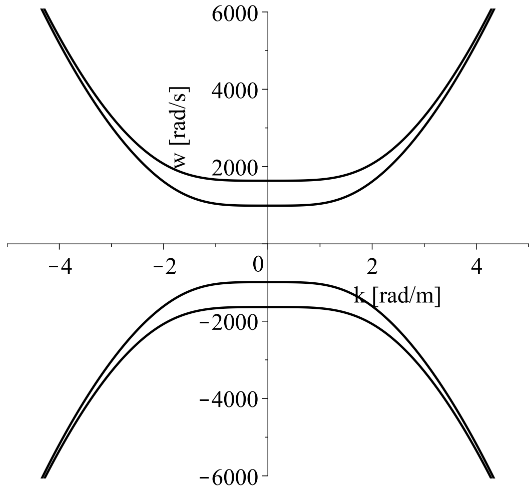

Figure 7.4: Dispersion curves for flexural waves in the Euler-Bernoulli beam on lateral and vertical homogeneous elastic foundation.

The bifurcation curves are now determined in exactly the same manner as described in Chapter 5. Interestingly, as for the beam model from Chapter 5, the dispersion relation is hidden within the characteristic equation that defines the natural frequencies of the equivalent system; looking at Eq. (7.51)—in which s is replaced by $i\omega_n$—one can see the resemblance to Eq. (7.83) combined with Eq. (5.18), though in the former case the assumed waveform exhibits a phase with different signage: $\omega t + kx$ instead of $\omega t - kx$. This observation hints to why the solid curves of Fig. (7.3) are referred to as 'bifurcation' curves; investigating how the wavenumber roots of Eq. (7.51) behave in the complex plane as functions of the velocity and excitation (natural) frequency, two out of eight complex k's transform into real numbers once the first bifurcation curve is exceeded. Two additional roots become real once the V-Ω pair goes beyond the second bifurcation curve. Hence, in case the improper integrals of Eq. (7.48) to Eq. (7.50) are evaluated by means of the contour integration method, a contour that is indented along the real axis needs to be employed so as to be able to calculate the second natural frequency beyond the first bifurcation curve [1].

Recall that we are only interested in the non-damped (or sub-critical) motion of the point mass—motion that disperses evanescent waves in the beam and not harmonic ones; the latter would extract energy from the oscillating point mass, effectively damping its motion—which requires to make use of those second natural frequencies that are enclosed by the first bifurcation curve when computing the instability domains' center lines associated with (combination) parametric resonance. After all, as for the vertical-only beam model from Chapter 5, once the kinematic invariant passes the bifurcation curve, anomalous Doppler waves (harmonic waves) are generated, which causes wave-induced instability [13]; a form of instability that is not the focus of this chapter.

7.2.4 The solution

The lateral and vertical displacements of the point mass are described by the general expression for the motion of the undamped freely vibrating 2DoF system:

$$v_0^{(0)}(t) = V_A e^{i\omega_{n1}t} + V_B e^{-i\omega_{n1}t} + V_C e^{i\omega_{n2}t} + V_D e^{-i\omega_{n2}t} \tag{7.86}$$

$$w_0^{(0)}(t) = W_A e^{i\omega_{n1}t} + W_B e^{-i\omega_{n1}t} + W_C e^{i\omega_{n2}t} + W_D e^{-i\omega_{n2}t} \tag{7.87}$$

The natural frequencies are derived from Eq. (7.59)—see Fig. (7.3)—and the coefficients are determined by the four initial conditions of the concentrated mass once the ratios between these coefficients are known; see section 2.4.1 of reference [14]. The expression for the lateral deflection of the right beam domain ($\xi \geq 0$) reads:

$$\begin{aligned}
&v^{(0)+}(x,t) = \\
&V_{A1}e^{i\left(\omega_{n1}t-k_1^A\xi\right)} + V_{A2}e^{i\left(\omega_{n1}t-k_2^A\xi\right)} + V_{A3}e^{i\left(\omega_{n1}t-k_3^A\xi\right)} + V_{A4}e^{i\left(\omega_{n1}t-k_4^A\xi\right)} + \\
&V_{B1}e^{-i\left(\omega_{n1}t+k_1^B\xi\right)} + V_{B2}e^{-i\left(\omega_{n1}t+k_2^B\xi\right)} + V_{B3}e^{-i\left(\omega_{n1}t+k_3^B\xi\right)} + V_{B4}e^{-i\left(\omega_{n1}t+k_4^B\xi\right)} + \\
&V_{C1}e^{i\left(\omega_{n2}t-k_1^C\xi\right)} + V_{C2}e^{i\left(\omega_{n2}t-k_2^C\xi\right)} + V_{C3}e^{i\left(\omega_{n2}t-k_3^C\xi\right)} + V_{C4}e^{i\left(\omega_{n2}t-k_4^C\xi\right)} + \\
&V_{D1}e^{-i\left(\omega_{n2}t+k_1^D\xi\right)} + V_{D2}e^{-i\left(\omega_{n2}t+k_2^D\xi\right)} + V_{D3}e^{-i\left(\omega_{n2}t+k_3^D\xi\right)} + V_{D4}e^{-i\left(\omega_{n2}t+k_4^D\xi\right)}
\end{aligned} \tag{7.88}$$

and for the left domain ($\xi \leq 0$):

$$\begin{aligned}
&v^{(0)-}(x,t) = \\
&V_{A5}e^{i\left(\omega_{n1}t-k_5^A\xi\right)} + V_{A6}e^{i\left(\omega_{n1}t-k_6^A\xi\right)} + V_{A7}e^{i\left(\omega_{n1}t-k_7^A\xi\right)} + V_{A8}e^{i\left(\omega_{n1}t-k_8^A\xi\right)} + \\
&V_{B5}e^{-i\left(\omega_{n1}t+k_5^B\xi\right)} + V_{B6}e^{-i\left(\omega_{n1}t+k_6^B\xi\right)} + V_{B7}e^{-i\left(\omega_{n1}t+k_7^B\xi\right)} + V_{B8}e^{-i\left(\omega_{n1}t+k_8^B\xi\right)} + \\
&V_{C5}e^{i\left(\omega_{n2}t-k_5^C\xi\right)} + V_{C6}e^{i\left(\omega_{n2}t-k_6^C\xi\right)} + V_{C7}e^{i\left(\omega_{n2}t-k_7^C\xi\right)} + V_{C8}e^{i\left(\omega_{n2}t-k_8^C\xi\right)} + \\
&V_{D5}e^{-i\left(\omega_{n2}t+k_5^D\xi\right)} + V_{D6}e^{-i\left(\omega_{n2}t+k_6^D\xi\right)} + V_{D7}e^{-i\left(\omega_{n2}t+k_7^D\xi\right)} + V_{D8}e^{-i\left(\omega_{n2}t+k_8^D\xi\right)}
\end{aligned} \tag{7.89}$$

The expression for the vertical deflection of the right beam domain ($\xi \geq 0$) reads:

$$\begin{aligned}
&w^{(0)+}(x,t) = \\
&W_{A1}e^{i\left(\omega_{n1}t-k_1^A\xi\right)} + W_{A2}e^{i\left(\omega_{n1}t-k_2^A\xi\right)} + W_{A3}e^{i\left(\omega_{n1}t-k_3^A\xi\right)} + W_{A4}e^{i\left(\omega_{n1}t-k_4^A\xi\right)} + \\
&W_{B1}e^{-i\left(\omega_{n1}t+k_1^B\xi\right)} + W_{B2}e^{-i\left(\omega_{n1}t+k_2^B\xi\right)} + W_{B3}e^{-i\left(\omega_{n1}t+k_3^B\xi\right)} + W_{B4}e^{-i\left(\omega_{n1}t+k_4^B\xi\right)} + \\
&W_{C1}e^{i\left(\omega_{n2}t-k_1^C\xi\right)} + W_{C2}e^{i\left(\omega_{n2}t-k_2^C\xi\right)} + W_{C3}e^{i\left(\omega_{n2}t-k_3^C\xi\right)} + W_{C4}e^{i\left(\omega_{n2}t-k_4^C\xi\right)} + \\
&W_{D1}e^{-i\left(\omega_{n2}t+k_1^D\xi\right)} + W_{D2}e^{-i\left(\omega_{n2}t+k_2^D\xi\right)} + W_{D3}e^{-i\left(\omega_{n2}t+k_3^D\xi\right)} + W_{D4}e^{-i\left(\omega_{n2}t+k_4^D\xi\right)}
\end{aligned} \tag{7.90}$$

and for the left domain ($\xi \leq 0$):

$$
\begin{aligned}
&w^{(0)-}(x,t) = \\
&W_{A5}e^{i\left(\omega_{n1}t-k_5^A\xi\right)} + W_{A6}e^{i\left(\omega_{n1}t-k_6^A\xi\right)} + W_{A7}e^{i\left(\omega_{n1}t-k_7^A\xi\right)} + W_{A8}e^{i\left(\omega_{n1}t-k_8^A\xi\right)} + \\
&W_{B5}e^{-i\left(\omega_{n1}t+k_5^B\xi\right)} + W_{B6}e^{-i\left(\omega_{n1}t+k_6^B\xi\right)} + W_{B7}e^{-i\left(\omega_{n1}t+k_7^B\xi\right)} + W_{B8}e^{-i\left(\omega_{n1}t+k_8^B\xi\right)} + \\
&W_{C5}e^{i\left(\omega_{n2}t-k_5^C\xi\right)} + W_{C6}e^{i\left(\omega_{n2}t-k_6^C\xi\right)} + W_{C7}e^{i\left(\omega_{n2}t-k_7^C\xi\right)} + W_{C8}e^{i\left(\omega_{n2}t-k_8^C\xi\right)} + \\
&W_{D5}e^{-i\left(\omega_{n2}t+k_5^D\xi\right)} + W_{D6}e^{-i\left(\omega_{n2}t+k_6^D\xi\right)} + W_{D7}e^{-i\left(\omega_{n2}t+k_7^D\xi\right)} + W_{D8}e^{-i\left(\omega_{n2}t+k_8^D\xi\right)}
\end{aligned}
\tag{7.91}
$$

How the V- and W-coefficients can be determined is outlined in Appendix F. The wavenumbers $k_{1,2,3,4,5,6,7,8}^{A,B,C,D}$ are derived from Eq. (7.83) combined with Eq. (5.18). Dealing with complex wavenumbers—the point mass's sub-critical behavior is considered—their imaginary part dictates which waves occupy the right beam domain and which ones the left beam domain: $\mathrm{Im}\left(k_{1,2,3,4}^{A,B,C,D}\right) < 0$ and $\mathrm{Im}\left(k_{5,6,7,8}^{A,B,C,D}\right) > 0$. See Chapter 2.

7.3 Analysis of the perturbed problem

In this section, the system of Eq. (7.22) to Eq. (7.29) is analyzed in order to determine under which conditions parametric resonance occurs. Substituting Eq. (7.88) to Eq. (7.91) in Eq. (7.22) and Eq. (7.23) while setting $c_f = 0$ and using Eq. (5.26), the right-hand side of the perturbed equations of motion for $x \geq Vt$ can be rewritten as:

$$
\begin{aligned}
&\rho A\frac{\partial^2 v^{(1)}}{\partial t^2} + EI\frac{\partial^4 v^{(1)}}{\partial x^4} + k_{f,y}v^{(1)} + k_{f,c}w^{(1)} = \\
&\quad -\frac{1}{2}\sum_{a=A}^{D}\sum_{b=1}^{4}\sum_{c=1}^{2}\left(k_{f,y}V_{ab} + k_{f,c}W_{ab}\right)e^{i\left(k_b^aV+\Omega_a\right)t}e^{i\left((-1)^c\chi-k_b^a\right)x}
\end{aligned}
\tag{7.92}
$$

$$
\begin{aligned}
&\rho A\frac{\partial^2 w^{(1)}}{\partial t^2} + EI\frac{\partial^4 w^{(1)}}{\partial x^4} + k_{f,z}w^{(1)} + k_{f,c}v^{(1)} = \\
&\quad -\frac{1}{2}\sum_{a=A}^{D}\sum_{b=1}^{4}\sum_{c=1}^{2}\left(k_{f,c}V_{ab} + k_{f,z}W_{ab}\right)e^{i\left(k_b^aV+\Omega_a\right)t}e^{i\left((-1)^c\chi-k_b^a\right)x}
\end{aligned}
\tag{7.93}
$$

and for $x \leq Vt$ as:

$$
\begin{aligned}
&\rho A\frac{\partial^2 v^{(1)}}{\partial t^2} + EI\frac{\partial^4 v^{(1)}}{\partial x^4} + k_{f,y}v^{(1)} + k_{f,c}w^{(1)} = \\
&\quad -\frac{1}{2}\sum_{a=A}^{D}\sum_{b=5}^{8}\sum_{c=1}^{2}\left(k_{f,y}V_{ab} + k_{f,c}W_{ab}\right)e^{i\left(k_b^aV+\Omega_a\right)t}e^{i\left((-1)^c\chi-k_b^a\right)x}
\end{aligned}
\tag{7.94}
$$

$$
\begin{aligned}
&\rho A\frac{\partial^2 w^{(1)}}{\partial t^2} + EI\frac{\partial^4 w^{(1)}}{\partial x^4} + k_{f,z}w^{(1)} + k_{f,c}v^{(1)} = \\
&\quad -\frac{1}{2}\sum_{a=A}^{D}\sum_{b=5}^{8}\sum_{c=1}^{2}\left(k_{f,c}V_{ab} + k_{f,z}W_{ab}\right)e^{i\left(k_b^aV+\Omega_a\right)t}e^{i\left((-1)^c\chi-k_b^a\right)x}
\end{aligned}
\tag{7.95}
$$

in which $\Omega_A = -\Omega_B = \omega_{n1}$ and $\Omega_C = -\Omega_D = \omega_{n2}$. The following solutions are proposed:

$$v^{(1)} = v_h^{(1)} + v_p^{(1)}, \quad w^{(1)} = w_h^{(1)} + w_p^{(1)} \tag{7.96}$$

The particular solutions for $x \geq Vt$ are defined as:

$$v_p^{(1)}(x,t) = \sum_{a=A}^{D}\sum_{b=1}^{4}\sum_{c=1}^{2} C_{abc}^{v} e^{i\left(k_b^a V + \Omega_a\right)t} e^{i\left((-1)^c \chi - k_b^a\right)x} \tag{7.97}$$

$$w_p^{(1)}(x,t) = \sum_{a=A}^{D}\sum_{b=1}^{4}\sum_{c=1}^{2} C_{abc}^{w} e^{i\left(k_b^a V + \Omega_a\right)t} e^{i\left((-1)^c \chi - k_b^a\right)x} \tag{7.98}$$

and for $x \leq Vt$:

$$v_p^{(1)}(x,t) = \sum_{a=A}^{D}\sum_{b=5}^{8}\sum_{c=1}^{2} C_{abc}^{v} e^{i\left(k_b^a V + \Omega_a\right)t} e^{i\left((-1)^c \chi - k_b^a\right)x} \tag{7.99}$$

$$w_p^{(1)}(x,t) = \sum_{a=A}^{D}\sum_{b=5}^{8}\sum_{c=1}^{2} C_{abc}^{w} e^{i\left(k_b^a V + \Omega_a\right)t} e^{i\left((-1)^c \chi - k_b^a\right)x} \tag{7.100}$$

The C-coefficients are defined in Appendix F. The system of partial differential equations that governs the homogeneous solutions $v_h^{(1)}$ and $w_h^{(1)}$ reads as follows—with $\Omega_1 = \omega_{n1}$ and $\Omega_2 = \omega_{n2}$.

- The equations of motion (EoMs):

$$\rho A \frac{\partial^2 v_h^{(1)}}{\partial t^2} + EI \frac{\partial^4 v_h^{(1)}}{\partial x^4} + k_{f,y} v_h^{(1)} + k_{f,c} w_h^{(1)} = 0 \tag{7.101}$$

$$\rho A \frac{\partial^2 w_h^{(1)}}{\partial t^2} + EI \frac{\partial^4 w_h^{(1)}}{\partial x^4} + k_{f,z} w_h^{(1)} + k_{f,c} v_h^{(1)} = 0 \tag{7.102}$$

- The interface conditions (ICs):

$$\begin{aligned}\left[v_h^{(1)}\right]_{x=Vt} &= D_{01}^{v} e^{-it(V\chi-\Omega_1)} + D_{02}^{v} e^{it(V\chi+\Omega_1)} + D_{03}^{v} e^{-it(V\chi+\Omega_1)} + D_{04}^{v} e^{it(V\chi-\Omega_1)} + \\ &D_{05}^{v} e^{-it(V\chi-\Omega_2)} + D_{06}^{v} e^{it(V\chi+\Omega_2)} + D_{07}^{v} e^{-it(V\chi+\Omega_2)} + D_{08}^{v} e^{it(V\chi-\Omega_2)}\end{aligned} \tag{7.103}$$

$$\begin{aligned}\left[w_h^{(1)}\right]_{x=Vt} &= D_{01}^{w} e^{-it(V\chi-\Omega_1)} + D_{02}^{w} e^{it(V\chi+\Omega_1)} + D_{03}^{w} e^{-it(V\chi+\Omega_1)} + D_{04}^{w} e^{it(V\chi-\Omega_1)} + \\ &D_{05}^{w} e^{-it(V\chi-\Omega_2)} + D_{06}^{w} e^{it(V\chi+\Omega_2)} + D_{07}^{w} e^{-it(V\chi+\Omega_2)} + D_{08}^{w} e^{it(V\chi-\Omega_2)}\end{aligned} \tag{7.104}$$

$$\left[\frac{\partial v_h^{(1)}}{\partial x}\right]_{x=Vt} = D_{11}^v e^{-it(V\chi-\Omega_1)} + D_{12}^v e^{it(V\chi+\Omega_1)} + D_{13}^v e^{-it(V\chi+\Omega_1)} + D_{14}^v e^{it(V\chi-\Omega_1)} + D_{15}^v e^{-it(V\chi-\Omega_2)} + D_{16}^v e^{it(V\chi+\Omega_2)} + D_{17}^v e^{-it(V\chi+\Omega_2)} + D_{18}^v e^{it(V\chi-\Omega_2)} \tag{7.105}$$

$$\left[\frac{\partial w_h^{(1)}}{\partial x}\right]_{x=Vt} = D_{11}^w e^{-it(V\chi-\Omega_1)} + D_{12}^w e^{it(V\chi+\Omega_1)} + D_{13}^w e^{-it(V\chi+\Omega_1)} + D_{14}^w e^{it(V\chi-\Omega_1)} + D_{15}^w e^{-it(V\chi-\Omega_2)} + D_{16}^w e^{it(V\chi+\Omega_2)} + D_{17}^w e^{-it(V\chi+\Omega_2)} + D_{18}^w e^{it(V\chi-\Omega_2)} \tag{7.106}$$

$$\left[\frac{\partial^2 v_h^{(1)}}{\partial x^2}\right]_{x=Vt} = D_{21}^v e^{-it(V\chi-\Omega_1)} + D_{22}^v e^{it(V\chi+\Omega_1)} + D_{23}^v e^{-it(V\chi+\Omega_1)} + D_{24}^v e^{it(V\chi-\Omega_1)} + D_{25}^v e^{-it(V\chi-\Omega_2)} + D_{26}^v e^{it(V\chi+\Omega_2)} + D_{27}^v e^{-it(V\chi+\Omega_2)} + D_{28}^v e^{it(V\chi-\Omega_2)} \tag{7.107}$$

$$\left[\frac{\partial^2 w_h^{(1)}}{\partial x^2}\right]_{x=Vt} = D_{21}^w e^{-it(V\chi-\Omega_1)} + D_{22}^w e^{it(V\chi+\Omega_1)} + D_{23}^w e^{-it(V\chi+\Omega_1)} + D_{24}^w e^{it(V\chi-\Omega_1)} + D_{25}^w e^{-it(V\chi-\Omega_2)} + D_{26}^w e^{it(V\chi+\Omega_2)} + D_{27}^w e^{-it(V\chi+\Omega_2)} + D_{28}^w e^{it(V\chi-\Omega_2)} \tag{7.108}$$

- The relations that constitute the balance of forces at the interface (BoFs):

$$F_{s,y}^{(1)} = EI\left[\frac{\partial^3 v_h^{(1)}}{\partial x^3}\right]_{x=Vt} - EI\begin{pmatrix} D_{31}^v e^{-it(V\chi-\Omega_1)} + D_{32}^v e^{it(V\chi+\Omega_1)} + \\ D_{33}^v e^{-it(V\chi+\Omega_1)} + D_{34}^v e^{it(V\chi-\Omega_1)} + \\ D_{35}^v e^{-it(V\chi-\Omega_2)} + D_{36}^v e^{it(V\chi+\Omega_2)} + \\ D_{37}^v e^{-it(V\chi+\Omega_2)} + D_{38}^v e^{it(V\chi-\Omega_2)} \end{pmatrix} \tag{7.109}$$

$$F_{s,y}^{(1)} = -m\frac{d^2 v_0^{(1)}}{dt^2} \tag{7.110}$$

$$F_{s,z}^{(1)} = EI\left[\frac{\partial^3 w_h^{(1)}}{\partial x^3}\right]_{x=Vt} - EI\begin{pmatrix} D_{31}^w e^{-it(V\chi-\Omega_1)} + D_{32}^w e^{it(V\chi+\Omega_1)} + \\ D_{33}^w e^{-it(V\chi+\Omega_1)} + D_{34}^w e^{it(V\chi-\Omega_1)} + \\ D_{35}^w e^{-it(V\chi-\Omega_2)} + D_{36}^w e^{it(V\chi+\Omega_2)} + \\ D_{37}^w e^{-it(V\chi+\Omega_2)} + D_{38}^w e^{it(V\chi-\Omega_2)} \end{pmatrix} \tag{7.111}$$

$$F_{s,z}^{(1)} = -m\frac{d^2 w_0^{(1)}}{dt^2} \tag{7.112}$$

- The continuity conditions (CCs):

$$F_{s,y}^{(1)} = k_{con,yy}\left(v_0^{(1)} - v_h^{(1)}\Big|_{x=Vt}\right) + k_{con,yy}\begin{pmatrix} D_{41}^{v}e^{-it(V\chi-\Omega_1)} + D_{42}^{v}e^{it(V\chi+\Omega_1)} + \\ D_{43}^{v}e^{-it(V\chi+\Omega_1)} + D_{44}^{v}e^{it(V\chi-\Omega_1)} + \\ D_{45}^{v}e^{-it(V\chi-\Omega_2)} + D_{46}^{v}e^{it(V\chi+\Omega_2)} + \\ D_{47}^{v}e^{-it(V\chi+\Omega_2)} + D_{48}^{v}e^{it(V\chi-\Omega_2)} \end{pmatrix} \tag{7.113}$$

$$F_{s,z}^{(1)} = k_{con,zz}\left(w_0^{(1)} - w_h^{(1)}\Big|_{x=Vt}\right) + k_{con,zz}\begin{pmatrix} D_{41}^{w}e^{-it(V\chi-\Omega_1)} + D_{42}^{w}e^{it(V\chi+\Omega_1)} + \\ D_{43}^{w}e^{-it(V\chi+\Omega_1)} + D_{44}^{w}e^{it(V\chi-\Omega_1)} + \\ D_{45}^{w}e^{-it(V\chi-\Omega_2)} + D_{46}^{w}e^{it(V\chi+\Omega_2)} + \\ D_{47}^{w}e^{-it(V\chi+\Omega_2)} + D_{48}^{w}e^{it(V\chi-\Omega_2)} \end{pmatrix} \tag{7.114}$$

The definitions of the D-coefficients are listed in Appendix F. It can be readily seen by looking at the BoFs that in case of combination parametric resonance, four conditions for parametric instability emerge:

$$V\chi = 2\Omega_1 \tag{7.115}$$

$$V\chi = 2\Omega_2 \tag{7.116}$$

$$V\chi = \Omega_2 \pm \Omega_1 \tag{7.117}$$

Note that $V > 0$, $\chi > 0$ and $\Omega_2 (= \omega_{n2}) > \Omega_1 (= \omega_{n1}) > 0$; of the eight excitation frequencies in Eq. (7.109) and Eq. (7.111), only four are physically admissible to balance with the first and second natural frequency of the unperturbed system. Compare Eq. (7.101) and Eq. (7.102) to Eq. (7.14) respectively Eq. (7.15).

7.4 The center lines of the instability domains

Eq. (7.115) to Eq. (7.117) define the instability domains' centers, which are curves in the velocity-mass parameter space. See Fig. (7.5). Based on the data of Fig. (7.3) that is enclosed by bifurcation curve 1, these center lines are plotted by checking numerically for each mass value which combination of velocity and natural frequency Eq. (7.115), Eq. (7.116) and Eq. (7.117) balance. Fig. (7.3) clearly shows that $\Omega_2 > \Omega_1$, which explains why the center lines are ordered with respect to V as they are in Fig. (7.5).

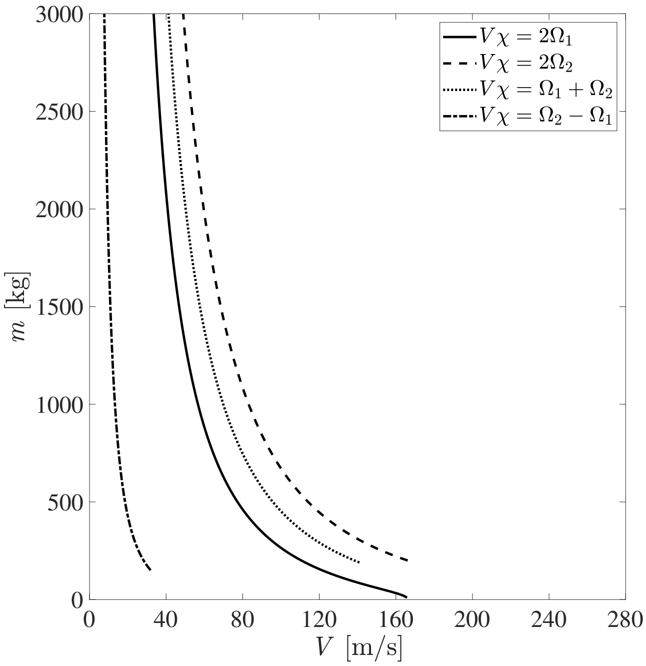

Figure 7.5: Center lines of the instability domains for a period of inhomogeneity $d = 0.6$ m without contact springs ($k_{con,yy} \to \infty$, $k_{con,zz} \to \infty$).

Repeating this procedure for three different valuations of χ, one can observe by looking at Fig. (7.6) that an increase in the period of inhomogeneity leads to an elevation of the critical mass; the velocity at which parametric instability occurs increases. The same effect has been observed for the vertical-only model from Chapter 5. See Fig. (5.4).

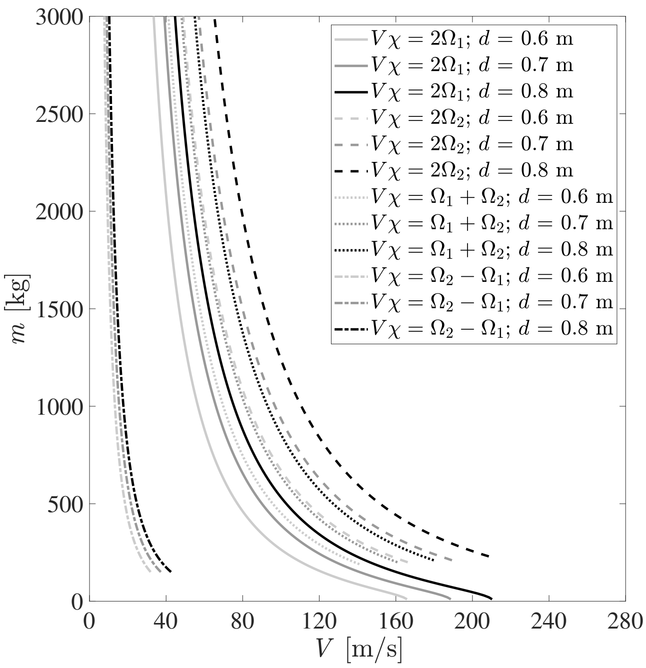

Figure 7.6: The effect of an increasing period of inhomogeneity on the instability domains' center lines.

The effect of vehicle-structure interaction is investigated by including the contact springs ($k_{con,yy} = k_{con,zz} = 7.4 \times 10^7\ \mathrm{N\,m^{-1}}$). See Fig. (7.7). As for the vertical-only model from Chapter 6, the contact springs reduce the critical mass; the velocity at which parametric instability occurs decreases. Compare to Fig. (6.3).

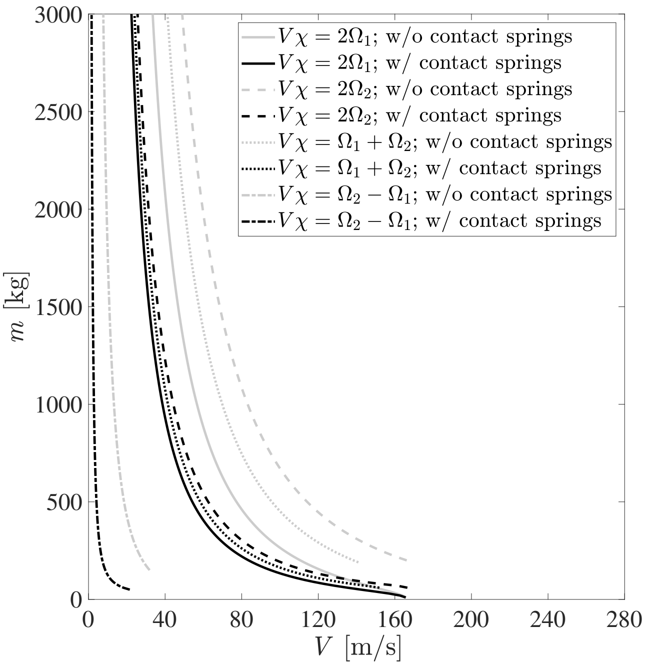

Figure 7.7: The effect of vehicle-structure interaction.

Chapter 8

Conclusions and recommendations

The aim of this thesis project was to investigate the stability of lateral and vertical vibrations of a vehicle that moves uniformly along an infinite Euler-Bernoulli beam on a coupled lateral-vertical periodically inhomogeneous foundation. It has been shown that these vibrations can become unstable as a result of combination parametric resonance; a form of instability that is caused by periodic variation of the coupled foundation stiffnesses.

The first-order instability domains have been derived by using a perturbation method under the assumption that the amplitudes of the harmonically varying foundation stiffnesses are small compared to the mean stiffness values. It has been found that the lateral-vertical beam model yields four instability domains, as opposed to the one for the vertical-only model. The center lines of these four instability domains are defined by the following conditions: $V\chi = 2\Omega_1$, $V\chi = 2\Omega_2$ and $V\chi = \Omega_2 \pm \Omega_1$, in which $V\chi$ is the frequency of the stiffness variation and Ω_1 and Ω_2 is the first respectively second natural frequency of the moving mass along the homogeneous lateral-vertical beam.

It has been shown that the period of inhomogeneity significantly affects the position of the instability domains. As for the vertical-only model, the center lines shift towards the right in the velocity-mass parameter space with increasing period of inhomogeneity. The effect of vehicle-structure interaction has also been investigated; the inclusion of contact springs makes the center lines reposition themselves towards the left in the parameter space.

In order to obtain complete instability domains for combination parametric resonance, the boundaries also have to be derived. To this end, reference [23] provides a method that can be extended to the lateral-vertical case, though it is recommended to augment the more efficient method presented in reference [12]. The reason for this is threefold. First of all, the paper of Metrikine (2008) uses a more realistic foundation model; instead of applying a harmonically varying support with small amplitude, actual discrete supports with constant spacing are used. Secondly, the method enables to derive directly the total instability domain as described by its boundary in the velocity-mass parameter space—no distinction is made between center lines and deviation lines. Higher-order domains will also emerge in the parameter space. Finally, foundation damping can be taken into account more easily such that its effect on the instability domain's boundary can be studied. This is of practical importance, because it needs to be examined if the instability domains will completely vanish once the damping exceeds a threshold value as is shown for the parametric oscillator described by Mathieu's equation.

References

[1] N.H. Asmar and L. Grafakos. *Complex Analysis with Applications*. Undergraduate Texts in Mathematics. Springer International Publishing, 1st edition, 2018.

[2] M. Bell. A note on mathieu functions. *Proceedings of the Glasgow Mathematical Association*, 3(3):132–134, 1957.

[3] W.E. Boyce and R.C. DiPrima. *Elementary Differential Equations and Boundary Value Problems*. Wiley, 10th edition, 2013.

[4] Y. Cai, S.S. Chen, T.M. Mulcahy, and D.M. Rote. Dynamic Stability of Maglev Systems. Technical report, Argonne National Laboratory, 1993.

[5] G.G. Denisov, E.K. Kugusheva, and V.V. Novikov. On the problem of the stability of one-dimensional unbounded elastic systems. *Journal of Applied Mathematics and Mechanics*, 49(4):533 – 537, 1985.

[6] H. A. Dieterman and A. Metrikine. Critical Velocities of a Harmonic Load Moving Uniformly Along an Elastic Layer. *Journal of Applied Mechanics*, 64(3):596–600, 09 1997.

[7] H. Goldstein, C.P. Poole, and J.L. Safko. *Classical Mechanics*. Pearson Education Limited, 3rd edition, 2014.

[8] K.F. Graff. *Wave Motion in Elastic Solids*. Dover, 1991.

[9] T. Houter, M. van der Meijs, M. Geuze, and S. Lamme. The Hyperloop Concept. Technical report, Hardt Hyperloop, 2019. Confidential.

[10] I. Kovacic, R. Rand, and S. Mohamed Sah. Mathieu's Equation and Its Generalizations: Overview of Stability Charts and Their Features. *Applied Mechanics Reviews*, 70(2), 02 2018. 020802.

[11] L.D. Landau and E.M. Lifshitz. *Mechanics*, volume 1 of *Course of Theoretical Physics*. Pergamon Press, 1960.

[12] A. V. Metrikine. Parametric Instability of a Moving Particle on a Periodically Supported Infinitely Long String. *Journal of Applied Mechanics*, 75(1), 01 2008. 011006.

[13] A.V. Metrikine. Unstable lateral oscillations of an object moving uniformly along an elastic guide as a result of an anomalous doppler effect. *Acoustical Physics*, 40(1), 1994.

[14] A.V. Metrikine. Lecture notes CT4145: Dynamics, Slender Structures and an Introduction to Continuum Mechanics, August 2006.

[15] A.V. Metrikine and H.A. Dieterman. Instability of vibrations of a mass moving uniformly along an axially compressed beam on a viscoelastic foundation. *Journal of Sound and Vibration*, 201(5):567 – 576, 1997.

[16] A.V. Metrikine and A.W.C.M. Vrouwenvelder. Lecture notes CT4140: Dynamics of Structures - Part 2 Wave Dynamics, December 2006.

[17] A.H. Nayfeh. *Perturbation Methods*. Wiley-VCH, 2004.

[18] M.I. Rabinovich and D.I. Trubetskov. *Oscillations and Waves in Linear and Nonlinear Systems*, volume 50 of *Mathematics and Its Applications*. Kluwer Academic Publishers, 1989.

[19] D.M. Rote and Y. Cai. Review of Dynamic Stability of Repulsive-Force Maglev Suspension Systems. *IEEE Transactions on Magnetics*, 38(2):1383–1390, 2002.

[20] C.T. Sun. On the Equations for a Timoshenko Beam Under Initial Stress. *Journal of Applied Mechanics*, 39(1):282–285, 03 1972.

[21] J. van de Craats. *Vervolgboek wiskunde*. Pearson Education Benelux, 5th edition, June 2013.

[22] S. N. Verichev and A. V. Metrikine. Dynamic rigidity of a beam in a moving contact. *Journal of Applied Mechanics and Technical Physics*, 41(6):1111–1117, Nov 2000.

[23] S.N. Verichev and A.V. Metrikine. Instability of vibrations of a mass that moves uniformly along a beam on a periodically inhomogeneous foundation. *Journal of Sound and Vibration*, 260(5):901 – 925, 2003.

Appendix A

Second order approximation of equation 4.23

To obtain a better approximation of the first instability domain for parametric resonance, the expression for the SDoF's motion $x(t)$ is extended according to Eq. (4.24) with $q = 2$ while considering the coefficients a_p and b_p to be constant; the notion that the boundaries of the instability domain are associated with constant coefficients is exploited in order to speed up the derivation.

$$\begin{aligned} x\left(t\right) =& A_1 \cos\left(\left(\omega_0 + \mu^2\delta\right)t\right) + B_1 \sin\left(\left(\omega_0 + \mu^2\delta\right)t\right) + \\ & A_2 \cos\left(3\left(\omega_0 + \mu^2\delta\right)t\right) + B_2 \sin\left(3\left(\omega_0 + \mu^2\delta\right)t\right) \end{aligned} \tag{A.1}$$

Substitution in Eq. (4.3), with $\omega_p = 2\left(\omega_0 + \mu^2\delta\right)$, yields:

$$\begin{aligned} & -A_1\left(\omega_0 + \mu^2\delta\right)^2 \cos\left(\left(\omega_0 + \mu^2\delta\right)t\right) - B_1\left(\omega_0 + \mu^2\delta\right)^2 \sin\left(\left(\omega_0 + \mu^2\delta\right)t\right) - \\ & \quad 9A_2\left(\omega_0 + \mu^2\delta\right)^2 \cos\left(3\left(\omega_0 + \mu^2\delta\right)t\right) - 9B_2\left(\omega_0 + \mu^2\delta\right)^2 \sin\left(3\left(\omega_0 + \mu^2\delta\right)t\right) + \\ & \quad A_1\omega_0^2 \cos\left(\left(\omega_0 + \mu^2\delta\right)t\right) + B_1\omega_0^2 \sin\left(\left(\omega_0 + \mu^2\delta\right)t\right) + \\ & \quad A_2\omega_0^2 \cos\left(3\left(\omega_0 + \mu^2\delta\right)t\right) + B_2\omega_0^2 \sin\left(3\left(\omega_0 + \mu^2\delta\right)t\right) + \\ & \quad A_1\omega_0^2\mu \cos\left(2\left(\omega_0 + \mu^2\delta\right)t\right) \cos\left(\left(\omega_0 + \mu^2\delta\right)t\right) + \\ & \quad B_1\omega_0^2\mu \cos\left(2\left(\omega_0 + \mu^2\delta\right)t\right) \sin\left(\left(\omega_0 + \mu^2\delta\right)t\right) + \\ & \quad A_2\omega_0^2\mu \cos\left(2\left(\omega_0 + \mu^2\delta\right)t\right) \cos\left(3\left(\omega_0 + \mu^2\delta\right)t\right) + \\ & \quad B_2\omega_0^2\mu \cos\left(2\left(\omega_0 + \mu^2\delta\right)t\right) \sin\left(3\left(\omega_0 + \mu^2\delta\right)t\right) = 0 \end{aligned} \tag{A.2}$$

Using the trigonometric identities from Eq. (4.12) and Eq. (4.13) and omitting terms that exhibit the frequency '$5(\omega_0+\mu^2\delta)$' reduces Eq. (A.2) to:

$$\begin{aligned}
&\left[-A_1\left(2\omega_0\mu^2\delta+\mu^4\delta^2-\frac{1}{2}\omega_0^2\mu\right)+\frac{1}{2}A_2\omega_0^2\mu\right]\cos\left(\left(\omega_0+\mu^2\delta\right)t\right)+\\
&\left[-B_1\left(2\omega_0\mu^2\delta+\mu^4\delta^2+\frac{1}{2}\omega_0^2\mu\right)+\frac{1}{2}B_2\omega_0^2\mu\right]\sin\left(\left(\omega_0+\mu^2\delta\right)t\right)+\\
&\left[-A_2\left(8\omega_0^2+18\omega_0\mu^2\delta+9\mu^4\delta^2\right)+\frac{1}{2}A_1\omega_0^2\mu\right]\cos\left(3\left(\omega_0+\mu^2\delta\right)t\right)+\\
&\left[-B_2\left(8\omega_0^2+18\omega_0\mu^2\delta+9\mu^4\delta^2\right)+\frac{1}{2}B_1\omega_0^2\mu\right]\sin\left(3\left(\omega_0+\mu^2\delta\right)t\right)=0
\end{aligned} \tag{A.3}$$

In order to satisfy Eq. (A.3) the expressions enclosed by the square brackets must vanish. To this end, for the first two terms of Eq. (A.3), only terms between the brackets that are proportional to the perturbation parameter up to and including the second order $\mathcal{O}(\mu^2)$ are considered while for the latter two terms only zero- and first-order bracketed terms are taken into account:[1]

$$-8A_2\omega_0^2+\frac{1}{2}A_1\omega_0^2\mu=0\Rightarrow A_2=\frac{\mu}{16}A_1 \tag{A.4}$$

$$-8B_2\omega_0^2+\frac{1}{2}B_1\omega_0^2\mu=0\Rightarrow B_2=\frac{\mu}{16}B_1 \tag{A.5}$$

Substitution in:

$$-2A_1\omega_0\mu^2\delta+\frac{1}{2}A_1\omega_0^2\mu+\frac{1}{2}A_2\omega_0^2\mu=0 \tag{A.6}$$

$$-2B_1\omega_0\mu^2\delta-\frac{1}{2}B_1\omega_0^2\mu+\frac{1}{2}B_2\omega_0^2\mu=0 \tag{A.7}$$

gives:

$$\delta=\left(\pm\frac{1}{4\mu}+\frac{1}{64}\right)\omega_0 \tag{A.8}$$

Inserting Eq. (A.8) into the second order perturbation of the first condition for parametric resonance:

$$\omega_p=2\left(\omega_0+\mu^2\delta\right) \tag{A.9}$$

yields the second order approximation of the first instability domain for parametric resonance:

$$2\omega_0\left(1-\frac{1}{4}\mu+\frac{1}{64}\mu^2\right)<\omega_p<2\omega_0\left(1+\frac{1}{4}\mu+\frac{1}{64}\mu^2\right) \tag{A.10}$$

Compared to Eq. (4.23) the second order approximation adds $\omega_0\mu^2/32$ to its first order counterpart.

[1] Cf. Eq. (4.14); only terms of the order $\mathcal{O}(\mu^1)$ are included; terms proportional to μ^0 are omitted. Why do we include zero-order terms in the second order approximation, but not in the first order approximation? See reference [11].

Appendix B

Derivation of equation 4.37

The following solution of the second order is used to derive the second instability domain:[1]

$$\begin{aligned} x(t) = & A_1 \cos\left(\left(\omega_0 + \mu^2\delta\right)t\right) + B_1 \sin\left(\left(\omega_0 + \mu^2\delta\right)t\right) + \\ & A_2 \cos\left(2\left(\omega_0 + \mu^2\delta\right)t\right) + B_2 \sin\left(2\left(\omega_0 + \mu^2\delta\right)t\right) + C \end{aligned} \tag{B.1}$$

Substitution in Eq. (4.3), with $\omega_p = \omega_0 + \mu^2\delta$, yields:

$$\begin{aligned} & -A_1\left(\omega_0 + \mu^2\delta\right)^2 \cos\left(\left(\omega_0 + \mu^2\delta\right)t\right) - B_1\left(\omega_0 + \mu^2\delta\right)^2 \sin\left(\left(\omega_0 + \mu^2\delta\right)t\right) - \\ & \quad 4A_2\left(\omega_0 + \mu^2\delta\right)^2 \cos\left(2\left(\omega_0 + \mu^2\delta\right)t\right) - 4B_2\left(\omega_0 + \mu^2\delta\right)^2 \sin\left(2\left(\omega_0 + \mu^2\delta\right)t\right) + \\ & \quad A_1\omega_0^2 \cos\left(\left(\omega_0 + \mu^2\delta\right)t\right) + B_1\omega_0^2 \sin\left(\left(\omega_0 + \mu^2\delta\right)t\right) + \\ & \quad A_2\omega_0^2 \cos\left(2\left(\omega_0 + \mu^2\delta\right)t\right) + B_2\omega_0^2 \sin\left(2\left(\omega_0 + \mu^2\delta\right)t\right) + C\omega_0^2 + \\ & \quad A_1\omega_0^2\mu \cos\left(\left(\omega_0 + \mu^2\delta\right)t\right) \cos\left(\left(\omega_0 + \mu^2\delta\right)t\right) + \\ & \quad B_1\omega_0^2\mu \cos\left(\left(\omega_0 + \mu^2\delta\right)t\right) \sin\left(\left(\omega_0 + \mu^2\delta\right)t\right) + \\ & \quad A_2\omega_0^2\mu \cos\left(\left(\omega_0 + \mu^2\delta\right)t\right) \cos\left(2\left(\omega_0 + \mu^2\delta\right)t\right) + \\ & \quad B_2\omega_0^2\mu \cos\left(\left(\omega_0 + \mu^2\delta\right)t\right) \sin\left(2\left(\omega_0 + \mu^2\delta\right)t\right) + \\ & \quad C\omega_0^2\mu \cos\left(\left(\omega_0 + \mu^2\delta\right)t\right) = 0 \end{aligned} \tag{B.2}$$

Using Eq. (4.12) and Eq. (4.13) and omitting terms that exhibit the frequency '$3(\omega_0+\mu^2\delta)$'

[1]The first order solution '$x(t) = A\cos((\omega_0 + \mu\delta)t) + B\sin((\omega_0 + \mu\delta)t) + C$' returns a zero-width interval and is therefore not suitable to derive the second instability domain.

reduces Eq. (B.2) to:

$$\begin{aligned}
&\left[-A_1\left(2\omega_0\mu^2\delta+\mu^4\delta^2\right)+\frac{1}{2}A_2\omega_0^2\mu+C\omega_0^2\mu\right]\cos\left(\left(\omega_0+\mu^2\delta\right)t\right)+\\
&\left[-B_1\left(2\omega_0\mu^2\delta+\mu^4\delta^2\right)+\frac{1}{2}B_2\omega_0^2\mu\right]\sin\left(\left(\omega_0+\mu^2\delta\right)t\right)+\\
&\left[-A_2\left(3\omega_0^2+8\omega_0\mu^2\delta+4\mu^4\delta^2\right)+\frac{1}{2}A_1\omega_0^2\mu\right]\cos\left(2\left(\omega_0+\mu^2\delta\right)t\right)+\\
&\left[-B_2\left(3\omega_0^2+8\omega_0\mu^2\delta+4\mu^4\delta^2\right)+\frac{1}{2}B_1\omega_0^2\mu\right]\sin\left(2\left(\omega_0+\mu^2\delta\right)t\right)+\\
&\frac{1}{2}A_1\omega_0^2\mu+C\omega_0^2=0
\end{aligned}\tag{B.3}$$

In order to satisfy Eq. (B.3) the expressions between the square brackets must vanish. To this end, bracketed terms up to $\mathcal{O}(\mu^2)$ are considered for the first two terms of Eq. (B.3) while for the latter two terms only zero- and first-order bracket terms are taken into account. Note that the inclusion of the constant C in the proposed solution of Eq. (B.1) is necessary to avoid a trivial solution in which A_1 is required to be equal to zero.

$$-3A_2\omega_0^2+\frac{1}{2}A_1\omega_0^2\mu=0\Rightarrow A_2=\frac{\mu}{6}A_1\tag{B.4}$$

$$-3B_2\omega_0^2+\frac{1}{2}B_1\omega_0^2\mu=0\Rightarrow B_2=\frac{\mu}{6}B_1\tag{B.5}$$

$$\frac{1}{2}A_1\omega_0^2\mu+C\omega_0^2=0\Rightarrow C=-\frac{\mu}{2}A_1\tag{B.6}$$

Substitution in:

$$-2A_1\omega_0\mu^2\delta+\frac{1}{2}A_2\omega_0^2\mu+C\omega_0^2\mu=0\tag{B.7}$$

$$-2B_1\omega_0\mu^2\delta+\frac{1}{2}B_2\omega_0^2\mu=0\tag{B.8}$$

gives:

$$-\frac{5}{24}\omega_0<\delta<\frac{1}{24}\omega_0\tag{B.9}$$

Inserting Eq. (B.9) into $\omega_p=\omega_0+\mu^2\delta$ yields the second order approximation of the second instability domain for parametric resonance:

$$\omega_0\left(1-\frac{5}{24}\mu^2\right)<\omega_p<\omega_0\left(1+\frac{1}{24}\mu^2\right)\tag{B.10}$$

In case the frequency of inhomogeneity ω_p lies within this interval, it is assumed that the oscillations as well as the energy content grow exponentially with time; in reference [23] it is stated that this growth is linear, not exponential. This latter claim can be checked by adopting slowly varying time functions as coefficients in Eq. (B.1) and redoing the analysis of chapter 4.

Appendix C

Derivation of equation 5.4

Newton's second law of motion is used to derive Eq. (5.4); displacing the beam segment at the interface in the positive upward direction results in vertical shear forces acting on this segment. See Fig. (C.1).

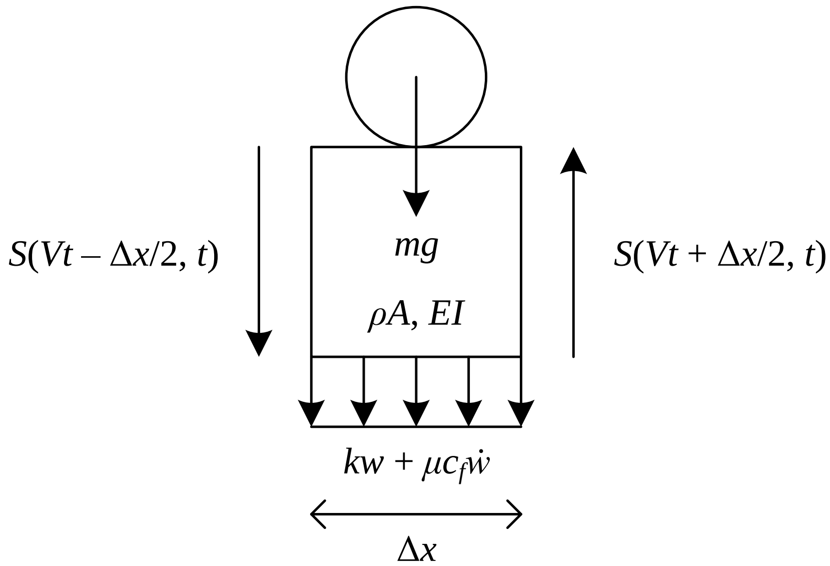

Figure C.1: Forces acting on the displaced beam segment at the interface.

Scalar format of Newton's second law of motion:

$$F_{net} = ma \tag{C.1}$$

Adapted to the problem of Fig. (C.1):

$$-S^{-} + S^{+} - mg - (kw + \mu c_f \dot{w})\, \Delta x = (m + \rho A \Delta x)\, \ddot{w} \tag{C.2}$$

With $\Delta x \to 0$ and $S = -EI\partial^3 w/\partial x^3$, Eq. (C.2) reduces to:

$$EI \left[\frac{\partial^3 w}{\partial x^3} \right]_{x=Vt} = -m \frac{\partial^2 w}{\partial t^2} - mg \tag{C.3}$$

Finally, the first term on the right-hand side of Eq. (C.3) is rewritten by virtue of Eq. (5.5):

$$EI \left[\frac{\partial^3 w}{\partial x^3} \right]_{x=Vt} = -m \frac{d^2 w_0}{dt^2} - mg \tag{C.4}$$

Appendix D

Coefficient definitions for chapter 5

The W-coefficients of Eq. (5.25):

$$W_{n1} = -W_n \frac{\left(k_2^n - k_3^n\right)\left(k_2^n - k_4^n\right)}{\left(k_1^n + k_2^n - k_3^n - k_4^n\right)\left(k_1^n - k_2^n\right)}, \quad W_{n2} = W_n \frac{\left(k_1^n - k_3^n\right)\left(k_1^n - k_4^n\right)}{\left(k_1^n + k_2^n - k_3^n - k_4^n\right)\left(k_1^n - k_2^n\right)},$$

$$W_{n3} = W_n \frac{\left(k_1^n - k_4^n\right)\left(k_2^n - k_4^n\right)}{\left(k_1^n + k_2^n - k_3^n - k_4^n\right)\left(k_3^n - k_4^n\right)}, \quad W_{n4} = -W_n \frac{\left(k_1^n - k_3^n\right)\left(k_2^n - k_3^n\right)}{\left(k_1^n + k_2^n - k_3^n - k_4^n\right)\left(k_3^n - k_4^n\right)}$$

$n = A, B$

The C-coefficients of Eq. (5.29):

$$C_{11} = \frac{-k_f W_{A1}}{2\left(-\rho A(k_1^A V + \Omega)^2 + EI(\chi - k_1^A)^4 + k_f\right)}, \quad C_{12} = \frac{-k_f W_{A2}}{2\left(-\rho A(k_2^A V + \Omega)^2 + EI(\chi - k_2^A)^4 + k_f\right)},$$

$$C_{21} = \frac{-k_f W_{A1}}{2\left(-\rho A(k_1^A V + \Omega)^2 + EI(\chi + k_1^A)^4 + k_f\right)}, \quad C_{22} = \frac{-k_f W_{A2}}{2\left(-\rho A(k_2^A V + \Omega)^2 + EI(\chi + k_2^A)^4 + k_f\right)},$$

$$C_{31} = \frac{-k_f W_{B1}}{2\left(-\rho A(k_1^B V - \Omega)^2 + EI(\chi - k_1^B)^4 + k_f\right)}, \quad C_{32} = \frac{-k_f W_{B2}}{2\left(-\rho A(k_2^B V - \Omega)^2 + EI(\chi - k_2^B)^4 + k_f\right)},$$

$$C_{41} = \frac{-k_f W_{B1}}{2\left(-\rho A(k_1^B V - \Omega)^2 + EI(\chi + k_1^B)^4 + k_f\right)}, \quad C_{42} = \frac{-k_f W_{B2}}{2\left(-\rho A(k_2^B V - \Omega)^2 + EI(\chi + k_2^B)^4 + k_f\right)}$$

$$C_{13} = \frac{-k_f W_{A3}}{2\left(-\rho A(k_3^A V + \Omega)^2 + EI(\chi - k_3^A)^4 + k_f\right)}, \quad C_{14} = \frac{-k_f W_{A4}}{2\left(-\rho A(k_4^A V + \Omega)^2 + EI(\chi - k_4^A)^4 + k_f\right)},$$

$$C_{23} = \frac{-k_f W_{A3}}{2\left(-\rho A(k_3^A V + \Omega)^2 + EI(\chi + k_3^A)^4 + k_f\right)}, \quad C_{24} = \frac{-k_f W_{A4}}{2\left(-\rho A(k_4^A V + \Omega)^2 + EI(\chi + k_4^A)^4 + k_f\right)},$$

$$C_{33} = \frac{-k_f W_{B3}}{2\left(-\rho A(k_3^B V - \Omega)^2 + EI(\chi - k_3^B)^4 + k_f\right)}, \quad C_{34} = \frac{-k_f W_{B4}}{2\left(-\rho A(k_4^B V - \Omega)^2 + EI(\chi - k_4^B)^4 + k_f\right)},$$

$$C_{43} = \frac{-k_f W_{B3}}{2\left(-\rho A(k_3^B V - \Omega)^2 + EI(\chi + k_3^B)^4 + k_f\right)}, \quad C_{44} = \frac{-k_f W_{B4}}{2\left(-\rho A(k_4^B V - \Omega)^2 + EI(\chi + k_4^B)^4 + k_f\right)}$$

The D-coefficients of Eq. (5.30):

$$D_{n1} = \left(+i\left(\chi - k_3^A\right)\right)^n C_{13} + \left(+i\left(\chi - k_4^A\right)\right)^n C_{14} - \left(+i\left(\chi - k_1^A\right)\right)^n C_{11} - \left(+i\left(\chi - k_2^A\right)\right)^n C_{12},$$

$$D_{n2} = \left(-i\left(\chi + k_3^A\right)\right)^n C_{23} + \left(-i\left(\chi + k_4^A\right)\right)^n C_{24} - \left(-i\left(\chi + k_1^A\right)\right)^n C_{21} - \left(-i\left(\chi + k_2^A\right)\right)^n C_{22},$$

$$D_{n3} = \left(+i\left(\chi - k_3^B\right)\right)^n C_{33} + \left(+i\left(\chi - k_4^B\right)\right)^n C_{34} - \left(+i\left(\chi - k_1^B\right)\right)^n C_{31} - \left(+i\left(\chi - k_2^B\right)\right)^n C_{32},$$

$$D_{n4} = \left(-i\left(\chi + k_3^B\right)\right)^n C_{43} + \left(-i\left(\chi + k_4^B\right)\right)^n C_{44} - \left(-i\left(\chi + k_1^B\right)\right)^n C_{41} - \left(-i\left(\chi + k_2^B\right)\right)^n C_{42}$$

$n = 0, 1, 2, 3$

$$D_{41} = -C_{11} - C_{12}, \quad D_{42} = -C_{21} - C_{22}, \quad D_{43} = -C_{31} - C_{32}, \quad D_{44} = -C_{41} - C_{42}$$

Appendix E

Derivation of equations 6.1 and 6.2

The displacement method is used in order to derive Eq. (6.1) and Eq. (6.2). Now that (linear) inertia is present at two separate points, these two bodies of mass are to be displaced individually, so as to be able to see clearly the forces that are exerted on the connecting spring. See Fig. (E.1).

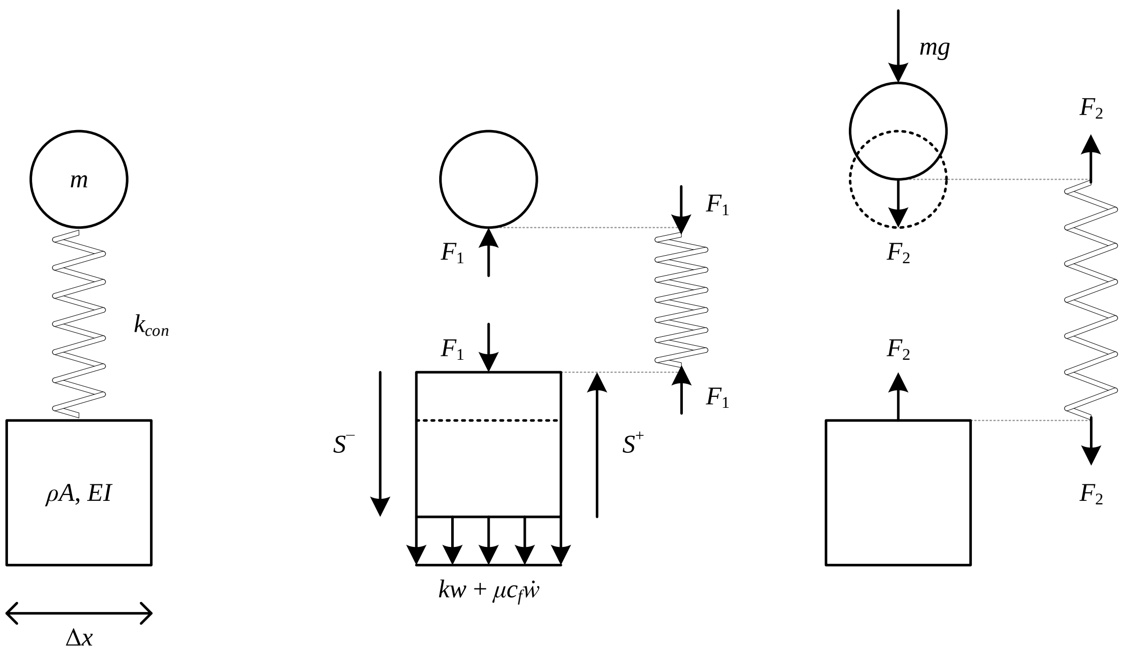

Figure E.1: Forces acting on the beam segment at the interface and the point mass as a result of displacing both inertia elements in the positive upward direction.

Newton's second law of motion applied to each inertia element:

$$-S^- + S^+ - F_1 + F_2 - \left(kw + \mu c_f \frac{\partial w}{\partial t}\right)\Delta x = \rho A \Delta x \frac{\partial^2 w}{\partial t^2} \tag{E.1}$$

$$-mg + F_1 - F_2 = m\frac{d^2 w_0}{dt^2} \tag{E.2}$$

in which the spring forces are defined as:

$$F_1 = k_{con}\, w|_{x=Vt}, \quad F_2 = k_{con} w_0 \tag{E.3}$$

By convention, compressive spring force is negative while tensile spring force is considered positive. The total spring force then reads:

$$F_s = -F_1 + F_2 = k_{con} \left(w_0 - w|_{x=Vt} \right) \tag{E.4}$$

With $\Delta x \to 0$ and $S = -EI\partial^3 w/\partial x^3$, Eq. (E.1) and Eq. (E.2) reduce to:

$$EI \left[\frac{\partial^3 w}{\partial x^3} \right]_{x=Vt} = F_s \tag{E.5}$$

$$m \frac{d^2 w_0}{dt^2} = -F_s - mg \tag{E.6}$$

Combining Eq. (E.5) and Eq. (E.6) recovers the balance of vertical forces at the interface for the model that excludes the contact spring. If the spring stiffness concurrently goes to infinity in Eq. (E.4), the associated continuity condition is retrieved as well:

$$\lim_{k_{con} \to \infty} F_s/k_{con} = w_0 - w|_{x=Vt} = 0 \Rightarrow w|_{x=Vt} = w_0 \tag{E.7}$$

This shows that the definition of the spring force—Eq. (E.4)—forms the new continuity condition and that Eq. (E.5) together with Eq. (E.6) compose the new balance of vertical forces at the interface.

Appendix F

Coefficient definitions for chapter 7

To define the V- and W-coefficients of Eq. (7.88) to Eq. (7.91), these latter four equations are to be substituted in Eq. (7.14) and Eq. (7.15) from which a relationship between the amplitudes V and W ensue. Being left with 32 instead of 64 unknowns, the remaining equations that describe the unperturbed problem—Eq. (7.16) to Eq. (7.21)—allow to define these unknowns; the eight relations that are used to this end, read (see also Chapter 6):

$$v^{(0)\ +}\big|_{x=Vt} = v_0^{(0)} + \frac{m}{k_{con,yy}}\frac{d^2 v_0^{(0)}}{dt^2}, \quad v^{(0)\ -}\big|_{x=Vt} = v_0^{(0)} + \frac{m}{k_{con,yy}}\frac{d^2 v_0^{(0)}}{dt^2},$$

$$\left.\frac{\partial v^{(0)\ +}}{\partial x}\right|_{x=Vt} = \left.\frac{\partial v^{(0)\ -}}{\partial x}\right|_{x=Vt}, \quad \left.\frac{\partial^2 v^{(0)\ +}}{\partial x^2}\right|_{x=Vt} = \left.\frac{\partial^2 v^{(0)\ -}}{\partial x^2}\right|_{x=Vt}$$

$$w^{(0)\ +}\big|_{x=Vt} = w_0^{(0)} + \frac{m}{k_{con,zz}}\frac{d^2 w_0^{(0)}}{dt^2}, \quad w^{(0)\ -}\big|_{x=Vt} = w_0^{(0)} + \frac{m}{k_{con,zz}}\frac{d^2 w_0^{(0)}}{dt^2},$$

$$\left.\frac{\partial w^{(0)\ +}}{\partial x}\right|_{x=Vt} = \left.\frac{\partial w^{(0)\ -}}{\partial x}\right|_{x=Vt}, \quad \left.\frac{\partial^2 w^{(0)\ +}}{\partial x^2}\right|_{x=Vt} = \left.\frac{\partial^2 w^{(0)\ -}}{\partial x^2}\right|_{x=Vt}$$

Substituting the expressions for the lateral and vertical deflections of the right ($+$) and left ($-$) beam domain—with the W-coefficients now expressed in terms of V-coefficients—in the above relations, yields for each time signature (A, B, C and D) a system of eight algebraic equations, which can be solved.

The C-coefficients of Eq. (7.97) to Eq. (7.100):

$$C_{abc}^{v} = -\frac{\left(Q_{abc}^{z}k_{f,y} - k_{f,c}^{2}\right)V_{ab} + \left(Q_{abc}^{z} - k_{f,z}\right)k_{f,c}W_{ab}}{2\left(Q_{abc}^{y}Q_{abc}^{z} - k_{f,c}^{2}\right)}$$

$$C_{abc}^{w} = -\frac{\left(Q_{abc}^{y} - k_{f,y}\right)k_{f,c}V_{ab} + \left(Q_{abc}^{y}k_{f,z} - k_{f,c}^{2}\right)W_{ab}}{2\left(Q_{abc}^{y}Q_{abc}^{z} - k_{f,c}^{2}\right)}$$

in which:

$$Q_{abc}^{y} = -\left(k_b^a V + \Omega_a\right)^2 \rho A + \left((-1)^c \chi - k_b^a\right)^4 EI + k_{f,y}$$

$$Q_{abc}^{z} = -\left(k_b^a V + \Omega_a\right)^2 \rho A + \left((-1)^c \chi - k_b^a\right)^4 EI + k_{f,z}$$

and:

$$\Omega_A = -\Omega_B = \omega_{n1}$$

$$\Omega_C = -\Omega_D = \omega_{n2}$$

for $x \geq Vt$: $b = 1, 2, 3, 4$

for $x \leq Vt$: $b = 5, 6, 7, 8$

$c = 1, 2$

The D-coefficients of Eq. (7.103) to Eq. (7.109) and Eq. (7.111):

$$D_{n1}^{v/w} = \left(-i\left(\chi + k_5^A\right)\right)^n C_{A51}^{v/w} + \left(-i\left(\chi + k_6^A\right)\right)^n C_{A61}^{v/w} + \left(-i\left(\chi + k_7^A\right)\right)^n C_{A71}^{v/w} + \left(-i\left(\chi + k_8^A\right)\right)^n C_{A81}^{v/w} - \left(-i\left(\chi + k_1^A\right)\right)^n C_{A11}^{v/w} - \left(-i\left(\chi + k_2^A\right)\right)^n C_{A21}^{v/w} - \left(-i\left(\chi + k_3^A\right)\right)^n C_{A31}^{v/w} - \left(-i\left(\chi + k_4^A\right)\right)^n C_{A41}^{v/w}$$

$$D_{n2}^{v/w} = \left(i\left(\chi - k_5^A\right)\right)^n C_{A52}^{v/w} + \left(i\left(\chi - k_6^A\right)\right)^n C_{A62}^{v/w} + \left(i\left(\chi - k_7^A\right)\right)^n C_{A72}^{v/w} + \left(i\left(\chi - k_8^A\right)\right)^n C_{A82}^{v/w} - \left(i\left(\chi - k_1^A\right)\right)^n C_{A12}^{v/w} - \left(i\left(\chi - k_2^A\right)\right)^n C_{A22}^{v/w} - \left(i\left(\chi - k_3^A\right)\right)^n C_{A32}^{v/w} - \left(i\left(\chi - k_4^A\right)\right)^n C_{A42}^{v/w}$$

$$D_{n3}^{v/w} = \left(-i\left(\chi + k_5^B\right)\right)^n C_{B51}^{v/w} + \left(-i\left(\chi + k_6^B\right)\right)^n C_{B61}^{v/w} + \left(-i\left(\chi + k_7^B\right)\right)^n C_{B71}^{v/w} + \left(-i\left(\chi + k_8^B\right)\right)^n C_{B81}^{v/w} - \left(-i\left(\chi + k_1^B\right)\right)^n C_{B11}^{v/w} - \left(-i\left(\chi + k_2^B\right)\right)^n C_{B21}^{v/w} - \left(-i\left(\chi + k_3^B\right)\right)^n C_{B31}^{v/w} - \left(-i\left(\chi + k_4^B\right)\right)^n C_{B41}^{v/w}$$

$$D_{n4}^{v/w} = \left(i\left(\chi - k_5^B\right)\right)^n C_{B52}^{v/w} + \left(i\left(\chi - k_6^B\right)\right)^n C_{B62}^{v/w} + \left(i\left(\chi - k_7^B\right)\right)^n C_{B72}^{v/w} + \left(i\left(\chi - k_8^B\right)\right)^n C_{B82}^{v/w} - \left(i\left(\chi - k_1^B\right)\right)^n C_{B12}^{v/w} - \left(i\left(\chi - k_2^B\right)\right)^n C_{B22}^{v/w} - \left(i\left(\chi - k_3^B\right)\right)^n C_{B32}^{v/w} - \left(i\left(\chi - k_4^B\right)\right)^n C_{B42}^{v/w}$$

$$D_{n5}^{v/w} = \left(-i\left(\chi + k_5^C\right)\right)^n C_{C51}^{v/w} + \left(-i\left(\chi + k_6^C\right)\right)^n C_{C61}^{v/w} + \left(-i\left(\chi + k_7^C\right)\right)^n C_{C71}^{v/w} + \left(-i\left(\chi + k_8^C\right)\right)^n C_{C81}^{v/w} - \left(-i\left(\chi + k_1^C\right)\right)^n C_{C11}^{v/w} - \left(-i\left(\chi + k_2^C\right)\right)^n C_{C21}^{v/w} - \left(-i\left(\chi + k_3^C\right)\right)^n C_{C31}^{v/w} - \left(-i\left(\chi + k_4^C\right)\right)^n C_{C41}^{v/w}$$

$$D_{n6}^{v/w} = \left(i\left(\chi - k_5^C\right)\right)^n C_{C52}^{v/w} + \left(i\left(\chi - k_6^C\right)\right)^n C_{C62}^{v/w} + \left(i\left(\chi - k_7^C\right)\right)^n C_{C72}^{v/w} + \left(i\left(\chi - k_8^C\right)\right)^n C_{C82}^{v/w} - \left(i\left(\chi - k_1^C\right)\right)^n C_{C12}^{v/w} - \left(i\left(\chi - k_2^C\right)\right)^n C_{C22}^{v/w} - \left(i\left(\chi - k_3^C\right)\right)^n C_{C32}^{v/w} - \left(i\left(\chi - k_4^C\right)\right)^n C_{C42}^{v/w}$$

$$D_{n7}^{v/w} = \left(-i\left(\chi + k_5^D\right)\right)^n C_{D51}^{v/w} + \left(-i\left(\chi + k_6^D\right)\right)^n C_{D61}^{v/w} + \left(-i\left(\chi + k_7^D\right)\right)^n C_{D71}^{v/w} + \left(-i\left(\chi + k_8^D\right)\right)^n C_{D81}^{v/w} - \left(-i\left(\chi + k_1^D\right)\right)^n C_{D11}^{v/w} - \left(-i\left(\chi + k_2^D\right)\right)^n C_{D21}^{v/w} - \left(-i\left(\chi + k_3^D\right)\right)^n C_{D31}^{v/w} - \left(-i\left(\chi + k_4^D\right)\right)^n C_{D41}^{v/w}$$

$$D_{n8}^{v/w} = \left(i\left(\chi - k_5^D\right)\right)^n C_{D52}^{v/w} + \left(i\left(\chi - k_6^D\right)\right)^n C_{D62}^{v/w} + \left(i\left(\chi - k_7^D\right)\right)^n C_{D72}^{v/w} + \left(i\left(\chi - k_8^D\right)\right)^n C_{D82}^{v/w} - \left(i\left(\chi - k_1^D\right)\right)^n C_{D12}^{v/w} - \left(i\left(\chi - k_2^D\right)\right)^n C_{D22}^{v/w} - \left(i\left(\chi - k_3^D\right)\right)^n C_{D32}^{v/w} - \left(i\left(\chi - k_4^D\right)\right)^n C_{D42}^{v/w}$$

$n = 0, 1, 2, 3$

The D-coefficients of Eq. (7.113) and Eq. (7.114):

$$D_{41}^{v/w} = -C_{A11}^{v/w} - C_{A21}^{v/w} - C_{A31}^{v/w} - C_{A41}^{v/w}, \quad D_{42}^{v/w} = -C_{A12}^{v/w} - C_{A22}^{v/w} - C_{A32}^{v/w} - C_{A42}^{v/w},$$

$$D_{43}^{v/w} = -C_{B11}^{v/w} - C_{B21}^{v/w} - C_{B31}^{v/w} - C_{B41}^{v/w}, \quad D_{44}^{v/w} = -C_{B12}^{v/w} - C_{B22}^{v/w} - C_{B32}^{v/w} - C_{B42}^{v/w},$$

$$D_{45}^{v/w} = -C_{C11}^{v/w} - C_{C21}^{v/w} - C_{C31}^{v/w} - C_{C41}^{v/w}, \quad D_{46}^{v/w} = -C_{C12}^{v/w} - C_{C22}^{v/w} - C_{C32}^{v/w} - C_{C42}^{v/w},$$

$$D_{47}^{v/w} = -C_{D11}^{v/w} - C_{D21}^{v/w} - C_{D31}^{v/w} - C_{D41}^{v/w}, \quad D_{48}^{v/w} = -C_{D12}^{v/w} - C_{D22}^{v/w} - C_{D32}^{v/w} - C_{D42}^{v/w}$$

Static Euler-Bernoulli beam (1)

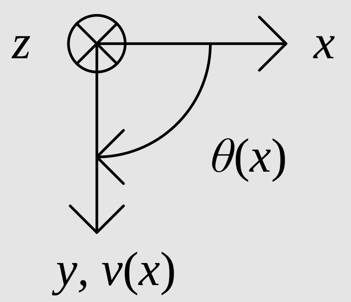

By convention, positive bending moment generates tension along the positive vertical axis. Also, curvature follows angle. Consequently, moment and deflection are negatively related; regardless which of the four sign conventions is chosen.

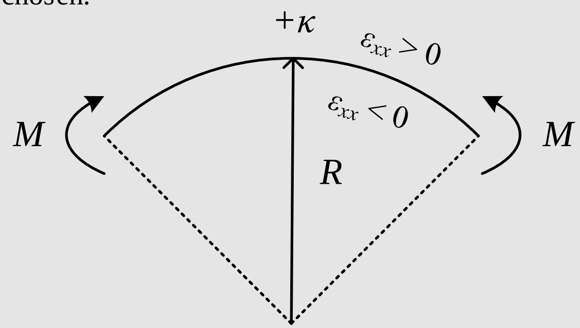

v

$\varepsilon_{xx} = -y/R = -y\kappa$

$\theta = dv/dx$

$M = \int dM = \int \sigma_{xx} y dA$

$\kappa = d\theta/dx = d^2v/dx^2$

$M = -EI\kappa = -EId^2v/dx^2$

$V = dM/dx = -EId^3v/dx^3$

$q = -dV/dx = EId^4v/dx^4$

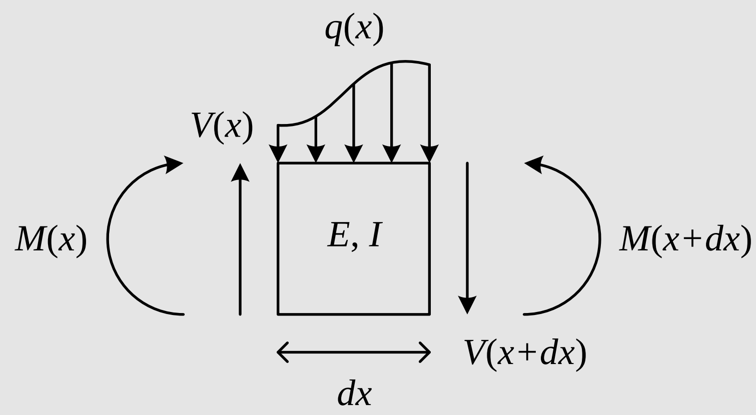

Taylor expansions around x of the quantities at the right end of the beam segment:

$$M(x+dx) = M(x) + dM/dx dx + O(dx^2)$$

$$V(x+dx) = V(x) + dV/dx dx + O(dx^2)$$

Considering static moment equilibrium around an arbitrary point and static force equilibrium along the vertical direction while neglecting second and higher order terms w.r.t. dx, gives the following differential equations:

$$V = dM/dx$$

$$q = -dV/dx$$

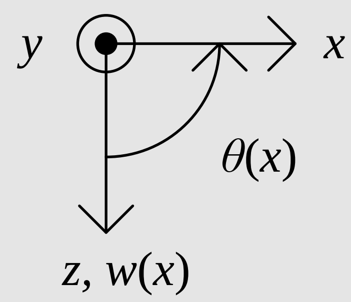

$\varepsilon_{xx} = z/R = z\kappa$

$M = \int dM = \int \sigma_{xx} z dA$

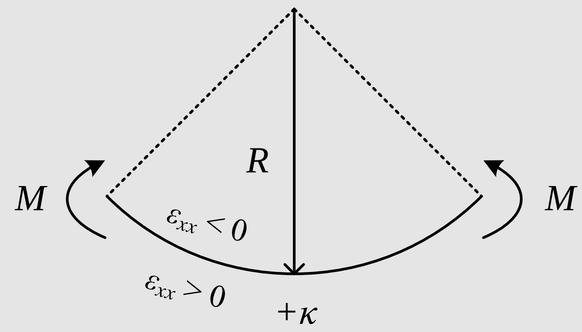

w

$\theta = -dw/dx$

$\kappa = d\theta/dx = -d^2w/dx^2$

$M = EI\kappa = -EId^2w/dx^2$

$V = dM/dx = -EId^3w/dx^3$

$q = -dV/dx = EId^4w/dx^4$

Static Euler-Bernoulli beam (2)

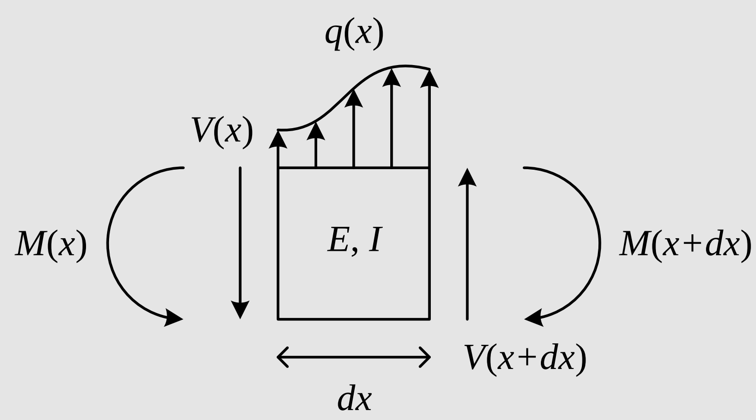

Taylor expansions around x of the quantities at the right end of the beam segment:

$$M(x+dx) = M(x) + dM/dx dx + O(dx^2)$$

$$V(x+dx) = V(x) + dV/dx dx + O(dx^2)$$

Considering static moment equilibrium around an arbitrary point and static force equilibrium along the vertical direction while neglecting second and higher order terms w.r.t. dx, gives the following differential equations:

$$V = dM/dx$$

$$q = -dV/dx$$

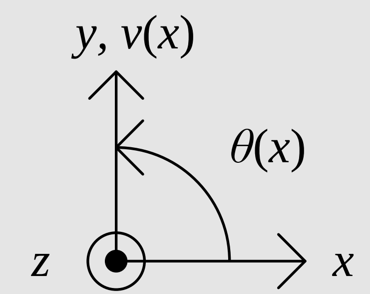

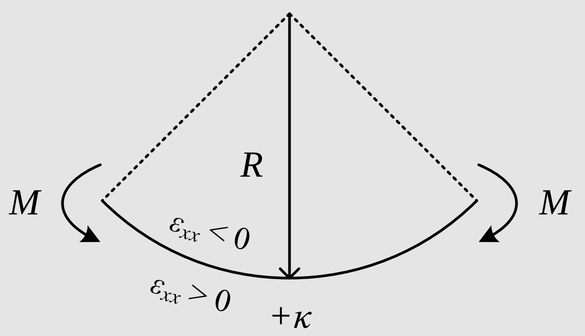

$$\varepsilon_{xx} = -y/R = -y\kappa$$

$$M = \int dM = \int \sigma_{xx} y dA$$

v

$$\theta = dv/dx$$

$$\kappa = d\theta/dx = d^2v/dx^2$$

$$M = -EI\kappa = -EId^2v/dx^2$$

$$V = dM/dx = -EId^3v/dx^3$$

$$q = -dV/dx = EId^4v/dx^4$$

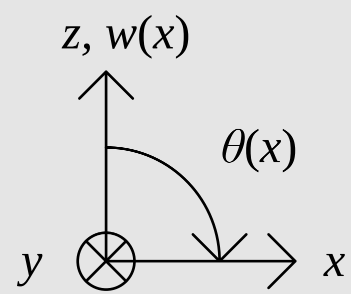

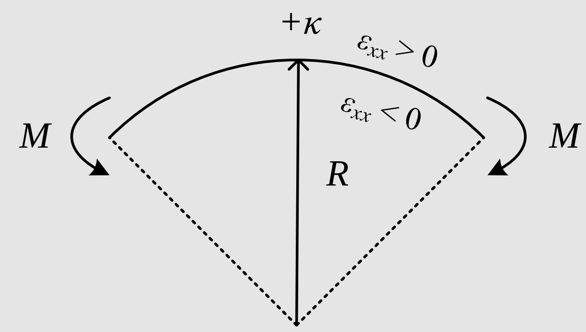

$$\varepsilon_{xx} = z/R = z\kappa$$

$$M = \int dM = \int \sigma_{xx} z dA$$

w

$$\theta = -dw/dx$$

$$\kappa = d\theta/dx = -d^2w/dx^2$$

$$M = EI\kappa = -EId^2w/dx^2$$

$$V = dM/dx = -EId^3w/dx^3$$

$$q = -dV/dx = EId^4w/dx^4$$

Dynamic Euler-Bernoulli beam (1)

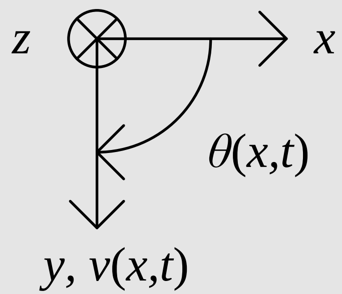

By convention, positive bending moment generates tension along the positive vertical axis. Also, curvature follows angle. Consequently, moment and deflection are negatively related; regardless which of the four sign conventions is chosen.

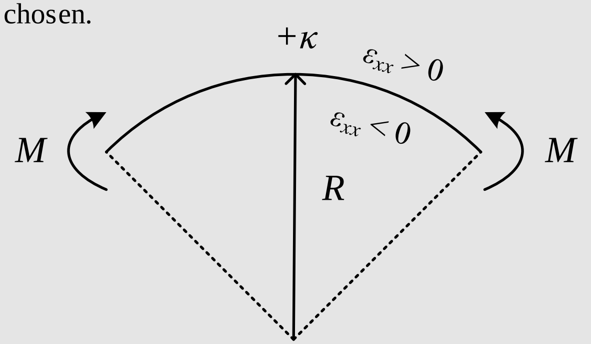

v

$\varepsilon_{xx} = -y/R = -y\kappa$

$\theta = \partial v/\partial x$

$M = \int dM = \int \sigma_{xx} y dA$

$\kappa = \partial\theta/\partial x = \partial^2 v/\partial x^2$

$M = -EI\kappa = -EI\partial^2 v/\partial x^2$

$V = \partial M/\partial x = -EI\partial^3 v/\partial x^3$

$q = EI\partial^4 v/\partial x^4 + \rho A\partial^2 v/\partial t^2$

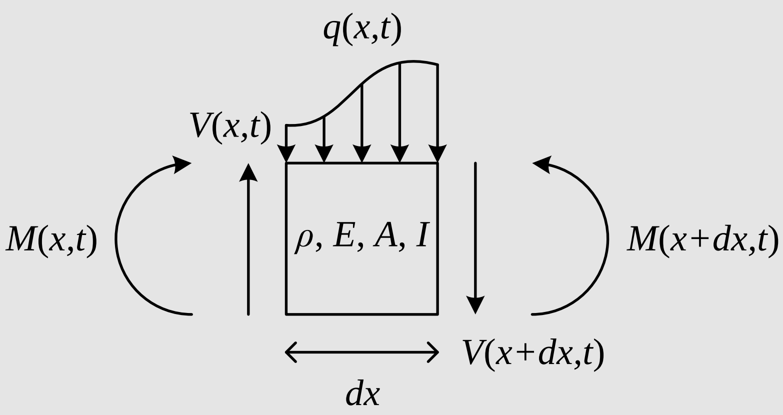

Taylor expansions around x of the quantities at the right end of the beam segment:

$M(x+dx,t) = M(x,t) + \partial M/\partial x dx + O(dx^2)$

$V(x+dx,t) = V(x,t) + \partial V/\partial x dx + O(dx^2)$

Considering static moment equilibrium around an arbitrary point and dynamic force equilibrium along the vertical direction while neglecting second and higher order terms w.r.t. dx, gives the following differential equations:

$V = \partial M/\partial x$

$q + \partial V/\partial x = \rho A\partial^2 v/\partial t^2$

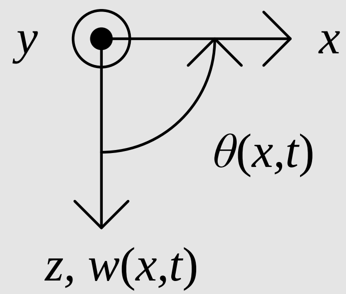

$\varepsilon_{xx} = z/R = z\kappa$

$M = \int dM = \int \sigma_{xx} z dA$

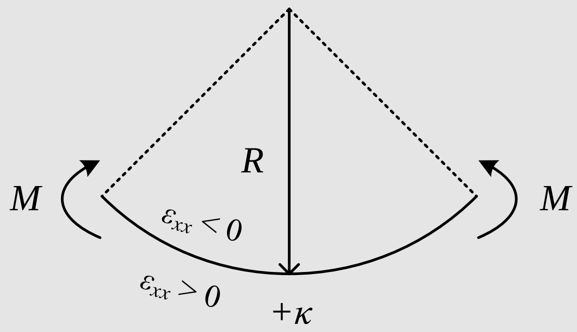

w

$\theta = -\partial w/\partial x$

$\kappa = \partial\theta/\partial x = -\partial^2 w/\partial x^2$

$M = EI\kappa = -EI\partial^2 w/\partial x^2$

$V = \partial M/\partial x = -EI\partial^3 w/\partial x^3$

$q = EI\partial^4 w/\partial x^4 + \rho A\partial^2 w/\partial t^2$

Dynamic Euler-Bernoulli beam (2)

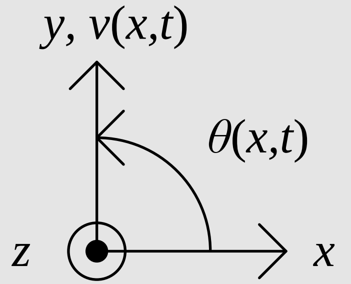

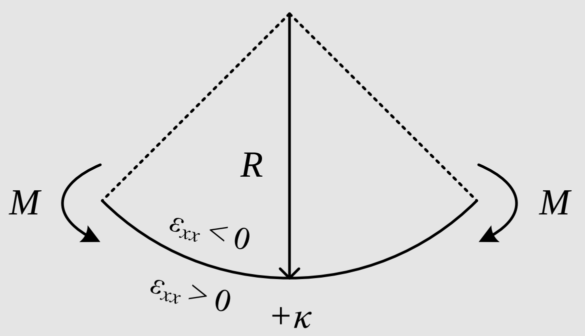

$\varepsilon_{xx} = -y/R = -y\kappa$

$M = \int dM = \int \sigma_{xx} y dA$

v

$\theta = \partial v/\partial x$

$\kappa = \partial\theta/\partial x = \partial^2 v/\partial x^2$

$M = -EI\kappa = -EI\partial^2 v/\partial x^2$

$V = \partial M/\partial x = -EI\partial^3 v/\partial x^3$

$q = EI\partial^4 v/\partial x^4 + \rho A\partial^2 v/\partial t^2$

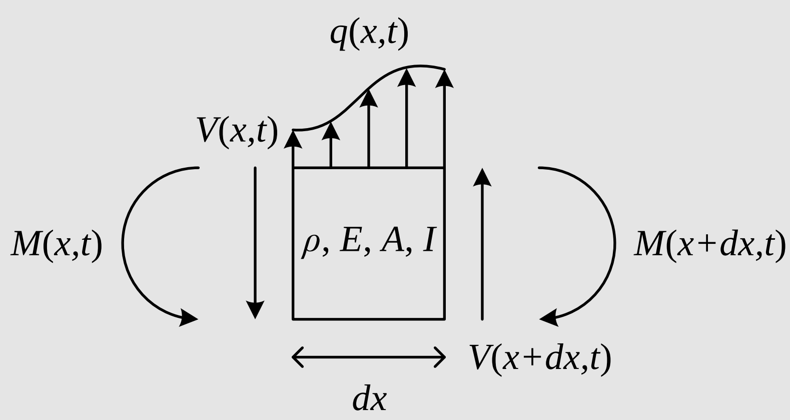

Taylor expansions around x of the quantities at the right end of the beam segment:

$M(x+dx,t) = M(x,t) + \partial M/\partial x dx + O(dx^2)$

$V(x+dx,t) = V(x,t) + \partial V/\partial x dx + O(dx^2)$

Considering static moment equilibrium around an arbitrary point and dynamic force equilibrium along the vertical direction while neglecting second and higher order terms w.r.t. dx, gives the following differential equations:

$V = \partial M/\partial x$

$q + \partial V/\partial x = \rho A\partial^2 v/\partial t^2$

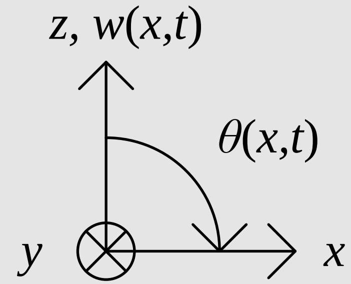

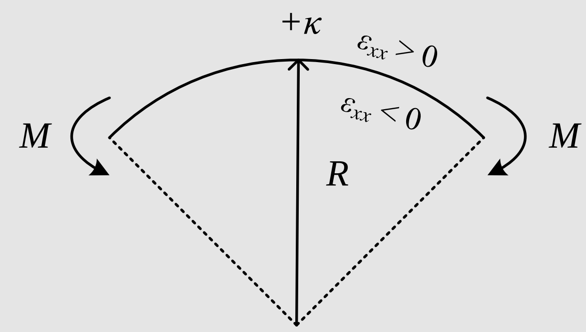

$\varepsilon_{xx} = z/R = z\kappa$

$M = \int dM = \int \sigma_{xx} z dA$

w

$\theta = -\partial w/\partial x$

$\kappa = \partial\theta/\partial x = -\partial^2 w/\partial x^2$

$M = EI\kappa = -EI\partial^2 w/\partial x^2$

$V = \partial M/\partial x = -EI\partial^3 w/\partial x^3$

$q = EI\partial^4 w/\partial x^4 + \rho A\partial^2 w/\partial t^2$

Rayleigh beam (1)

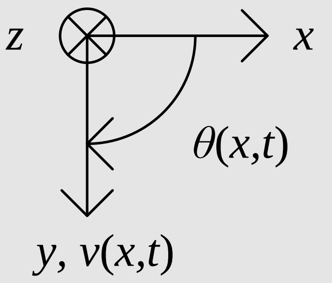

$J_z = \int_V r^2 \rho dV =$

$\rho\int_A y^2 dA dx =$

$\rho I_{yy} dx =$

$\rho I dx =$

J

By convention, positive bending moment generates tension along the positive vertical axis. Also, curvature follows angle. Consequently, moment and deflection are negatively related; regardless which of the four sign conventions is chosen.

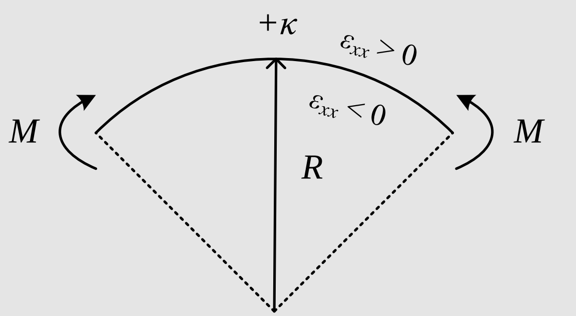

v

$\varepsilon_{xx} = -y/R = -y\kappa$

$\theta = \partial v/\partial x$

$M = \int dM = \int \sigma_{xx} y dA$

$\kappa = \partial\theta/\partial x = \partial^2 v/\partial x^2$

$M = -EI\kappa = -EI\partial^2 v/\partial x^2$

$V = -EI\partial^3 v/\partial x^3 + \rho I\partial^3 v/\partial x\partial t^2$

$q = EI\partial^4 v/\partial x^4 - \rho I\partial^4 v/\partial x^2\partial t^2 + \rho A\partial^2 v/\partial t^2$

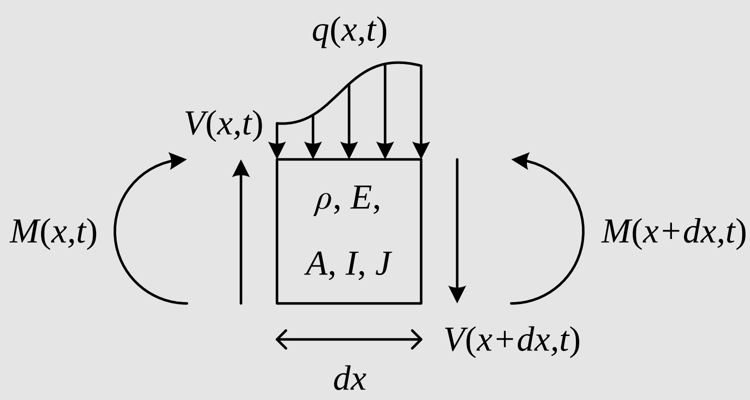

Taylor expansions around x of the quantities at the right end of the beam segment:

$M(x+dx,t) = M(x,t) + \partial M/\partial x dx + O(dx^2)$

$V(x+dx,t) = V(x,t) + \partial V/\partial x dx + O(dx^2)$

Considering dynamic moment equilibrium around an arbitrary point and dynamic force equilibrium along the vertical direction while neglecting second and higher order terms w.r.t. dx, gives the following differential equations:

$\circlearrowright$: $V - \partial M/\partial x = J/dx\partial^2\theta/\partial t^2 = \rho I\partial^2\theta/\partial t^2$

$\circlearrowleft$: $-V + \partial M/\partial x = J/dx\partial^2\theta/\partial t^2 = \rho I\partial^2\theta/\partial t^2$

$q + \partial V/\partial x = \rho A\partial^2 v/\partial t^2$

$J_y = \int_V r^2 \rho dV =$

$\rho\int_A z^2 dA dx =$

$\rho I_{zz} dx =$

$\rho I dx =$

J

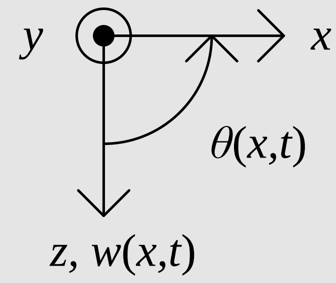

$\varepsilon_{xx} = z/R = z\kappa$

$M = \int dM = \int \sigma_{xx} z dA$

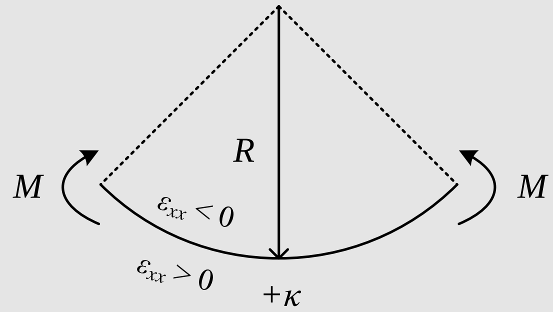

w

$\theta = -\partial w/\partial x$

$\kappa = \partial\theta/\partial x = -\partial^2 w/\partial x^2$

$M = EI\kappa = -EI\partial^2 w/\partial x^2$

$V = -EI\partial^3 w/\partial x^3 + \rho I\partial^3 w/\partial x\partial t^2$

$q = EI\partial^4 w/\partial x^4 - \rho I\partial^4 w/\partial x^2\partial t^2 + \rho A\partial^2 w/\partial t^2$

Rayleigh beam (2)

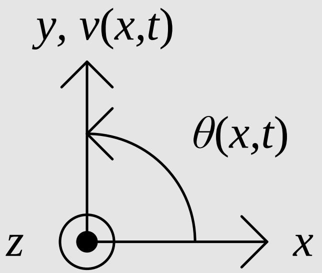

$J_z = \int_V r^2 \rho dV =$

$\rho \int_A y^2 dA dx =$

$\rho I_{yy} dx =$

$\rho I dx =$

J

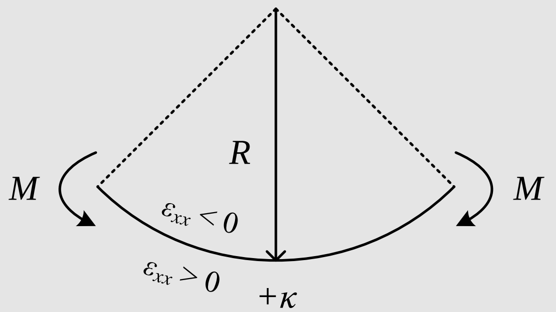

$\varepsilon_{xx} = -y/R = -y\kappa$

v

$M = \int dM = \int \sigma_{xx} y dA$

$\theta = \partial v/\partial x$

$\kappa = \partial\theta/\partial x = \partial^2 v/\partial x^2$

$M = -EI\kappa = -EI\partial^2 v/\partial x^2$

$V = -EI\partial^3 v/\partial x^3 + \rho I\partial^3 v/\partial x\partial t^2$

$q = EI\partial^4 v/\partial x^4 - \rho I\partial^4 v/\partial x^2\partial t^2 + \rho A\partial^2 v/\partial t^2$

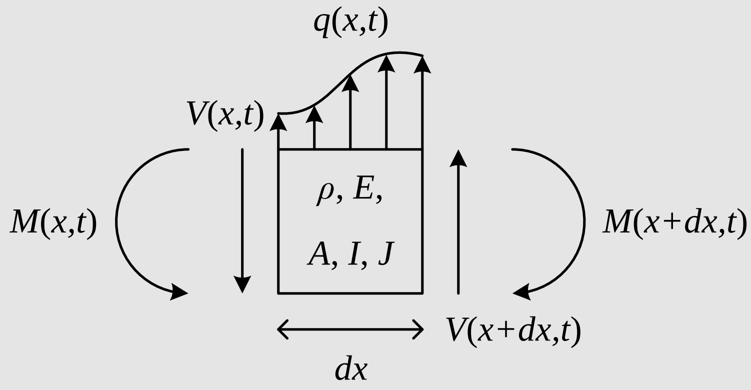

Taylor expansions around x of the quantities at the right end of the beam segment:

$M(x+dx,t) = M(x,t) + \partial M/\partial x dx + O(dx^2)$

$V(x+dx,t) = V(x,t) + \partial V/\partial x dx + O(dx^2)$

Considering dynamic moment equilibrium around an arbitrary point and dynamic force equilibrium along the vertical direction while neglecting second and higher order terms w.r.t. dx, gives the following differential equations:

$\circlearrowleft$: $V - \partial M/\partial x = J/dx\,\partial^2\theta/\partial t^2 = \rho I\partial^2\theta/\partial t^2$

$\circlearrowright$: $-V + \partial M/\partial x = J/dx\,\partial^2\theta/\partial t^2 = \rho I\partial^2\theta/\partial t^2$

$q + \partial V/\partial x = \rho A\partial^2 v/\partial t^2$

$J_y = \int_V r^2 \rho dV =$

$\rho \int_A z^2 dA dx =$

$\rho I_{zz} dx =$

$\rho I dx =$

J

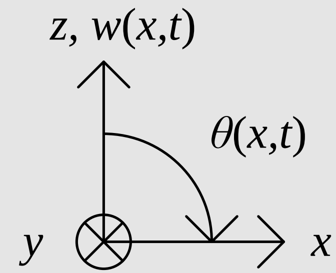

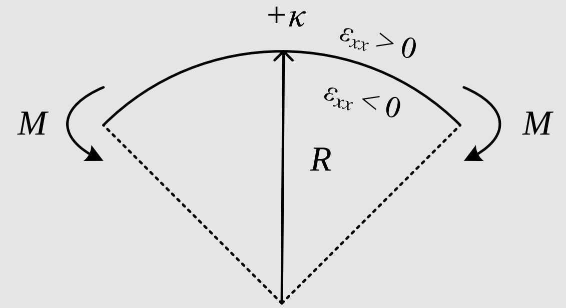

$\varepsilon_{xx} = z/R = z\kappa$

$M = \int dM = \int \sigma_{xx} z dA$

w

$\theta = -\partial w/\partial x$

$\kappa = \partial\theta/\partial x = -\partial^2 w/\partial x^2$

$M = EI\kappa = -EI\partial^2 w/\partial x^2$

$V = -EI\partial^3 w/\partial x^3 + \rho I\partial^3 w/\partial x\partial t^2$

$q = EI\partial^4 w/\partial x^4 - \rho I\partial^4 w/\partial x^2\partial t^2 + \rho A\partial^2 w/\partial t^2$

Dynamic Timoshenko beam (1)

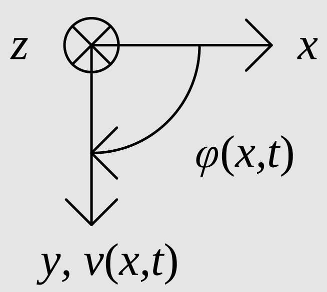

$J_z = \int_V r^2 \rho dV =$

$\rho \int_A y^2 dA dx =$

$\rho I_{yy} dx =$

$\rho I dx =$

J

By convention, positive bending moment generates tension along the positive vertical axis. Also, curvature follows angle.

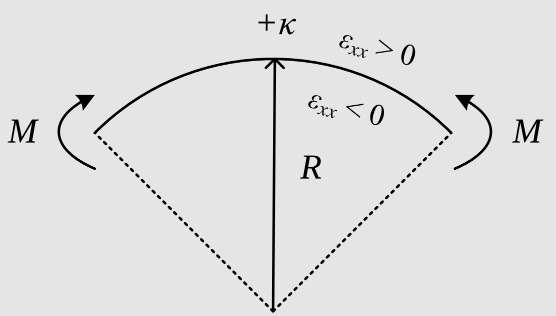

v

$\varepsilon_{xx} = -y/R = -y\kappa$

$\varphi = \partial v/\partial x - \gamma_0$

$M = \int dM = \int \sigma_{xx} y dA$

$\kappa = \partial\varphi/\partial x$

$M = -EI\kappa = -EI\partial\varphi/\partial x$

$V = GA\beta\gamma_0 = GA\beta(\partial v/\partial x - \varphi)$

$\rightarrow GA\beta(\partial v/\partial x - \varphi) + EI\partial^2\varphi/\partial x^2 = \rho I\partial^2\varphi/\partial t^2$

$q = GA\beta(\partial\varphi/\partial x - \partial^2 v/\partial x^2) + \rho A\partial^2 v/\partial t^2$

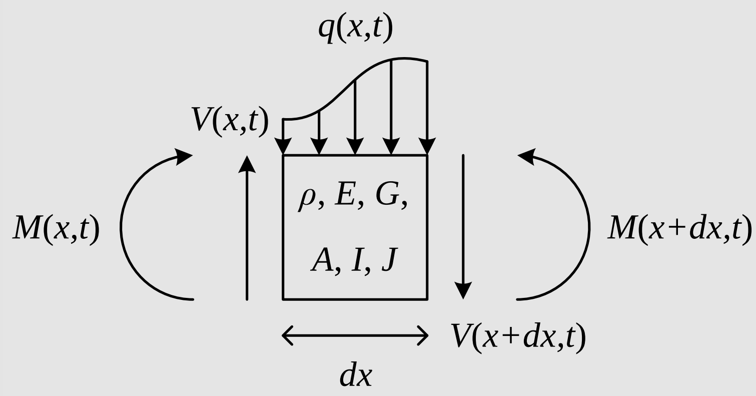

Taylor expansions around x of the quantities at the right end of the beam segment:

$$M(x+dx,t) = M(x,t) + \partial M/\partial x dx + O(dx^2)$$

$$V(x+dx,t) = V(x,t) + \partial V/\partial x dx + O(dx^2)$$

Considering dynamic moment equilibrium around an arbitrary point and dynamic force equilibrium along the vertical direction while neglecting second and higher order terms w.r.t. dx, gives the following differential equations:

$$\circlearrowright: V - \partial M/\partial x = J/dx\,\partial^2\varphi/\partial t^2 = \rho I\partial^2\varphi/\partial t^2$$

$$\circlearrowleft: -V + \partial M/\partial x = J/dx\,\partial^2\varphi/\partial t^2 = \rho I\partial^2\varphi/\partial t^2$$

$$q + \partial V/\partial x = \rho A\partial^2 v/\partial t^2$$

To obtain the two equations that govern Timoshenko's beam model, the two constitutive relations—relating bending moment to curvature and shear force to shear strain/angle—are substituted in the above dynamic equilibrium equations.

Note how the chosen coordinate system affects the sign of the terms in the governing equations associated with the shear stiffness. The β in these terms denotes the Timoshenko shear coefficient to account for the actual shear strain distribution along the surface of the cross-section; not just the shear strain/angle at the centroidal level γ_0.

$J_y = \int_V r^2 \rho dV =$

$\rho \int_A z^2 dA dx =$

$\rho I_{zz} dx =$

$\rho I dx =$

J

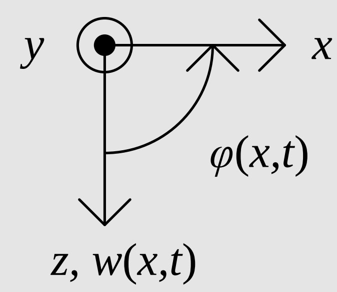

$\varepsilon_{xx} = z/R = z\kappa$

$M = \int dM = \int \sigma_{xx} z dA$

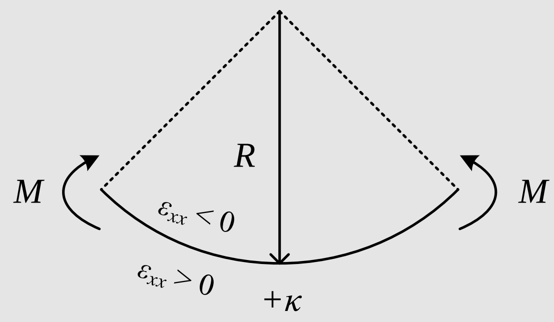

w

$\varphi = -\partial w/\partial x + \gamma_0$

$\kappa = \partial\varphi/\partial x$

$M = EI\kappa = EI\partial\varphi/\partial x$

$V = GA\beta\gamma_0 = GA\beta(\partial w/\partial x + \varphi)$

$\rightarrow -GA\beta(\partial w/\partial x + \varphi) + EI\partial^2\varphi/\partial x^2 = \rho I\partial^2\varphi/\partial t^2$

$q = -GA\beta(\partial\varphi/\partial x + \partial^2 w/\partial x^2) + \rho A\partial^2 w/\partial t^2$

Dynamic Timoshenko beam (2)

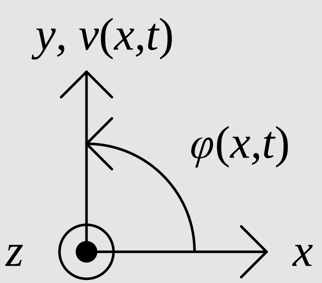

$J_z = \int_V r^2 \rho dV =$

$\rho \int_A y^2 dA dx =$

$\rho I_{yy} dx =$

$\rho I dx =$

J

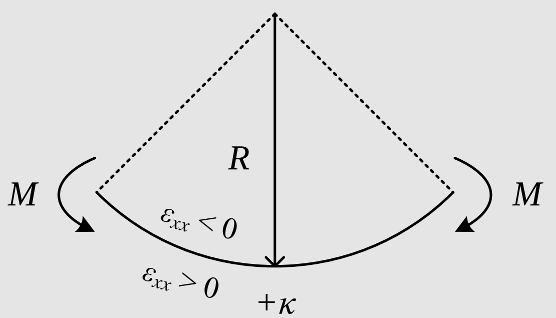

$\varepsilon_{xx} = -y/R = -y\kappa$

v $\quad M = \int dM = \int \sigma_{xx} y dA$

$\varphi = \partial v/\partial x - \gamma_0$

$\kappa = \partial \varphi/\partial x$

$M = -EI\kappa = -EI\partial\varphi/\partial x$

$V = GA\beta\gamma_0 = GA\beta(\partial v/\partial x - \varphi)$

$\rightarrow GA\beta(\partial v/\partial x - \varphi) + EI\partial^2\varphi/\partial x^2 = \rho I \partial^2\varphi/\partial t^2$

$q = GA\beta(\partial\varphi/\partial x - \partial^2 v/\partial x^2) + \rho A \partial^2 v/\partial t^2$

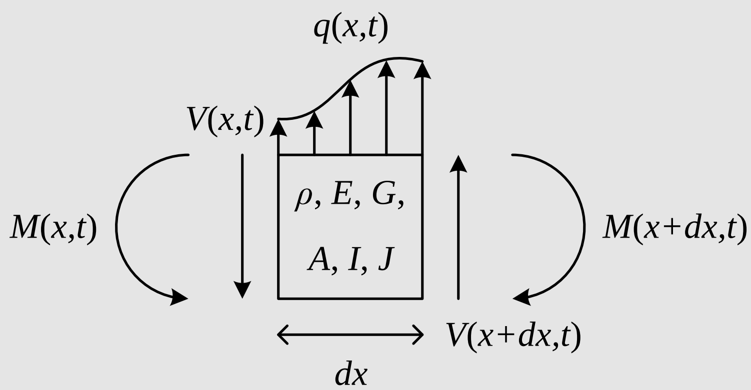

Taylor expansions around x of the quantities at the right end of the beam segment:

$M(x+dx,t) = M(x,t) + \partial M/\partial x dx + O(dx^2)$

$V(x+dx,t) = V(x,t) + \partial V/\partial x dx + O(dx^2)$

Considering dynamic moment equilibrium around an arbitrary point and dynamic force equilibrium along the vertical direction while neglecting second and higher order terms w.r.t. dx, gives the following differential equations:

$\circlearrowleft$: $V - \partial M/\partial x = J/dx \partial^2\varphi/\partial t^2 = \rho I \partial^2\varphi/\partial t^2$

$\circlearrowright$: $-V + \partial M/\partial x = J/dx \partial^2\varphi/\partial t^2 = \rho I \partial^2\varphi/\partial t^2$

$q + \partial V/\partial x = \rho A \partial^2 v/\partial t^2$

To obtain the two equations that govern Timoshenko's beam model, the two constitutive relations—relating bending moment to curvature and shear force to shear strain/angle—are substituted in the above dynamic equilibrium equations.

Note how the chosen coordinate system affects the sign of the terms in the governing equations associated with the shear stiffness. The β in these terms denotes the Timoshenko shear coefficient to account for the actual shear strain distribution along the surface of the cross-section; not just the shear strain/angle at the centroidal level γ_0.

$J_y = \int_V r^2 \rho dV =$

$\rho \int_A z^2 dA dx =$

$\rho I_{zz} dx =$

$\rho I dx =$

J

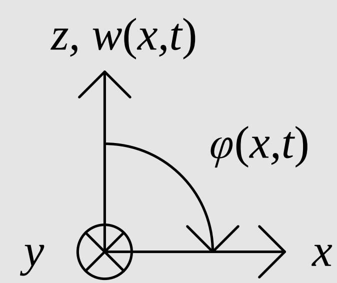

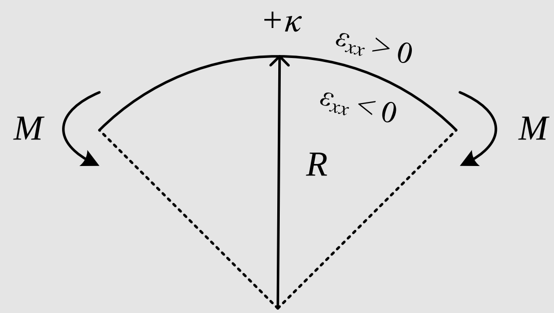

$\varepsilon_{xx} = z/R = z\kappa$

$M = \int dM = \int \sigma_{xx} z dA$ $\quad w$

$\varphi = -\partial w/\partial x + \gamma_0$

$\kappa = \partial\varphi/\partial x$

$M = EI\kappa = EI\partial\varphi/\partial x$

$V = GA\beta\gamma_0 = GA\beta(\partial w/\partial x + \varphi)$

$\rightarrow -GA\beta(\partial w/\partial x + \varphi) + EI\partial^2\varphi/\partial x^2 = \rho I \partial^2\varphi/\partial t^2$

$q = -GA\beta(\partial\varphi/\partial x + \partial^2 w/\partial x^2) + \rho A \partial^2 w/\partial t^2$

Static Timoshenko beam (1)

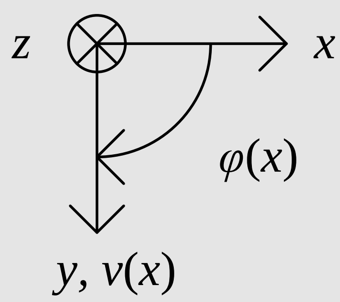

By convention, positive bending moment generates tension along the positive vertical axis. Also, curvature follows angle.

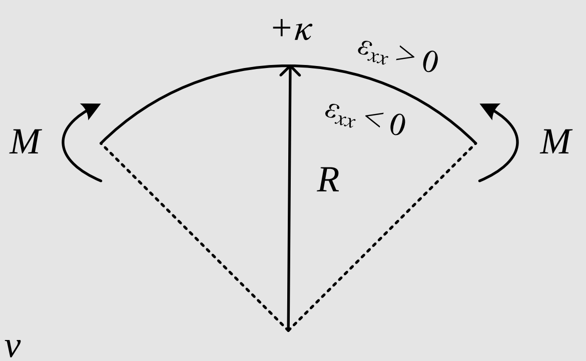

$$\varepsilon_{xx} = -y/R = -y\kappa$$

$$\varphi = dv/dx - \gamma_0$$

$$M = \int dM = \int \sigma_{xx} y dA$$

$$\kappa = d\varphi/dx$$

$$M = -EI\kappa = -EI d\varphi/dx$$

$$V = GA\beta\gamma_0 = GA\beta(dv/dx - \varphi)$$

$$\rightarrow GA\beta(dv/dx - \varphi) + EId^2\varphi/dx^2 = 0$$

$$q = GA\beta(d\varphi/dx - d^2v/dx^2)$$

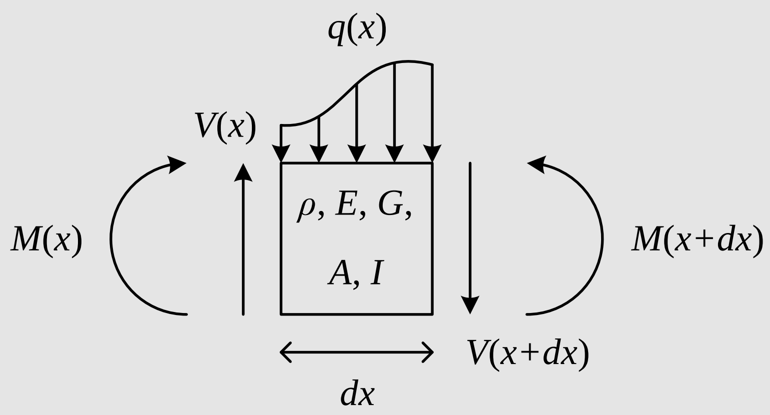

Taylor expansions around x of the quantities at the right end of the beam segment:

$$M(x+dx) = M(x) + dM/dxdx + O(dx^2)$$

$$V(x+dx) = V(x) + dV/dxdx + O(dx^2)$$

Considering dynamic moment equilibrium around an arbitrary point and dynamic force equilibrium along the vertical direction while neglecting second and higher order terms w.r.t. dx, gives the following differential equations:

$$V = dM/dx$$

$$q = -dV/dx$$

To obtain the two equations that govern Timoshenko's beam model, the two constitutive relations—relating bending moment to curvature and shear force to shear strain/angle—are substituted in the above static equilibrium equations.

Note how the chosen coordinate system affects the sign of the terms in the governing equations associated with the shear stiffness. The β in these terms denotes the Timoshenko shear coefficient to account for the actual shear strain distribution along the surface of the cross-section; not just the shear strain/angle at the centroidal level γ_0.

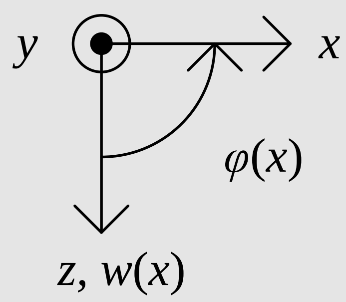

$$\varepsilon_{xx} = z/R = z\kappa$$

$$M = \int dM = \int \sigma_{xx} z dA$$

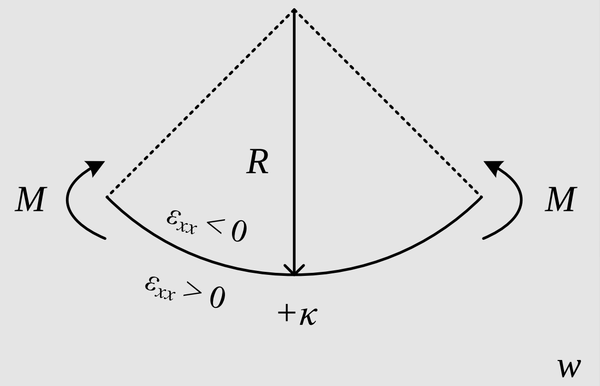

$$\varphi = -dw/dx + \gamma_0$$

$$\kappa = d\varphi/dx$$

$$M = EI\kappa = EI d\varphi/dx$$

$$V = GA\beta\gamma_0 = GA\beta(dw/dx + \varphi)$$

$$\rightarrow -GA\beta(dw/dx + \varphi) + EId^2\varphi/dx^2 = 0$$

$$q = -GA\beta(d\varphi/dx + d^2w/dx^2)$$

Static Timoshenko beam (2)

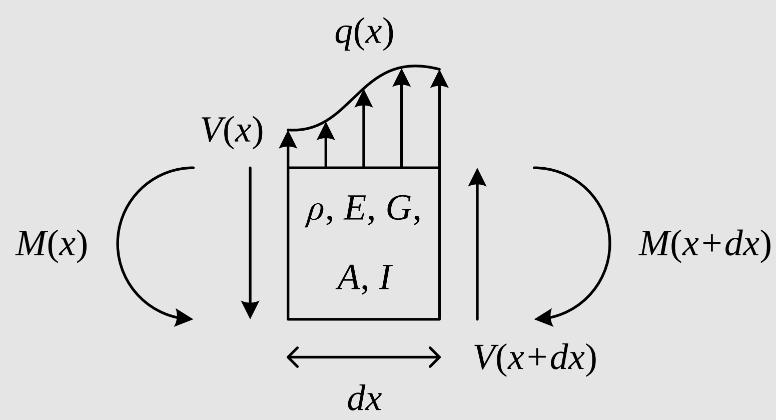

Taylor expansions around x of the quantities at the right end of the beam segment:

$$M(x+dx) = M(x) + dM/dxdx + O(dx^2)$$

$$V(x+dx) = V(x) + dV/dxdx + O(dx^2)$$

Considering dynamic moment equilibrium around an arbitrary point and dynamic force equilibrium along the vertical direction while neglecting second and higher order terms w.r.t. dx, gives the following differential equations:

$$V = dM/dx$$

$$q = -dV/dx$$

To obtain the two equations that govern Timoshenko's beam model, the two constitutive relations—relating bending moment to curvature and shear force to shear strain/angle—are substituted in the above static equilibrium equations.

Note how the chosen coordinate system affects the sign of the terms in the governing equations associated with the shear stiffness. The β in these terms denotes the Timoshenko shear coefficient to account for the actual shear strain distribution along the surface of the cross-section; not just the shear strain/angle at the centroidal level γ_0.

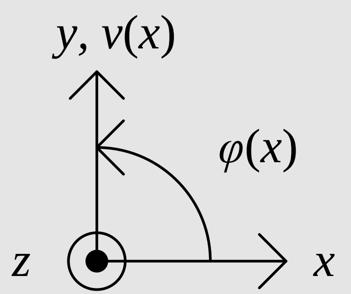

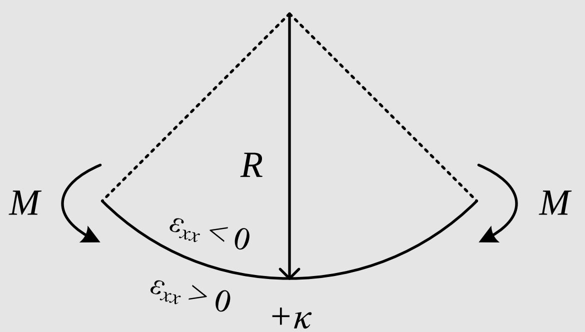

$$\varepsilon_{xx} = -y/R = -y\kappa$$

v

$$M = \int dM = \int \sigma_{xx} y dA$$

$$\varphi = dv/dx - \gamma_0$$

$$\kappa = d\varphi/dx$$

$$M = -EI\kappa = -EId\varphi/dx$$

$$V = GA\beta\gamma_0 = GA\beta(dv/dx - \varphi)$$

$$\rightarrow GA\beta(dv/dx - \varphi) + EId^2\varphi/dx^2 = 0$$

$$q = GA\beta(d\varphi/dx - d^2v/dx^2)$$

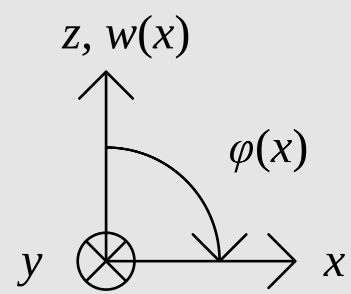

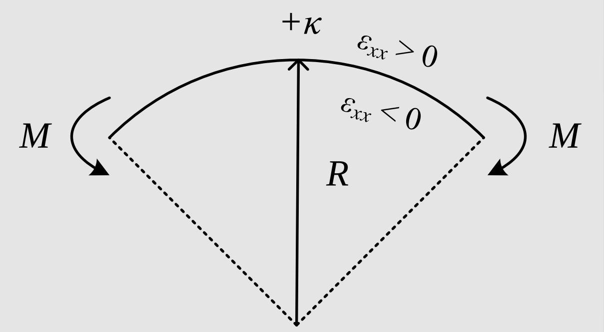

$$\varepsilon_{xx} = z/R = z\kappa$$

$$M = \int dM = \int \sigma_{xx} z dA$$

w

$$\varphi = -dw/dx + \gamma_0$$

$$\kappa = d\varphi/dx$$

$$M = EI\kappa = EId\varphi/dx$$

$$V = GA\beta\gamma_0 = GA\beta(dw/dx + \varphi)$$

$$\rightarrow -GA\beta(dw/dx + \varphi) + EId^2\varphi/dx^2 = 0$$

$$q = -GA\beta(d\varphi/dx + d^2w/dx^2)$$